Implementation of a Testbed for MISO OFDM Communication Systems

Submitted by

Weziwe Mfanafuthi Duma

In fulfillment of the Masters Degree in Electronic Engineering,

Faculty of Engineering, University of KwaZulu Natal

Submission date: 30 July 2012

Supervised by

Prof. S. H. Mneney

Declarations

Supervisor

As the candidate's Supervisor I agree/do not agree to the submission of this thesis.

_____

Name

_____ _____

Signature Date

Student

DECLARATION

I Weziwe Mfanafuthi Duma declare that

(i) The research reported in this dissertation/thesis, except where otherwise indicated, is my original work.

(ii) This dissertation/thesis has not been submitted for any degree or examination at any other university.

(iii) This dissertation/thesis does not contain other persons' data, pictures, graphs or other information, unless specifically acknowledged as being sourced from other persons.

(iv) This dissertation/thesis does not contain other persons' writing, unless specifically acknowledged as being sourced from other researchers. Where other written sources have been quoted, then:

a) their words have been re-written but the general information attributed to them has been referenced;

b) where their exact words have been used, their writing has been placed inside quotation marks, and referenced.

(v) Where I have reproduced a publication of which I am an author, co-author or editor, I have indicated in detail which part of the publication was actually written by myself alone and have fully referenced such publications.

(vi) This dissertation/thesis does not contain text, graphics or tables copied and pasted from the Internet, unless specifically acknowledged, and the source being detailed in the dissertation/thesis and in the References sections.

_____

Name

_____ _____

Signature Date

Acknowledgements

I would like to thank God for giving me the strength to pursue this degree and see it through till the end. I would like to thank my parents for the emotional support they gave me when days were dark and for giving me the confidence to tackle all the obstacles the project had.

I would like to thank my supervisor Prof. S. H. Mneney for his professional advice as well as his wisdom that I needed through my journey through the project. I would like to thank the technical staff at the School of Electrical, Electronic and Computer Engineering in particular, Mr Greg Loubser for his hardware expertise, Mr Ronald Koch for his technical assistance and Mr Urajh Roopnund for his technical expertise in RF hardware.

I would like to thank Dr Oyerinde, whose work my Masters Degree project was based, for giving me his support and advice throughout my time I spent on the degree. I would like to thank the other post graduates at the school whom I have gotten to know and who gave me support through the years I spent on the project.

Abstract

The thesis presents an implementation of a multiple input single output orthogonal frequency division multiplex (MISO OFDM) communication system testbed. The project was developed in order to evaluate whether the channel estimation algorithms developed by Dr Oyerinde [1] could be implemented in a real time communication system that uses today's technology. This implementation based validation would help determine the practicality of algorithms and methods that promise better performance for communication systems from a simulation point of view.

The benefits of using multiple orthogonal carriers are discussed as well as how an OFDM system works. The benefits of using multiple antennas at the transmitter, as opposed to using just one, are also discussed. The Alamouti scheme which allows space diversity to be achieved without the cost of having a lower data rate is presented.

Modules common to all communication systems, such as those dedicated to synchronization, channel estimation, symbol detection and channel coding, are discussed. The different methods of synchronization for OFDM communication systems are presented and compared. The channel estimation algorithm developed by Dr Oyerinde is presented and is adopted for an indoor channel. Most of the system blocks and parameters used in the testbed are the same as those used in [1] in order to easily compare the results obtained by simulation and those obtained by implementation.

The system bandwidth required for the project was too high for the processor chosen for the testbed. A qualitative evaluation of the practicality of Dr Oyerinde's channel estimation algorithms was performed instead. From this evaluation it was derived that Dr Oyerinde's non-iterative decision directed channel estimation algorithm was more suitable for real time non-iterative decision directed channel estimation communication systems than for iterative versions.. Apart from processing demands that couldn't be met, the other aspects of the project were implemented successfully.

Contents

Declarations ii

Acknowledgements iv

Abstract v

Glossary of Terms ix

Table of Figures xii

Table of Tables xiii

Chapter 1 1

Introduction 1

1.1 Research Motivation 4

1.1.1 Problem Definition 4

1.1.2 Research Question 5

1.2 Thesis Objectives 7

1.3 Thesis Outline 7

1.4 Contributions 8

1.5 Publications 9

Chapter 2 10

2 Background and Literature Review 10

2.1 Wireless Communication 10

2.2 Multiple Antenna Systems 13

2.2.1 SIMO Channel (Receive Diversity) 14

2.2.2 MISO Channel (Transmit Diversity) 15

2.2.3 MIMO Channel 16

2.2.4 Spatial Multiplexing 17

2.3 Indoor Channel 19

2.3.1 Model 1 20

2.3.2 Model 2 20

2.3.3 Model 3 21

2.4 OFDM Systems 23

2.5 MIMO OFDM 27

2.6 Conclusion 27
Chapter 3 29
3 System Model 29
3.1 SISO OFDM communication system 29
3.2 Orthogonal Frequency Division Multiplexing 30
3.2.1 Subcarrier Modulation and Demodulation 30
3.3 Multiple Input Single Output Orthogonal Frequency Division Multiplexing 32
3.4 Matlab Simulation of SISO and MISO OFDM 35
3.5 Conclusion 41
Chapter 4 42
4 Implementation Issues 42
4.1 Hardware Implementation 43
4.1.1 Processing Units 43
4.1.2 Data Converters 43
4.1.3 RF Stage Hardware 45
4.2 Synchronization 48
4.2.1 Synchronization Using 2 Repeated Parts 49
4.2.2 Synchronization using Cyclic Prefix 52
4.2.3 Synchronization using Multiple Repeated Parts 55
4.2.4 Fine Symbol Timing Synchronization 57
4.2.5 Fine Frequency Estimation 60
4.2.6 Chosen synchronization scheme 61
4.3 Detection 68
4.3.1 Symbol Detection 68
4.4 Channel Estimation 70
4.4.1 Channel Transfer Function Estimation 71
4.4.2 Channel Impulse Response Estimation 72
4.4.3 Channel Impulse Response Predictor 74
4.5 Channel Coding 76
4.5.1 Turbo Encoder 76
4.5.2 Turbo Decoder 81
4.6 Decision Directed Channel Estimation SISO OFDM systems 85

4.6.1 Non –Iterative 85
4.6.2 Iterative 89
4.7 Decision Directed Channel Estimation for MISO OFDM systems 91
4.7.1 Synchronization 92
4.7.2 Channel Estimation 93
4.8 Conclusion 96
Chapter 5 98
5 Results 98
5.1 Simulation Results 98
5.1 Implementation Results 105
5.2 DSP Implementation of a Baseband SISO OFDM Communication System 110
5.2.1 Transmitter 111
5.2.2 Receiver 114
5.3 Conclusion 119
Chapter 6 121
6 Conclusion and Recommendations 121
6.1 Conclusion 121
6.2 Recommendations and future work 123
8 References 124

Glossary of Terms

3GPP	-	3rd Generation Partnership Project
ADC	-	Analogue to digital converter
AWGN	-	Additive white Gaussian noise
BB	-	Base band
BIOS	-	Basic input output system
BPSK	-	Binary phase shift keying
CIR	-	Channel impulse response
CSI	-	Channel state information
CTF	-	Channel transfer function
DAC	-	Digital to analogue converter
DC	-	Direct current
DDCE	-	Decision directed channel estimation
DFT	-	Discrete Fourier transform
DSP	-	Digital signal processor
DVB-RCT	-	Digital Video Broadcasting - Return Channel Terrestrial
DVB-T	-	Digital Video Broadcasting - Terrestrial
EDMA	-	Enhanced direct memory access
EMIF	-	External memory interface
FD-CTF	-	Frequency domain – channel transfer function
FDD	-	Frequency division duplex
FDM	-	Frequency division multiplexing
FDPM	-	Fast data projection method

FEC	-	Forward error correction
FFT	-	Fast Fourier transform
FPGA	-	Field programmable gate array
FS	-	Fractionally spaced
HiperLAN	-	High performance local area network
ICI	-	Inter-carrier interference
IEEE	-	Institute of Electrical and Electronic Engineers
i.i.d.	-	Independently and identically distributed
IFFT	-	Inverse fast Fourier transform
ISI	-	Inter-symbol interference
LLR	-	Log likelihood ratio
LMS	-	Least mean squares
MIMO	-	Multiple input multiple output
MISO	-	Multiple input single output
ML	-	Maximum likelihood
MMSE	-	Minimum mean square error
MSE	-	Mean square error
MSPS	-	Megasamples per second
OFDM	-	Orthogonal frequency division multiplexing
PAPR	-	Peak to average power ratio
PASTd	-	Projection Approximation Subspace with deflation
PLL	-	Phase lock loop
PN	-	pseudo noise
QAM	-	Quadrature amplitude modulation
QPSK	-	Quadrature phase shift keying
RAM	-	Random access memory

RF	-	Radio frequency
RMS	-	Root mean square
SIMO	-	Single input multiple output
SISO	-	Single input single output
SNR	-	Signal to noise ratio
SOVA	-	Soft output Viterbi Algorithm
ST	-	Space time
TCP	-	Turbo-Decoder Coprocessor
V-BLAST	-	Vertical-Bell Laboratories Layered Space Time
VCO	-	Voltage controlled oscillator
VSSNLMS	-	Variable step size normalized least mean squares
WiMAX	-	Worldwide Interoperability for Microwave Access

Table of Figures

Figure 2-1: Multipath fading. (a) Outdoor channel. (b) Indoor channel. 13
Figure 2-2: SIMO channel with N transmit antennas and 1 receive antenna 15
Figure 2-3: MISO channel with N_T transmit antennas and 1 receive antenna 15
Figure 2-4: MIMO channel with N_R receiver and N_T transmitter antennas 16
Figure 2-5: OFDM Block Diagram 24
Figure 2-6: Modified OFDM block diagram 27
Figure 3-1 OFDM Communication system 30
Figure 3-2: BER Performance for SISO and MISO OFDM for a slow fading channel of normalized Doppler frequency fd=0.002. 38
Figure 3-3: BER Performance for SISO and MISO OFDM for a fast fading channel of normalized Doppler frequency fd=0.005. 39
Figure 3-4: BER Performance for SISO and MISO for a slow fading channel of normalized Doppler frequency fd=0.002 40
Figure 3-5: BER Performance for SISO and MISO OFDM for a slow fading channel of normalized Doppler frequency fd=0.005. 41
Figure 4-1: MISO OFDM Communication System 42
Figure 4-2: ADC and DAC interface with the DSP kit. 45
Figure 4-3: RF hardware functionality (a) modulator (b) demodulator 46
Figure 4-4: Testbed hardware (a) Transmitter (b) Receiver 48
Figure 4-5: OFDM symbol with repeated parts 50
Figure 4-6 Received OFDM symbols with cyclic extension 52
Figure 4-7: Timing metric trajectories for the different methods 57
Figure 4-8: Synchronization symbol pattern. 62
Figure 4-9: Signal buffering for synchronization (a) 1st symbol period (b) 2nd symbol period (c) subsequent symbol periods. 64
Figure 4-10: Decision Directed channel estimator for SISO OFDM 71
Figure 4-11: Turbo Code encoder 77
Figure 4-12: Convolutional Encoder (Non-Systematic) 78
Figure 4-13: (7.5) Recursive Systematic Convolutional Enconder 79
Figure 4-14: Turbo Code Decoder 81

Figure 4-15: Performance of the (7,5) Convolutional Code using a recursive systematic encoder....82
Figure 4-16: 3GPP Standard Turbo Encoder....84
Figure 4-17: Non- Iterative Decision Directed Channel Estimation for SISO OFDM 86
Figure 4-18: Modified Non- Iterative Decision Directed Channel Estimation....88
Figure 4-19: Iterative Decision Directed Channel Estimation 91
Figure 4-20: Decision directed channel estimation block diagram for MISO OFDM. 94
Figure 5-1: SISO OFDM system performance for different number of iterations 101
Figure 5-2: MISO OFDM system performance for different number of iterations 102
Figure 5-3: Performance of SISO and MISO OFDM systems for Non-Iterative DDCE....103
Figure 5-4: Performance of SISO and MISO OFDM systems for Iterative DDCE. 104
Figure 5-5: MISO OFDM spectrum for 16 subcarriers (a) 1st antenna contribution (b) 2nd antenna contribution (c) Total received MISO OFDM signal. 109
Figure 5-6: RF frequency MISO OFDM signal....110
Figure 5-7: Real part baseband signalxt. 113
Figure 5-8: Real part of Xk 113
Figure 5-9: Transmitted high frequency signal xct....114
Figure 5-10: Recovered real part of baseband signal after 4 OFDM symbol periods. 116
Figure 5-11: Received repeated OFDM signal's real part at low frequency after filtering. 116
Figure 5-12: $P(d)$....117
Figure 5-13: $E(d)$ 117
Figure 5-14: Λd and timing data 117
Figure 5-15: Real part of FFT of synchronized OFDM symbol after 4 periods. 118
Figure 5-16: Real part of Enlarged FFT of synchronized OFDM symbol after 4 periods. 119

Table of Tables

Table 2-1: Model parameters for the 3 models at 1.8 GHz....23
Table 3-1: Alamouti Scheme 33
Table 3-2: Power-delay profile for typical office environment with RMS delay spread of 50 ns 35
Table 5-1: Table of simulation parameters....99
Table 5-2: Profiling Statistics for the Receiver DSP 105

Chapter 1

Introduction

In our modern age, the demand for high data rate and good performing communication systems is ever increasing. Users want the transport of information from source to destination to be fast. They also want the transported information to be error free at the receiver. Users also want to be mobile during the transfer of information and this called for the use of wireless communication systems.

In any communication system, data is transmitted through a channel from the transmitter to the receiver. The channel between the transmitter and the receiver degrades the transmitted signal and this can cause the receiver to recover the transmitted information with errors. The wireless channel in wireless communication systems causes the transmitted signal to arrive at the receiver via different paths which have different lengths. This multipath transmission is caused by reflections from objects that lie in the environment between the transmitter and receiver. Since the paths have different lengths, the transmitted signal that travels along these paths arrives at the receiver at different times causing delay spreads at the receiver. The multipath signal interferes constructively and destructively resulting in what is referred to as multipath fading. Multipath fading causes signals that are transmitted in consecutive symbol periods to interfere with each other resulting in inter-symbol interference (ISI).

The wireless channel also corrupts the transmitted signal by adding noise to it. The noise alters the transmitted waveform and makes it difficult for the receiver to recover the transmitted information. Redundant symbols are transmitted with the information symbols and they are used with channel coding schemes to detect and correct errors in the transmitted information caused by noise and fading.

If either the transmitter or receiver or both are in motion during communication, the transmitted signal will experience a Doppler frequency shift (Doppler spread) at the receiver caused by the relative motion of the transmitter and receiver. This degrades the

synchronization of the receiver with the transmitter and causes inter-carrier interference in OFDM communication systems. The degraded synchronization between the transmitter and the receiver causes the receiver to detect incorrect information. This is because of the phase mismatch between the carriers of the transmitter and the receiver.

If the channel's impulse response is known at the receiver then the channel's effect on the transmitted signal can be cancelled out and the transmitted signal can be recovered. In general the channel impulse response is unknown at the receiver and it has to be recovered from the received signal. Accurate recovery of the transmitted signal at the receiver yields less errors in the data. The process of determining the channel's impulse response is called channel estimation. Channel estimation algorithms are employed in wireless communication systems in order to combat channel fading caused by delay and Doppler spread.

The channel estimation process is often hindered by the noise in the system. In a communication system where known symbols (pilots) are transmitted in order to estimate the channel's impulse response, if the signal to noise power ratio is low the estimated channel will be noisy and cause further errors in the detection process. A fast fading channel whose impulse response changes rapidly during the transmission of information, the channel estimation process has to be performed frequently in order to properly track the channel changes. If the channel estimation is not performed frequently, the receiver will use an outdated version of the channel in the detection process.

Since users demand high data rates from wireless communication systems, telecommunication engineers had to develop systems that can meet this demand without sacrificing the fidelity of the information. One of the schemes developed was Orthogonal Frequency Division Multiplexing (OFDM). Frequency division multiplexing allows the transmitter to transmit different information at different frequencies at the same time. This is done by modulating carriers which have different frequencies with different symbols. The data rate here is higher than in a single carrier system. If the carriers are multiples of the lowest frequency subcarrier then they become orthogonal to each other and they don't interfere with each other.

The modulated orthogonal carriers can overlap in the frequency domain which allows the system to use more carriers than an FDM system with non-orthogonal carriers within the same bandwidth since guard frequency bands are not required. Thus Orthogonal Frequency Division Multiplexing is spectrally efficient and has a high data rate since it doesn't waste bandwidth with the use of large frequency guard bands and it transmits data using many carriers.

Although OFDM has a lot of advantages it also has its disadvantages. OFDM is very sensitive to synchronization errors. Synchronization errors cause the carriers to no longer be orthogonal which results in inter-carrier interference (ICI). OFDM signals have a high peak to average power ratio (PAPR) and require the power amplifiers at the transmitter to be linear over a higher range and this leads to complexity in their design. Developments have been made to reduce the high PAPR in OFDM such as in [2] where the symbols in information carrying carriers are slightly disturbed and dummy symbols are used to modulate unused carriers.

In order to further increase the performance of wireless communication systems, space diversity is employed. A system with multiple antennas at the transmitter and the receiver is a multiple input and multiple output (MIMO) system. In a MIMO communication system the transmitted signal travels in different channels because it is transmitted with multiple antennas which are sufficiently spaced out such that the signals in these channels are uncorrelated. The signals are received at the receiver via different channels due to multiple receiver antennas. Sufficiently spaced out antennas at the transmitter and the receiver cause the signals travelling in different channels to be uncorrelated and this is how space diversity is achieved because the probability that there's severe fading on all the channels is reduced.

Where MIMO communication systems cannot be achieved due to space requirements or complexity in the implementation, single input multiple output (SIMO) and multiple input single output (MISO) communication systems are used. Space diversity can still be achieved because of the uncorrelated channels created by the multiple transmitter or the multiple receiver antennas. The signal from the transmitter arrives at the receiver via different channels and this yields diversity. The diversity gained in SMO and MISO communication systems is less than that in MIMO communication systems and hence MIMO communication systems have better performance than MISO and SIMO communication systems.

In this thesis, a MISO OFDM communication system is presented. MISO OFDM communication systems combine the benefits of MISO and OFDM communication systems thus yielding an even better performance than the two separate systems. With the use of an effective channel estimation algorithm and channel coding scheme, the performance is improved even further.

1.1 Research Motivation

1.1.1 Problem Definition

A lot of research has been done in channel estimation for SISO and MIMO OFDM and algorithms to perform channel estimation for these systems have been developed which give good performance for specific types of channels. Channel estimation algorithms have been developed for indoor, outdoor, slow fading, fast fading and frequency selective channels.

In signal processing we are often concerned about the complexity of algorithms as well as the performance. Usually algorithms that have good performance also have a lot of complexity as well and communication system designers have to find the right tradeoff between performance and complexity and choose the optimal option.

Often when algorithms are developed by researchers certain assumptions are made in the development, such as that synchronization is perfect, and they may not be true or possible in a real time implementation of the communication system. This was the case in [1] but for the real time testbed implementation, a synchronization scheme had to be investigated and implemented. Hardware also has limitations in terms of speed, memory, cost and availability which constrain communication system designers to using the most practical algorithms for their systems.

In order for us to know whether an algorithm can perform as promised in real systems, practical implementation of the algorithms has to be done to verify their viability. This can be done in 2 ways: simulation using target hardware simulators or practical implementation. Implementation using target processing hardware simulators allows designers to find out how fast the algorithms are and how much memory they use on the chip. Other aspects of the communication system, such as synchronization, space time coding and channel coding, can be simulated as well and the complexity of the whole communication system can be analyzed.

Simulations are cheap because only software is required however they cannot involve every aspect of the communication system. Analogue to digital (ADC) or digital to analogue (DAC) converters, amplifiers, modulators, demodulators and other hardware cannot be included in the software so their limitations cannot be factored in when analyzing the performance of the communication system. Simulation is usually not done in real time as well.

Practical implementation allows designers to analyze the performance of communication system as a whole and the communication between transmitter and receiver takes place in real time. Real hardware platforms are used and a full communication system is implemented on them. The communication system includes ADCs, DACs, amplifiers, filters and processors to realize a full communication system. The benefit of this type of validation is that all communication system modules which include synchronization and channel estimation are tested in a real environment in real time. The drawback is the high cost and development time required to realize a full system.

The method of validation carried out in this project is of the type which makes use of a hardware testbed. A full communication system is to be built to implement all the necessary modules for the task of validating the channel estimation algorithms developed in [1]. The simulation results produced are to be reproduced for a MISO OFDM communication system operating in an indoor environment. The design of the testbed is to be optimized for indoor environments.

1.1.2 Research Question

The questions to be answered are: Are the channel estimation algorithms for SISO and MIMO OFDM developed by Oyerinde [1] viable for real time implementation? Is it possible to achieve a good system performance in a real time implementation of a MISO OFDM communication system using these algorithms?

If indeed the algorithms perform in a real time communication system as promised then the work carried out in [1] would've benefitted research in the development of good channel estimation algorithms for MISO OFDM communication systems. It is expected that implemented communication systems do not perform as well as in their simulations due to hardware limitations and inaccurate assumptions made in the simulations. To determine if the developed channel estimation algorithms are viable for real time communication systems,

the performance as well as the complexity must not deviate by a large amount from the expected performance.

1.2 Thesis Objectives

The objective of the project was to implement the channel estimation algorithms developed for MIMO OFDM communication systems by Dr Olutayo Oyerinde [1]. He developed a variable step size normalized least mean squares (VSSNLMS) algorithm that is used with a subspace tracking algorithm called fast deflated projection method (FDPM) to perform channel estimation for SISO and MIMO OFDM communication systems. The task was to modify the algorithms for MISO OFDM and then build an indoor environment based communication system testbed that uses these algorithms.

Newly developed algorithms for communication systems which promise good performance must be investigated in order to evaluate their practical feasibility for real time applications using currently available hardware. This was the motivation for the project.

With the testbed, the algorithms were to be evaluated in terms of complexity and real time performance. If the algorithms were too complex then it would be impractical to use them with the currently available hardware. It may also imply that more expensive and high performance hardware must be purchased in order to cope with the complexity of the algorithms. If the algorithms were implemented with success and the system performs sufficiently similar to the theoretical predictions then a good contribution to research in MISO OFDM communication systems would have been made in the implementation and verification of the algorithms through measurements.

The objective of the thesis is to present the design and results of the testbed implementation. In the thesis the SISO and MIMO OFDM channel estimation algorithms developed in [1] are modified for indoor MISO OFDM communication systems and the results are presented.

1.3 Thesis Outline

The thesis is organized as follows:

In Chapter 2 a literature survey is presented that discusses the fundamental concepts that are used in the thesis. In this chapter, wireless communication systems are discussed and

concepts such as fading and inter-symbol interference which degrade the performance of a wireless communication system are explained. Multi-antenna systems which include MISO, SIMO and MIMO are introduced and their configurations and performance are discussed. The testbed was designed for an indoor channel and in this chapter this channel is modeled. Orthogonal frequency division multiplexing (OFDM) is discussed in this chapter and its benefits are mentioned and the implementation is also discussed.

In Chapter 3 a full OFDM communication system including the RF stage is presented. The combination of MISO and OFDM to form MISO OFDM is discussed where and the Alamouti space time coding scheme is used to achieve transmitter diversity while maintaining the same data rate as SISO OFDM. Simulations comparing SISO OFDM and MISO OFDM for slow fading and fast fading channels are given. Simulations of single carrier SISO and MISO communication systems are also performed in order to compare transmitter diversity benefits to single carrier system with OFDM systems.

In Chapter 4 the design of the testbed is presented. The hardware components used for the project are presented and their functionality, benefits and limitations are discussed. The signal processing component of the project is also presented and it included tasks such as synchronization, channel estimation, detection and decoding. The system blocks for SISO and MIMO OFDM developed in [1] were modified to suit an indoor channel and the SISO and MISO OFDM system blocks that resulted from the modifications are presented.

In Chapter 5 the results for the testbed implementation are presented. Achievements and limitations for the testbed are presented and a qualitative evaluation of the feasibility of the channel estimation algorithms developed in [1] is given.

Recommendations for the improvements of the testbed are given in Chapter 6. Methods to overcome the challenges and limitations addressed in Chapter 5 are suggested for future researchers who want to contribute to this field.

The thesis is concluded in Chapter 6.2

1.4 Contributions

- The channel estimation algorithms developed in [1] for SISO and MIMO OFDM communication systems were modified for MISO OFDM communication systems

operating in indoor channels. This contribution yielded new results for the research in MISO OFDM communication systems.

- Instead of using soft detected symbols to perform channel transfer function estimation using the minimum mean square error (MMSE) algorithm, soft decisions from the decoder were used. For the indoor slow fading channel, using decoded soft decisions yielded better results than using detected symbols as in [1] since the system used a frame consisting of more than one OFDM symbol.
- Synchronization algorithms from [3] which use multiple repeated parts were modified and made recursive and this reduced the computation time by a factor of N, where N is the fast Fourier transform (FFT) size.
- A full design and implementation of a MISO OFDM communication system test bed was achieved which used a TMS320C6416 Texas Instruments digital signal processor (DSP). The system could perform synchronization, channel estimation and also Turbo decoding with the DSP's Turbo Co-processor (TCP) module.

1.5 Publications

W. Duma, P. Motheeram and S.H. Mneney, *Wireless SIMO/MISO OFDM Testbed Implementation using the TMS320C6416 DSP Kits*, SATNAC Conference Proceedings, East London Convention Center, East London, 4 – 7 September 2011.

Chapter 2

2 Background and Literature Review

2.1 Wireless Communication

In wireless communication systems a radio link between transmitter and receiver is required in order to achieve communication. The radio link consists of electromagnetic waves that are transmitted at the transmitter and they propagate through free space towards the receiver. These electromagnetic waves are reflected and refracted by obstacles in the wireless channel on their way to the receiver. These reflections caused by the obstacles cause the signal from the transmitter to arrive at the receiver via different paths and at different times due to the different path lengths.

When the signals from the different paths arrive at the receiver they add constructively and destructively. If the different path delays are larger than the symbol period, this will result in inter-symbol interference (ISI). This type of signal distortion caused by the channel is called multipath fading. The largest amount of delay imposed on the signal by the channel's obstacles is called delay spread. Often the signal that arrives at the receiver via the path with the largest delay is the one that is attenuated the most because most channels have a decaying power-delay profile. Hence this signal contributes the least to ISI.

Telecommunication engineers instead use an RMS delay spread as a design guideline for their systems. The RMS delay spread is the effective delay spread experienced by the signal and is given by [4]

$$\tau_{RMS} = \sum_i P_i \tau_i^2 - (\bar{\tau})^2, \qquad 2\text{-}1$$

$$\bar{\tau} = \sum_i P_i \tau_i , \qquad 2\text{-}2$$

where τ_i is the delay of the i^{th} path, $\bar{\tau}$ is the average delay spread and P_i is the power of the i^{th} channel tap divided by the total power of all paths.

The reciprocal of the delay spread is called coherent bandwidth and is given by

$$B_c = \frac{1}{\tau_{max}}.$$

2-3

If the system bandwidth is higher than B_c the system will experience ISI which will cause the system performance to be degraded. This is because the delayed signals from previous symbol intervals arrive during the next symbol's interval at the receiver and these signals interfere with each other. Systems with a bandwidth higher than the coherent bandwidth experience frequency selective fading. Systems with a bandwidth lower than the coherent bandwidth experience flat fading which does not degrade the system performance.

In mobile communication systems the transmitter and/or the receiver are free to move around and still maintain a communication link. The relative motion of the receiver with respect to the transmitter causes the signal to experience a Doppler frequency shift. This Doppler frequency shift causes synchronization problems at the receiver due to the varying signal frequency. This motion also causes the channel through which the signal propagates to change. This is because the obstacles experienced by the signal on its way to the receiver and the signal path to the receiver change due to the mobility of the terminals through different environment configurations. This varying channel due to mobility makes it difficult to estimate the channel's impulse response to cancel out channel effects on the transmitted signal because it also changes as the channel changes.

Channels whose impulse responses change rapidly due the transmitter-receiver fast relative motion are said to be fast fading. If the transmitter-receiver relative motion is small the channel is considered slow fading. The channel fading caused by transmitter-receiver relative motion is characterized by the coherent time which is the reciprocal of the maximum Doppler frequency shift, denoted $f_{d\,max}$, and is given by

$$T_c = \frac{1}{f_{d\,max}}.$$

2-4

In indoor channels, the receiver and transmitter relative motion is often small because the speed of the terminals is restricted by the environment. Hence indoor channels are generally slow fading. Due to the close proximity of the walls and furniture to each other and to the receiver, the indoor channel has more multipath components than outdoor channels for isotropic radiating antennas. This is illustrated in Figure 2-1.

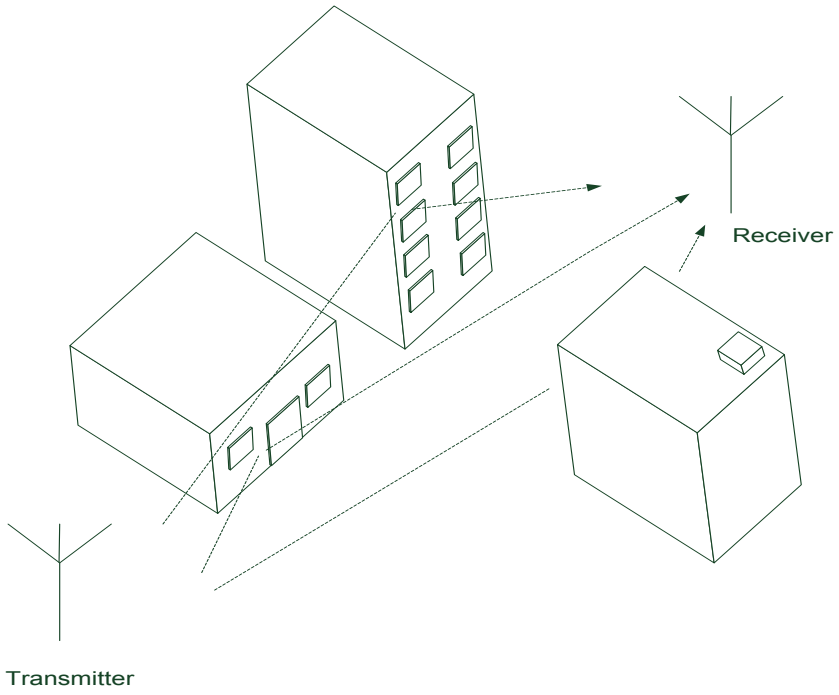

(a)

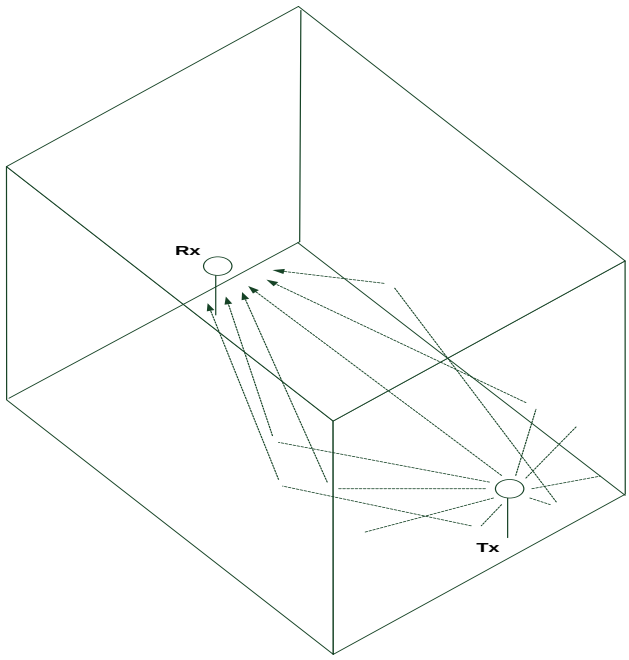

(b)

Figure 2-1: Multipath fading. (a) Outdoor channel. (b) Indoor channel.

2.2 Multiple Antenna Systems

Similar to time diversity, frequency diversity and coding diversity, MIMO offers spatial diversity in a communication system by using multiple antennas at the transmitter to transmit information and also at the receiver to receive the information. It allows independent data streams to be transmitted simultaneously in the same frequency band at the same time via spatial multiplexing which increases the capacity of the channel. It is better than frequency and time multiplexing because it doesn't need more bandwidth to achieve multiplexing [5].

By placing antennas at least $\lambda/2$ apart the signals transmitted with the different antennas are sent over different independent channels which will fade differently reducing the probability that all the paths are unreliable. Increased proximity of the antennas causes the channels to be correlated since the signals suffer the same scattering from the channels. The MIMO channel analysis will be broken up into SIMO and MISO channel analysis which yield receive and transmit diversity respectively.

2.2.1 SIMO Channel (Receive Diversity)

In this communication system there is only one transmitter antenna and N_R receiver antennas as depicted in Figure 2-2. The receiver receives N_R signals and has to select the corresponding transmitted signal based on the received signal. The signals arrive through independent and uncorrelated paths.

From [6] there are 2 types of gains that are obtained as N_R is increased. For BPSK the error probability is given by

$$p(e) = Q\left(\sqrt{2\|\boldsymbol{h}\|^2 SNR}\right), \quad 2\text{-}5$$

where $\boldsymbol{h}$ is the channel impulse response and SNR is the signal to noise ratio. The term $\|\boldsymbol{h}^2\|SNR$ can be written as $\frac{\|\boldsymbol{h}\|^2}{N_R} SNR.N_R$. The 1st term corresponds to a diversity gain; by averaging over multiple receive paths the probability that all the paths have small channel gains is reduced since

$$\frac{\|\boldsymbol{h}\|^2}{N_R} SNR = \frac{1}{N_R} \sum_{i=1}^{N_R} \left|h_i^2\right| \to 1 \; as \; N_R \to \infty,$$

if channel gains are normalized. The second term corresponds to a power gain from having many receive antennas and coherent combining at the receiver.

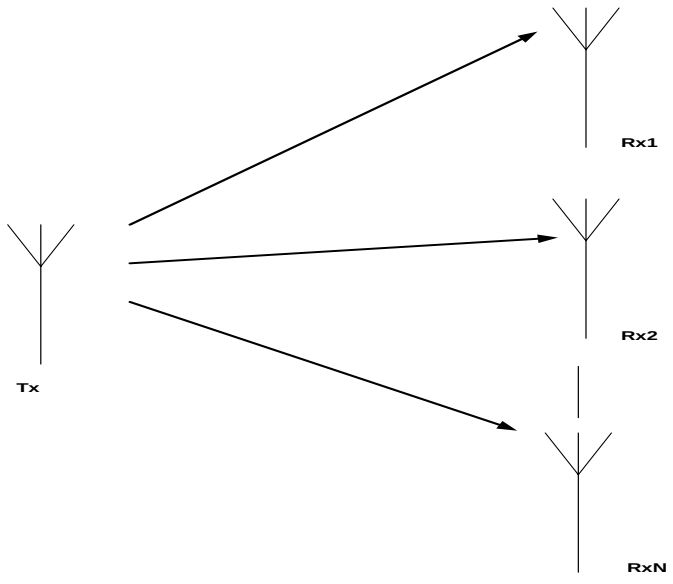

Figure 2-2: SIMO channel with N transmit antennas and 1 receive antenna

2.2.2 MISO Channel (Transmit Diversity)

In a MISO channel there are N_T transmitter antennas as depicted in Figure 2-3. There are many schemes used to achieve diversity such the repetition code and Alamouti [6]. There's no diversity gain when transmitting the same signal over different antennas. The repetition code achieves transmit diversity by transmitting the same signal over different antennas in different intervals with 1 antenna transmitting in each interval.

The repetition code is not efficient in using the available degrees of freedom from space diversity. It would cause delays in the transmission of information or require a higher transmission rate. In the Alamouti scheme 2 complex signals are transmitted over 2 symbol periods. In the 1st period

$x_1[1] = u_1, x_2[1] = u_2$ is transmitted and in the 2nd period

$x_1[2] = -u_2^*, x_2[2] = u_1^*$ is transmitted. If the channel is assumed to remain constant over the 2 symbol times then $h_1 = h_1[1] = h_1[2]$ and $h_2 = h_2[1] = h_2[2]$. Written in matrix form we obtain

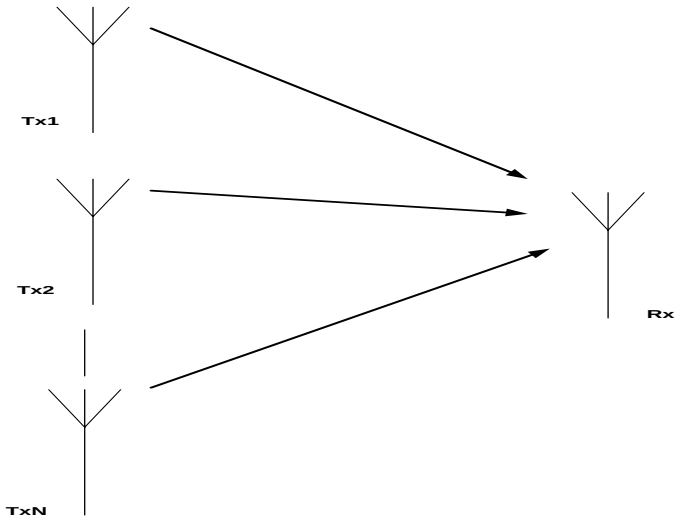

Figure 2-3: MISO channel with N_T transmit antennas and 1 receive antenna

$$[r[1]\, r[2]] = [h_1 \;\; h_2]\begin{bmatrix} u_1 & -u_2^* \\ u_2 & u_1^* \end{bmatrix} + [n[1] \;\; n[2]] = \begin{bmatrix} h_1 & -h_2^* \\ h_2 & h_1^* \end{bmatrix}[u_1 \;\; u_2] + [n[1] \;\; n[2]]$$

2-6

The square matrix has orthogonal columns which makes the problem of detecting u_1 and u_2 decompose to 2 separate orthogonal scalar problems. This makes the diversity gain 2 for the detection of each symbol since the signals x_1 and x_2 have been transmitted via 2 channels in 2 two symbol periods. This yields better bandwidth efficiency than the repetition code. The sacrifice is the power used to transmit each signal during the symbols period since 2 antennas are active during the symbol period each consuming half the total power. The diversity gain for the Alamouti scheme is 2 for the MISO channel.

2.2.3 MIMO Channel

The MIMO channel consists of N_R receiver antennas and N_T transmitter antennas as depicted in Figure 2-4. The diversity gain for the SIMO channel was N_R and for the MISO channel was N_T hence for a MIMO channel the maximum diversity gain is $N_R \times N_T$. Thus using multiple antennas at the transmitter and receiver increases the diversity of the system and hence the capacity. The other advantage of MIMO systems is discussed next which is spatial multiplexing.

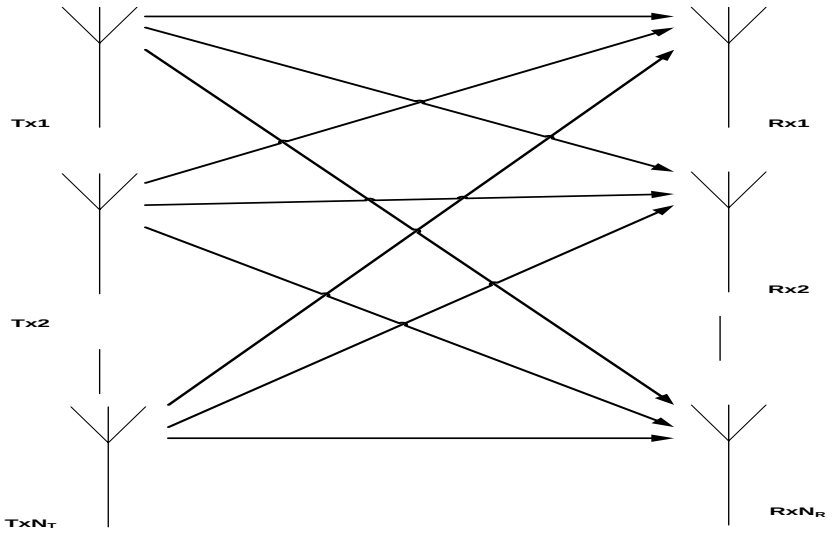

Figure 2-4: MIMO channel with N_R receiver and N_T transmitter antennas

For MISO, SIMO and MIMO communication systems, channel estimation is crucial since the channel needs to be known in order to perform detection. The combining of the signals that arrive at the receiver via multiple channels is achieved with the use of the channels' impulse responses or transfer functions, for example the Alamouti scheme. Thus channel estimation algorithms that are very accurate yield good performance for these systems and make them feasible.

2.2.4 Spatial Multiplexing

Multiplexing in communication systems is when multiple signals are sent simultaneously. In the space domain multiple signals are transmitted via different transmitter antennas and are received via different receiver antennas. This increases the data rate since instead of sending symbols via the same antenna serially one after the other, consecutive symbols equal to the number of transmitter antennas can be sent in parallel. Spatial multiplexing exploits the channels degrees of freedom which are limited by the minimum between the numbers of transmitter or receiver antennas.

An example of a spatial multiplexing is V-BLAST [6]. Here N_T signals are sent simultaneously through the channel with the different N_T transmitter antennas. The k^{th} signal is allocated a power P_k such that $\sum_{k=1}^{N_T} P_k = P$ which is the total transmitted power. The k^{th} data stream is encoded using a capacity achieving Gaussian code which achieves a rate R_k. The diversity of V-BLAST is at most N_R because each data stream is received via the N_R receiver antennas but is transmitted via only 1 transmitter antenna and not N_T antennas. This shows that there is less diversity when there is more spatial multiplexing and hence there is a tradeoff between spatial multiplexing and diversity gain.

From [6] it was shown that with channel state information (CSI) known at the receiver the capacity in a MIMO communication system with fast fading is given by

$$C = E\left[\log det\left(\mathbf{I}_{N_R} + \frac{SNR}{N_T}\mathbf{H}\mathbf{H}^*\right)\right],$$

2-7

where SNR is the common signal to noise ratio at each receiver antenna. If $\lambda_1 \geq \lambda_2 \geq \cdots \geq \lambda_{N_{min}}$ are the random and ordered singular values of $\mathbf{H}$ and N_{min} is the minimum of the number of receiver and transmitter antennas then

$$C = E\left[\sum_{i=1}^{N_{min}} \log\left(1 + \frac{SNR}{N_T}\,\lambda_i{}^2\right)\right] = \sum_{i=1}^{N_{min}} E\left[\log\left(1 + \frac{SNR}{N_T}\,\lambda_i{}^2\right)\right].$$

2-8

At high SNR the capacity reduces to

$$C \approx N_{min} \log\left(\frac{SNR}{N_T}\right) + E\left[\sum_{i=1}^{N_{min}} \lambda_i{}^2\right]$$

2-9

and at low SNR

$$C \approx N_R\, SNR \log_2 e$$

2-10

with a normalized channel covariance. This indicates that the capacity of a MIMO channel is increased by a factor N_{min}, which is the number of degrees of freedom of the channel, at high SNR and only by a factor N_R at low SNR which only yields a power gain which makes the communication system have a similar capacity to that of a 1 by N_R channel. Thus the capacity increase due to spatial multiplexing is only obtained at high SNR.

In a slow fading channel, the capacity is related to the outage probability which is given by

$$p_{out}(R) = P\left\{\log det\left(\mathbf{I}_{\mathrm{N_R}} + \frac{SNR}{\mathrm{N}_T}\mathbf{H}\mathbf{H}^*\right) < R\right\},$$

2-11

for an i.i.d. Rayleigh fading channel. Unlike an AWGN channel the slow fading channel is dependent on **H**, which is random and quasi static, and thus the slow fading channel cannot be characterized by capacity but by outage probability which is the probability that the information transmission rate is smaller than the target rate R. For SISO channel the outage probability at high SNR is given by

$$p_{out}(R) \approx \frac{(2^R-1)}{SNR},$$ 2-12

which decays as 1/SNR. For MIMO channel using a repetition scheme the outage probability decays as $1/SNR^{N_T N_R}$ and this is the upper bound of the decay of outage probability for a MIMO slow fading channel. The diversity from the use of multiple antennas improves the decaying compared to the SISO case hence there is a diversity gain.

V-BLAST works well in a fast fading channel but is not optimal in slow fading channels. This is because the data streams are transmitted via different antennas hence different channels. If one of the channels is in a deep fade all the data transmitted through it will be lost. In a fast fading channel the channel variations occur more often and so the channel wouldn't be in a deep fade for a long time such that all the data through is lost.

Spatial multiplexing achieves a higher data rate without having to use more bandwidth but this is achieved at the cost of diversity gain. One has to choose between the two benefits of MIMO channels.

2.3 Indoor Channel

The channel transfer function in a multipath environment is given by [7]

$$H(\omega, z) = \sum_i a_i e^{j\varphi_i} e^{j(-\omega\tau_i + z u_i)},$$ 2-13

where $a_i e^{j\varphi_i}$ is the complex amplitude, τ_i is the temporal delay, u_i is the spatial Doppler shift in rad.m^{-1} from the i^{th} multipath scatterer, ω is the base band angular frequency and z is the position along the direction of motion. The signal experiences attenuation a_i, a carrier phase shift φ_i, a base band phase shift $\omega\tau_i$ and a carrier spatial Doppler phase shift zu_i. The base band spatial Doppler phase shift is much smaller than that of the carrier signal hence it is neglected from (2-13). When the receiver moves along the z direction the received signal experiences a phase shift due to the time delay and the spatial Doppler phase shift.

The inverse Fourier transform of $H(\omega, z)$ is

$$a(\tau,u)=\frac{1}{2\pi}\int_{-\infty}^{\infty}\int_{-\infty}^{\infty}H(\omega,z)e^{j\omega\tau}e^{-jzu}\,d\omega dz=2\pi\sum_i a_i e^{j\varphi_i}\delta(\tau-\tau_i)\,\delta(u-u_i)\,,$$

2-14

which is the effective distribution of signals at the receiver antenna at a time delay τ and direction u. In an indoor channel the scatterers are closer together due to a large density of objects. The result of this is that there is more fading due to multipath. Since OFDM has an advantage of being immune to multipath fading then this will not pose a problem to the test bed implementation in an indoor channel as long as the transmission rate satisfies [8]

$$R_s\leq\frac{1}{2\pi T_m},$$

2-15

where T_m is the RMS delay spread. When there is no line of sight between the transmitter and receiver and the signal has to travel from one room to another the received signal will be weaker due to path loss. In [7] parametric models for an indoor channel path loss are presented. The models are based on experiments and the path loss is in dB (Hata power law).

2.3.1 Model 1

Here the path loss is given by

$$L=L_1+10nlog(d)\,,$$

2-16

where d is the distance from the transmitter, L_1 is the path loss at a distance 1m from the transmitter and n is to be determined experimentally and determines how rapidly the path loss increases with distance. In this model the path loss in dB increases linearly with distance.

2.3.2 Model 2

In this model the path loss is given by:

$$L = L_0 + L_C + \sum_i k_{wi} L_{wi} + k_f^{\left(\frac{k_f+2}{k_f+1} - b\right)} L_f \ ,$$

2-17

where L_0 is the free space path loss, L_C is a constant, k_{wi} is the number of walls penetrated of type i with wall loss L_{wi}, L_f is the loss between k_f adjacent floors and b is obtained empirically. From the above equation it is observable that the total floor loss is a non-linear function of the number of floors.

2.3.3 Model 3

In this model the path loss is given by:

$$L = L_0 + \propto d \ ,$$

2-18

where $\propto$ is an attenuation constant. This path loss is exponential (in dB). The path losses were found to be independent of frequency and the parameters of the models are to be determined experimentally. Once the parameters are obtained then the path loss can be obtained for any distance from the transmitter within the indoor channel. In [7] the parameters for the 3 models are presented which were obtained by 10 different institutions at an operating frequency of 1.8 GHz. These results are presented in Table 2-1.

The walls used in the experiment for Model 2 were L_{w1} , which was a light wall such as plaster board or light concrete, and L_{w2} which was a heavy and thick wall with thickness greater than 10cm made of concrete or brick. From the table it can be seen that the thicker wall contributes a higher loss than the thinner wall of a lighter material as expected. Other indoor channel models exist such as in [4] where standard DBV-T, DVB-RCT, WiMAX and IEEE 8 002.11g channel models are discussed.

In an indoor channel the receiver and the transmitter are either static or moving at slow speeds such that the Doppler spread is very small and the channel can be considered as a slow fading channel. The small Doppler spread in indoor channels will allow OFDM to

perform better since the carrier synchronization is less affected and thus the carriers will remain orthogonal.

Table 2-1: Model parameters for the 3 models at 1.8 GHz

	Model 1		Model 2				Model 3
Condition	L_1 (dB)	n	L_{w1} (dB)	L_{w2} (dB)	L_f (dB)	b	$\propto$ (dBm^{-1})
Dense							
One floor	33.3	4	3.4	6.9	18.3	0.46	0.62
Two floors	21.9	5.2					
Three floors	44.9	5.4					2.8
Open	42.7	1.9	3.4	6.9	18.3	0.46	0.22
Large	37.5	2	3.4	6.9	18.3	0.46	
Corridor	29.2	1.4	3.4	6.9	18.3	0.46	

In addition to slow movements making the channel slow fading, the indoor channel does not experience heavy weather conditions such as rain which attenuates the transmitted signal power causing errors at the receiver. The conditions in an indoor channel remain static for multiple symbol times even if is there are changes which can occur such as doors being opened and closed, changes in the occupancy of personnel in the room, movement of furniture etc.

The delay spread in the indoor channel is smaller than in the outdoor channel and this allows the communication to be at a higher data rate. This also allows wide band communication such as OFDM to be possible because the smaller delay spread corresponds to a wider coherence bandwidth which makes the channel flat fading as long as the transmission bandwidth is smaller than the coherence bandwidth.

2.4 OFDM Systems

Frequency division multiplexing is a communication scheme for sending multiple signals containing different information at the same time. This is done by modulating the different signals to different centre frequencies and then using the signals at different center frequencies to modulate a carrier signal which is transmitted. In OFDM the sub carrier frequencies are orthogonal i.e.

$$\int_0^T m_{k1}\, e^{k1\omega t} m_{k2} e^{k2\omega t} dt = 0, \quad k1 \neq k2\,,$$

2-19

where $k1$ and $k2$ are integers such that the signals do not interfere with each other and the receiver can easily distinguish between them and there's no inter-carrier interference (ICI). In OFDM the data symbols within a frame are sent at different orthogonal frequencies at the same time hence the modulation levels of the symbols in each sub carrier can be reduced in order to achieve the same data rate as for a single carrier system transmitting the same amount of symbols per unit time by having many modulation levels and decrease the symbol error probability. Figure 2-5 shows a block diagram of an OFDM block diagram.

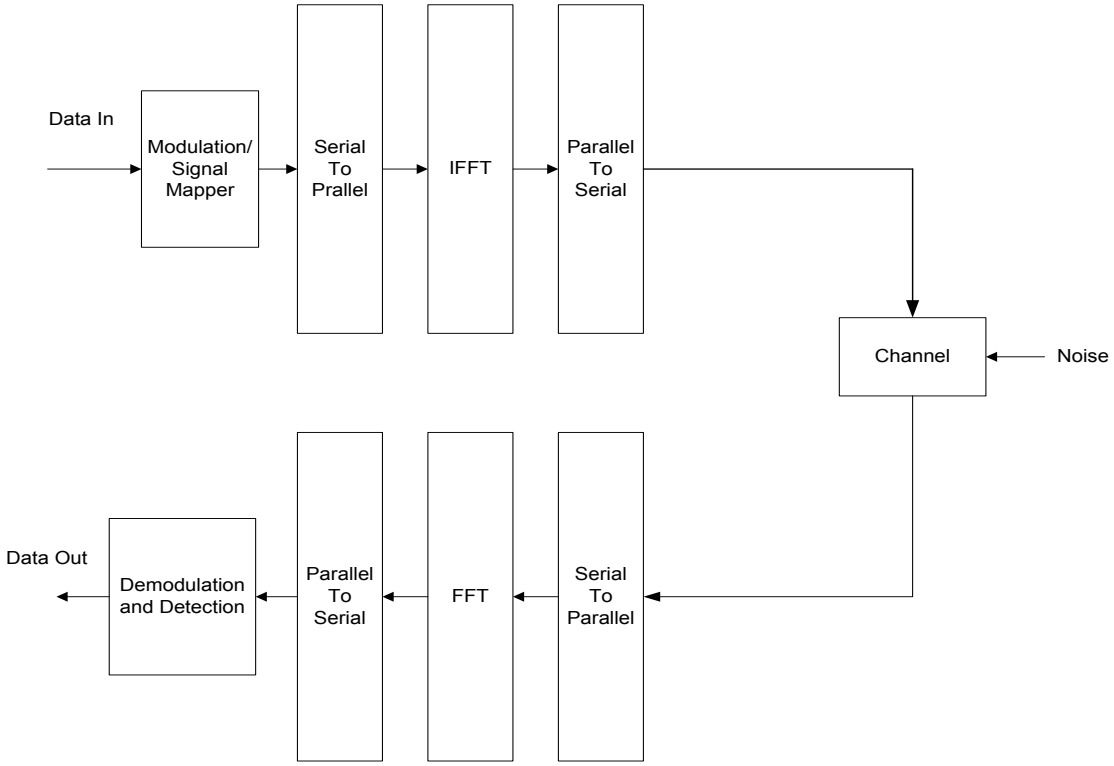

Figure 2-5: OFDM Block Diagram

The incoming serial data in the communication system is separated into frames of length N. The symbols in the frame are mapped in parallel into points on a constellation plane such that each symbol $s(i)$ is given by

$$s(i) = A_i e^{j\theta_i}, \quad 2\text{-}20$$

where A_i is the amplitude and θ_i is the phase. When the symbol $s(i)$ is multiplied with the carrier $e^{j2\pi f_i t}$, where f_i is the carrier frequency, the resulting signal is given by

$$x_i(t) = A_i e^{j\theta_i} e^{j2\pi f_i t}. \quad 2\text{-}21$$

Since the OFDM symbols are modulated at different frequencies that are integer multiples of each other and summed so that they can be transmitted at the same time the resulting signal is given by

$$x(t) = \sum_{i=1}^{N} x_i(t) = \sum_{i=1}^{N} A_i e^{j\theta_i} e^{j2\pi f_i t} = \sum_{i=1}^{N} A_i e^{j\theta_i} e^{j2\pi f_0 i t} = \sum_{i=1}^{N} s(i) e^{j2\pi f_0 i t}. \quad 2\text{-}22$$

It can be seen from (2-22) that $x(t)$is given by an inverse DFT of $s(i)$ since the frequencies are discrete and are multiples of f_0 . The DFT of a signal can be implemented more efficiently with a FFT when N is a power of 2. The mapped symbols given by $s(i)$ can now be replaced by X_i which is the FFT of $x(t)$. This means that OFDM can be implemented by taking the inverse FFT of the mapped symbols and thus at the receiver the received signal's FFT should be computed in order to obtain the symbols.

The high data rate of OFDM allows the communication system to make use of a guard interval which is greater than the channel's delay spread. The guard interval helps to mitigate the inter-symbol interference (ISI) caused by multipath. During the guard interval a cyclic prefix is transmitted instead of no transmission since that would cause harmonics at the FFT output. For every frame of symbols $s(i)$ of length N given by

$$s = \{s[0], s[1], s[2], \ldots\ldots\ldots, s[N-1]\}, \quad 2\text{-}23$$

a sub block of symbols of length L given by

$$s_g = \{s[N-L], s[N-L+1], s[N-L+2], \ldots\ldots, s[N-1]\},$$

2-24

is inserted before the original symbols and the overall frame to be transmitted is given by

$$d = \{s_g, s\} = \{s[N-L], s[N-L+1], .., s[N-1], s[0], s[1], s[2], .., s[N-1]\}.$$

2-25

The modified block diagram is shown in Figure 2-6. Since a whole frame of symbols is transmitted at the same time this makes the system able to combat short durations of noise bursts that are shorter than the symbol period [8]. Despite all the excellent advantages of OFDM there are also disadvantages which come from implementation. OFDM relies on the sub carriers being orthogonal and this makes it very sensitive to synchronization. Poor synchronization causes the carriers to be no longer orthogonal and this yields inter-carrier interference. Doppler frequency shift also causes poor synchronization and thus if the receiver and the transmitter are in motion relative to each other, ICI would also result in OFDM causing errors.

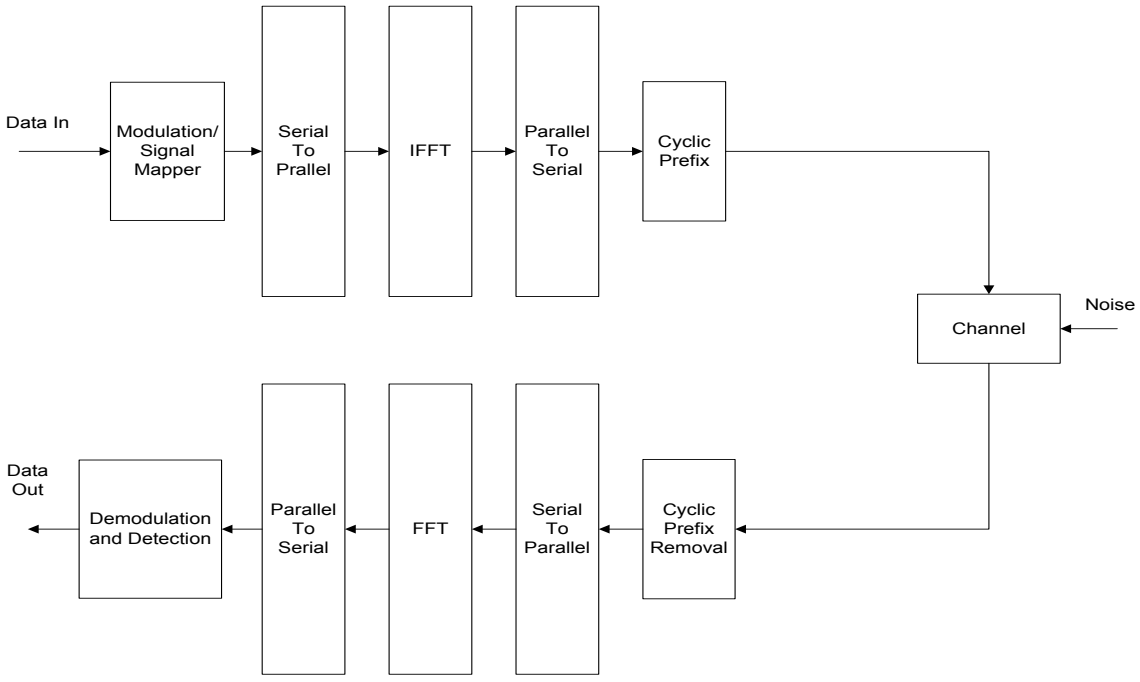

Figure 2-6: Modified OFDM block diagram

Since the sub carriers used in OFDM are multiples of each other they occur at discrete frequencies in the utilized bandwidth. This causes a high peak to average power ratio (PAPR) and requires the power amplifiers at the transmitter and the receiver to have a high dynamic range. Power amplifiers operating in a wide dynamic range are non-linear in nature and designing linear amplifiers is complex and thus more expensive. OFDM is more sensitive to distortion caused by non-linear amplifiers since it will cause ICI so OFDM needs more expensive amplifiers to be implemented. In [2] a method of reducing the peak to average power ratio (PAPR) in OFDM by slightly disturbing the symbols in carriers used to transmit information and also sending dummy symbols in unused carriers is presented. The reduction of the PAPR will reduce the cost of the power amplifiers needed to be used in the OFDM system.

2.5 MIMO OFDM

The use of OFDM increases the data rate since a serial data stream is transmitted in parallel via orthogonal sub carriers and if spatial multiplexing is used, via multiple transmitter antennas at the transmitter and multiple antennas at the receiver, the capacity and reliability of communication increases even further due to the diversity gained from the multiple antennas and spatial multiplexing. With spatial multiplexing each OFDM block can be sent with different antennas which will increase the data rate by a factor equal to the degree of freedom gain of the channel. With spatial diversity each OFDM of block will be sent through all the antennas at different times to achieve both transmit and receive diversity which reduces the symbol error rate.

2.6 Conclusion

A literature review was presented in this chapter. The concepts to be focused on in the thesis were introduced and they included space diversity where multiple antennas are used at the transmitter and/ or the receiver to send and receive signals via different channels. The

Orthogonal frequency division multiplexing (OFDM) communication system was introduced as well as the model for indoor channels.

Chapter 3

3 System Model

3.1 SISO OFDM communication system

The OFDM communication system developed in this chapter is given in Figure 3-1. Binary data is encoded by an encoder which adds parity bits that help with forward error correction (FEC) at the receiver. The channel coding scheme used was Turbo Coding so the encoder is a Turbo Encoder. The bits from Turbo Encoder are mapped into QPSK symbols. The serial QPSK symbols are converted into parallel symbols and are used to modulate OFDM subcarriers after applying an IFFT on them. The parallel IFFT samples are converted to serial in order to be transmitted in the time domain. In order to reduce inter-symbol interference (ISI) a cyclic prefix guard interval is added. The samples are converted to an analogue signal using a digital to analogue converter (DAC) and the real signal is used to modulate an in phase carrier and the imaginary signal is used to modulate a quadrature carrier. The resulting in-phase and quadrature components of the signal are summed and transmitted through the wireless channel.

The channel degrades the transmitted signal with multipath fading and it adds noise to the signal which is modeled as additive white Gaussian noise (AWGN). The received signal is split into 2 parts which are channeled through 2 paths. The signal in one path is multiplied by an in-phase carrier and the signal in the other path is multiplied by a quadrature carrier. The results are low pass filtered and the baseband real and imaginary parts of the transmitted signal are recovered. After converting the filtered analogue signals to digital they are combined to form a complex signal and the OFDM cyclic prefix is removed. The serial samples are converted to parallel and an FFT is performed on the samples. The result is converted back from parallel to serial. The frequency domain symbols are obtained after detection is performed. The detected symbols are then decoded in order to obtain the transmitted information symbols.

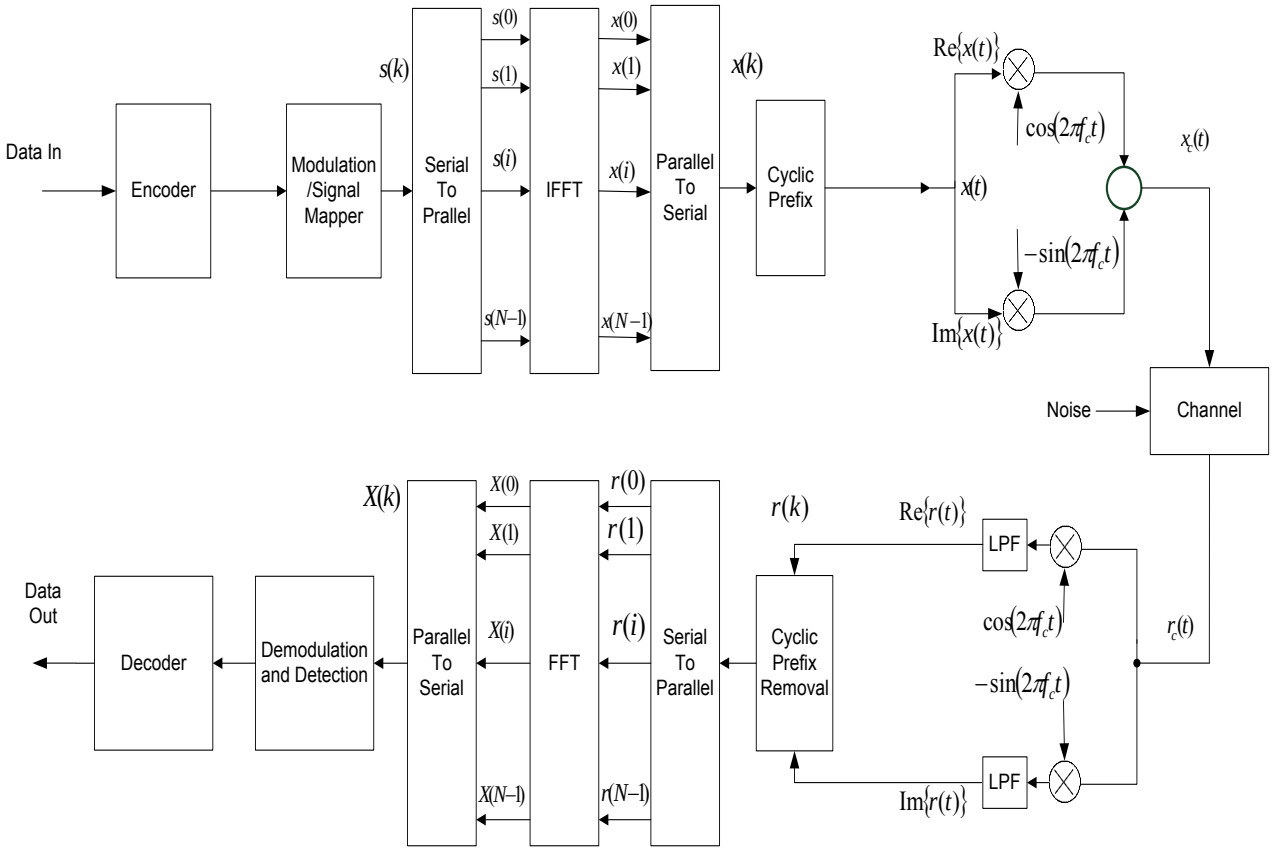

Figure 3-1 OFDM Communication system

3.2 Orthogonal Frequency Division Multiplexing

3.2.1 Subcarrier Modulation and Demodulation

The bits from the encoder are mapped to an M-ary constellation such as BPSK, QPSK or 4QAM. The mapped symbols are regarded as frequency domain symbols that have modulated their relevant subcarriers. An inverse fast Fourier Transform (IFFT) is performed on the symbols to convert the signal into time domain and the result is given by

$$x(t) = \sum_{k=0}^{N-1} s(k) e^{j2\pi k f_{BB} t},$$

3-1

where f_{BB} is the lowest baseband subcarrier frequency and $t = nT_s$ with n being the sample index and T_s is the sampling interval. Since $x(t)$ is a baseband signal, it must be translated to an RF frequency by multiplying it with an RF frequency carrier which will result in a signal given by [9]

$$x_c(t) = x(t)\cos(2\pi f_c t) = Re\left\{\sum_{k=0}^{N-1} A_k e^{j\theta_k} e^{j2\pi f_c t}\right\}$$

$$= \sum_{k=0}^{N-1} A_k e^{j\theta_k}\cos(2\pi(f_c + kf_{BB})t)$$

$$= \sum_{k=0}^{N-1} A_k e^{j\theta_k}[\cos(2\pi f_c t)\cos(2\pi k f_{BB} t) - \sin(2\pi f_c t)\sin(2\pi k f_{BB} t)]$$

$$= Re\{x(t)\}\cos(2\pi f_c t) - Im\{x(t)\}\sin(2\pi f_c t)\,.$$

3-2

At the receiver, the received signal is split into 2 paths where in one the signal is multiplied with a cosine and in the other it is multiplied with a sine signal. The real part of the baseband signal is recovered by multiplying the received signal with a cosine carrier signal and the result, neglecting channel degradations, is given by

$$Re\{r_{BB}(t)\} = r(t)\cos(2\pi f_c t)$$

$$= [Re\{x(t)\}\cos(2\pi f_c t) - Im\{x(t)\}\sin(2\pi f_c t)\,]\cos(2\pi f_c t)$$

$$= Re\{x(t)\}\cos(2\pi f_c t)\cos(2\pi f_c t) - Im\{x(t)\}\sin(2\pi f_c t)\cos(2\pi f_c t)$$

$$= \frac{1}{2}Re\{x(t)\}[1 + \cos(4\pi f_c t)] - \frac{1}{2}Im\{x(t)\}[\sin(0) + \sin(4\pi f_c t)]$$

3-3

The higher frequency terms are low pass filtered and the real part of the baseband signal is recovered. Applying the same procedure by multiplying the received signal with a sine

carrier signal and low pass filtering, the imaginary part of the baseband signal can be recovered. After digital to analogue conversion, the real and imaginary parts are combined to form a complex signal. An FFT is performed on the complex baseband signal and the frequency domain samples are given by

$$X(f) = \sum_{n=0}^{N-1} s(k) e^{-j2\pi n f_{BB} t} \quad 3\text{-}4$$

In the discrete time and frequency domains the IFFT and FFT of the signal is given by

$$x(n) = \sum_{k=0}^{N-1} s(k) e^{j2\pi nk/N}, \quad \text{and} \quad 3\text{-}5$$

$$X(k) = \sum_{n=0}^{N-1} r_{BB}(k) e^{-j2\pi nk/N} \quad 3\text{-}6$$

respectively, where $n = t/T_s$ and $f_{BB} = F_s/N$. Since the subcarrier frequencies are multiples of f_{BB}, the subcarriers are orthogonal to each other. The subcarriers being orthogonal allow the spectrum to be reduced by using closely spaced subcarriers while still avoiding inter-carrier interference. This is what makes OFDM bandwidth efficient.

3.3 Multiple Input Single Output Orthogonal Frequency Division Multiplexing

In order to improve the performance of communication systems, available diversity has to be exploited. Time diversity is achieved by repeating the transmitted signal over D symbol intervals. The receiver averages the received signal over the D symbol intervals and the average received signal yields better performance than using a single transmitted signal. The diversity order achieved is D at the expense of a lower information rate and a slower system.

With more than one antenna at the transmitter and/or at the receiver, space diversity can be achieved due to the transmitted signal arriving via different paths at the receiver, given that the antennas are at least half of a wavelength apart [6]. The separation of the antennas creates different independent channels for the transmitted signal to propagate through. The benefit of having multiple channels for the signal to travel through is that the probability that

overall signal will undergo severe fading is reduced [6] since the received signal is averaged over all the channels.

In a system with multiple transmitter and receiver antennas – a multiple input multiple output (MIMO) system - spatial multiplexing can also be achieved with the diversity. With spatial multiplexing the transmitter can transmit different signals over different antennas at the same time and receive these signals with different antennas at the receiver [6]. This increases the information rate because of the degrees of freedom created by the multiple channels. An example of a MIMO scheme that utilizes spatial multiplexing in order to increase the system capacity is V-BLAST.

As mentioned before transmitting the same symbol over different symbol intervals, as required by MISO communication systems, reduces the information rate. A scheme that maintains the information rate for a MISO system with 2 transmitter antennas is the Alamouti scheme.

During the 2 symbol periods, the transmitters transmit the following signals [10] given in Table 3-1.

Table 3-1: Alamouti Scheme

Time	Antenna 0	Antenna 1
t_0	s_0	s_1
t_1	$-s_1^*$	s_0^*

The received signal during the 1st symbols interval is given by

$$r_0 = h_0 s_0 + h_1 s_1 + n_0 \,, \tag{3-7}$$

and during the 2nd symbol interval it is given by

$$r_1 = -h_0 s_1^* + h_1 s_0^* + n_1, \tag{3-8}$$

where n_0 and n_1 are complex additive white Gaussian noise (AWGN) for interval t_0 and t_1 respectively with variances σ^2 and a power spectral densities of N/2 per dimension.

The receiver uses a maximum likelihood (ML) detector to choose the estimates of s_0 and s_1, given by $\hat{s}_0$ and $\hat{s}_1$ respectively, that minimize the distance metric given by

$$d^2(r_0, h_0\hat{s}_0 + h_1\hat{s}_1) + d^2(r_1, -h_0\hat{s}_1^* + h_1\hat{s}_0^*) = |r_0 - h_0\hat{s}_0 + h_1\hat{s}_1|^2 + |r_1 + h_0 s_1^* - h_1 s_0^*|^2 \quad \text{3-9}$$

Equations (3-7) and (3-8) are substituted in (3-9) to obtain the following representation of the maximum likelihood detection

$$(\hat{s}_0, \hat{s}_1) = \arg \min_{(\hat{s}_0, \hat{s}_1) \in C} (|h_0|^2 + |h_1|^2 - 1)(|\hat{s}_0|^2 + |\hat{s}_1|^2) + d^2(\tilde{s}_0, \hat{s}_0) + d^2(\tilde{s}_1, \hat{s}_1) \quad \text{3-10}$$

and C is the set of all possible modulated symbol pairs $(\hat{s}_0, \hat{s}_1)$. The decision statistics for detecting s_0 and s_1 ,$\tilde{s}_0$ and $\tilde{s}_1$, are given by

$$\tilde{s}_0 = h_0^* r_0 + h_1 r_1^* \quad \text{3-11}$$

$$\tilde{s}_1 = h_1^* r_0 - h_0 r_1^* \quad \text{3-12}$$

Substituting (3-7) and (3-8) in (3-11) and (3-12) results in

$$\tilde{s}_0 = (|h_0|^2 + |h_1|^2)s_0 + h_0^* n_0 + h_1 n_1^* \quad \text{3-13}$$

$$\tilde{s}_1 = (|h_0|^2 + |h_1|^2)s_1 + h_1^* n_0 - h_0 n_1^* \quad \text{3-14}$$

From here the maximum likelihood decoding rule (3-9) can be separated into 2 decoding rules for s_0 and s_1 which is given by

$$\hat{s}_0 = \arg\min_{\hat{s}_0 \in C}(|h_0|^2 + |h_1|^2 - 1)\,|\hat{s}_0|^2 + d^2(\tilde{s}_0, \hat{s}_0) \quad \text{3-15}$$

$$\hat{s}_1 = \arg\min_{\hat{s}_1 \in C}(|h_0|^2 + |h_1|^2 - 1)|\hat{s}_1|^2 + d^2(\tilde{s}_1, \hat{s}_1) \quad \text{3-16}$$

In the development of the above equations for decoding the Alamouti scheme, it was assumed that the channels h_0 and h_1 have constant fading over the 2 consecutive symbol intervals.

3.4 Matlab Simulation of SISO and MISO OFDM

SISO and MISO OFDM communications system were simulated for indoor slow and fast fading channels. The systems used a symbol length of 64 subcarriers where only 63 of them were active. The system utilized QPSK modulation and a 1/3 Turbo coding scheme from the 3GPP2 standard. A soft output Viterbi decoder was used for the component decoders of the Turbo Code scheme. The frame length comprised of 420 information bits which yielded 20 OFDM symbols per frame. Pilot symbols are transmitted at the beginning of each frame for channel estimation to be performed. A simple minimum mean square error channel estimator is used which is given by

$$\tilde{H}[n,k] = \frac{\bar{y}[n,k]z[n,k]}{|\bar{y}[n,k]|^2 + \frac{\sigma_W^2}{\sigma_H^2}} \quad \text{3-17}$$

where $\bar{y}[n,k]$ is the transmitted pilot symbol and $z[n,k]$ is the received symbol in nth OFDM symbol interval in the kth subcarrier. The parameters σ_W^2 and σ_H^2 are the noise and channel transfer function variance respectively.

The channel follows a hyperLAN/2 standard channel model and it was taken from [4] and its power-delay profile is given in Table 3-2.

Table 3-2: Power-delay profile for typical office environment with RMS delay spread of 50 ns

Tap	Power (dB)	Delay (ns)
1	0	0

2	-0.9	10
3	-1.7	20
4	-2.6	30
5	-3.5	40
6	-4.3	50
7	-5.2	60
8	-6.1	70
9	-6.9	80
10	-7.8	90
11	-4.7	110
12	-7.3	140
13	-9.9	170
14	-12.5	200
15	-13.7	240
16	-18	290
17	-22.4	340
18	-26.7	390

The power-delay profile in Table 3-2 is converted to a channel impulse response by the following equation [11]

$$h(t) = \sum_{l=0}^{M} h_l e^{-j2\pi f_c \tau_l},$$

3-18

and h_l is given by

$$h_l = \sqrt{10^{P_l/10}},$$

3-19

where P_l is the power of the l^{th} tap with respect to the 1st tap in the power-delay profile, f_c is the carrier frequency and τ_l is the delay of the l^{th} tap . The channel impulse response power is normalized to 1 [4]. The sum of the powers of the multipath signals that arrive at the receiver must be less or equal the total transmitted power hence $\sum|h_l|^2 = 1$.

With Doppler frequency shift taken into account, the channel impulse response is given by

$$h(t) = \sum_{l=0}^{M} h_l e^{-j2\pi(f_c+fd)\tau_l},$$

3-20

where fd is the RMS Doppler frequency shift. Single carrier SISO and MISO communication systems were also simulated. Their parameters were the same except for the frame length which was a length of 8 information bits. The symbol period for the single carrier and OFDM systems is the same hence the frame length of 8 bits here allowed both systems to perform channel estimation after the same frame interval. The channel estimation for the single carrier case is given by

$$\widetilde{H} = \frac{\bar{y}z}{|\bar{y}]|^2+\frac{\sigma_W^2}{\sigma_H^2}}.$$

3-21

As can be seen from Figure 3-2 and Figure 3-3, transmitter diversity improves the performance of an OFDM communication system. As in Chapter 6 of [1] where SISO and MIMO OFDM communication systems are compared, the SISO system performs slightly better at low SNR but MISO outperforms SISO at higher SNR. This is because at lower SNR up to about 12 dB, multi antenna systems' channel estimation methods are more affected by noise.

The power of the signal coming from each transmitter antenna in a MISO system is 1/M times that of a SISO system, where M is the number of transmitter antennas, since the total transmitted signal power for both systems is the same. Therefore the estimated channel for each transmitted signal path in a MISO system is more affected by noise than that of a SISO system since the signal power is M times lower which is the reason why at low SNR, the SISO system performs better.

As expected, systems operating in slow fading channels perform better than those operating in fast fading channels. This because the channel impulse response varies slightly from the estimated channel impulse response, estimated at the beginning of the frame, in subsequent symbol intervals. Since no channel tracking algorithm was used, the system operating in a fast fading environment use an outdated channel estimate to detect the transmitted symbols.

The single carrier systems perform similar to the OFDM systems with MISO offering better system performance over SISO. For a slow fading channel, the simulated QPSK modulated single carrier systems performed almost identically. For the fast fading case, transmitter diversity in the MISO system improved the system performance.

In the simulations OFDM outperformed single carrier systems. This could be attributed to the property of OFDM which is being immune to ISI distortion. Since the synchronization was assumed to be perfect, the OFDM systems weren't affected by the Doppler frequency shifts which cause synchronization errors. The Doppler frequency shifts only changed the channel impulse response from symbol period to symbol period.

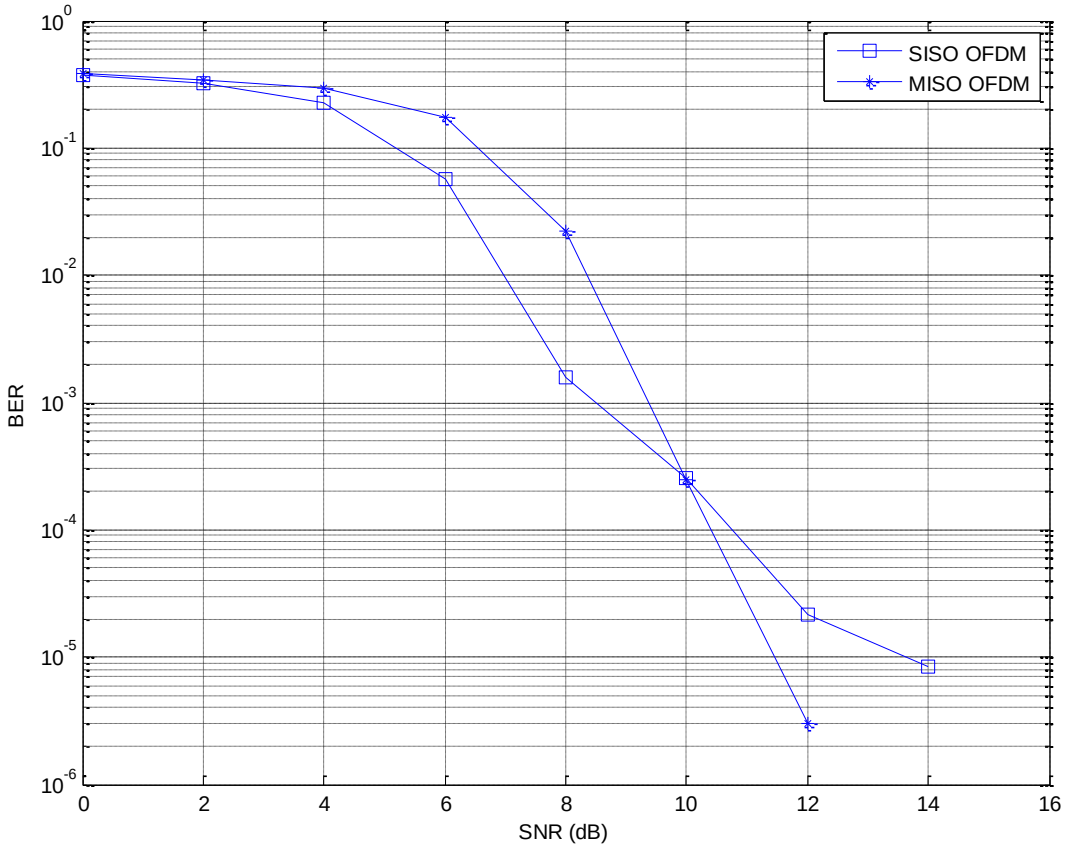

Figure 3-2: BER Performance for SISO and MISO OFDM for a slow fading channel of normalized Doppler frequency fd=0.002.

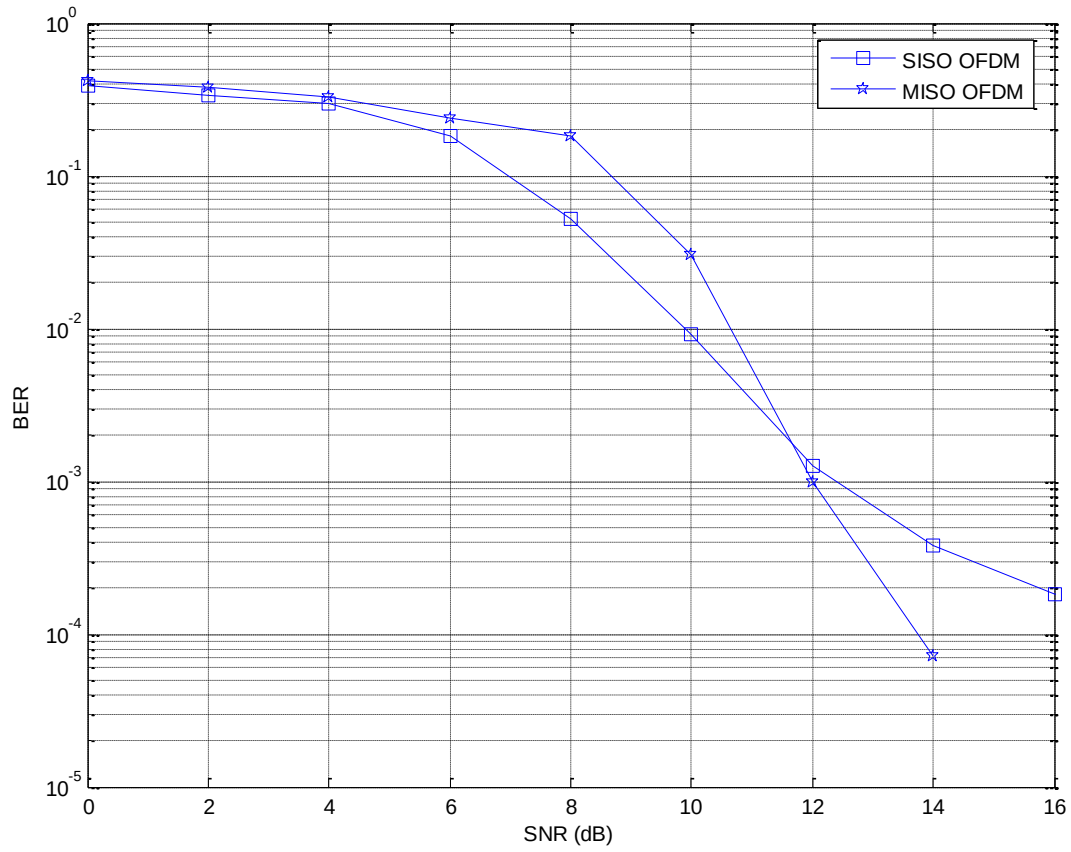

Figure 3-3: BER Performance for SISO and MISO OFDM for a fast fading channel of normalized Doppler frequency fd=0.005.

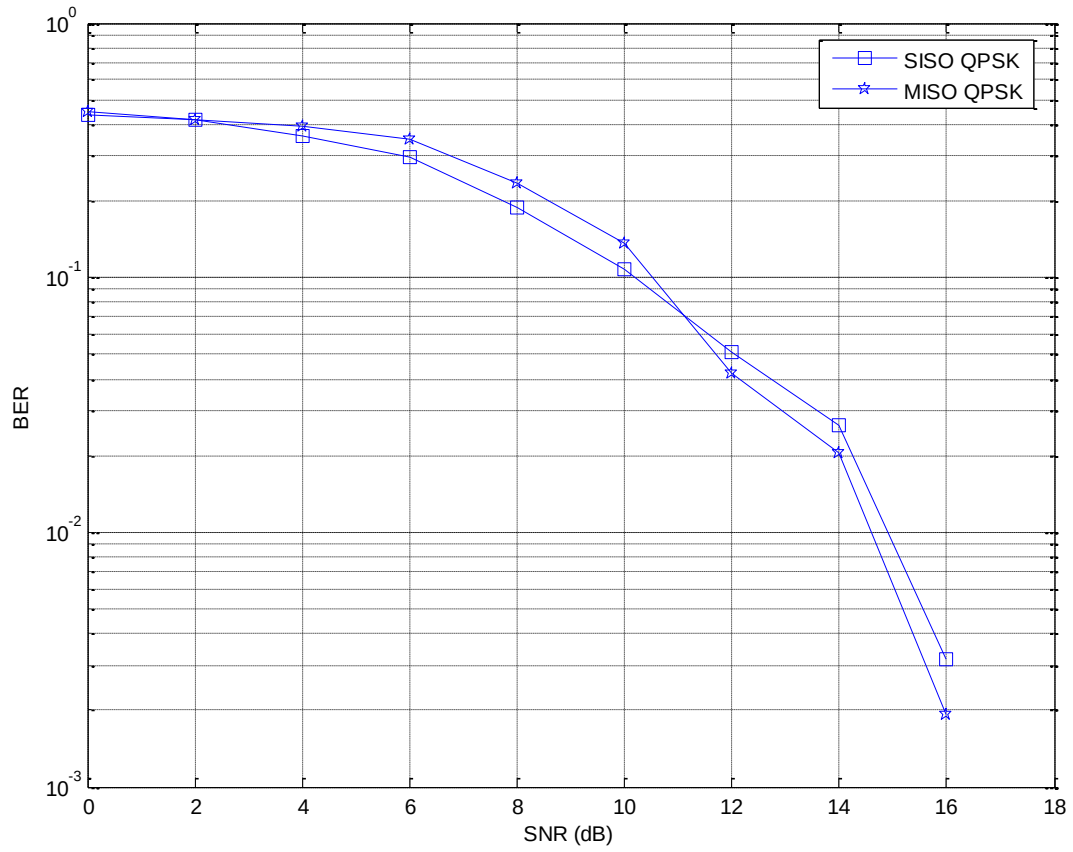

Figure 3-4: BER Performance for SISO and MISO for a slow fading channel of normalized Doppler frequency fd=0.002.

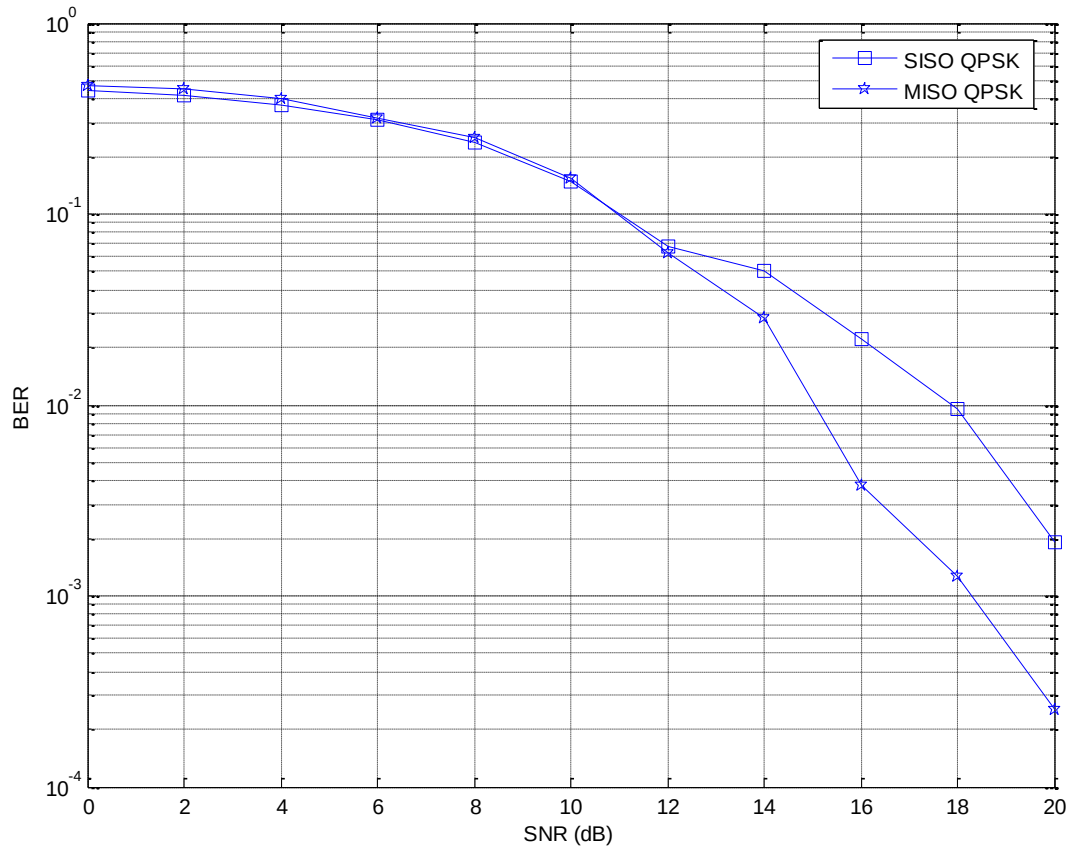

Figure 3-5: BER Performance for SISO and MISO for a slow fading channel of normalized Doppler frequency fd=0.005.

3.5 Conclusion

In this chapter a background of OFDM communication systems was presented. Implementation aspects of the communication system such as modulation and demodulation of subcarriers using the IFFT and FFT were discussed. Simulations of SISO and MISO OFDM for slow and fast fading channels were presented. Simulation of a single carrier communication system was also performed and results were given. The results showed that OFDM outperforms single carrier systems.

Chapter 4

4 Implementation Issues

The block diagram of a MISO OFDM Communication system is given in Figure 4-1. The hardware and software design to implement the communication system will be presented in this chapter. The hardware completed the platform for the testbed on which channel estimation algorithms were implemented.

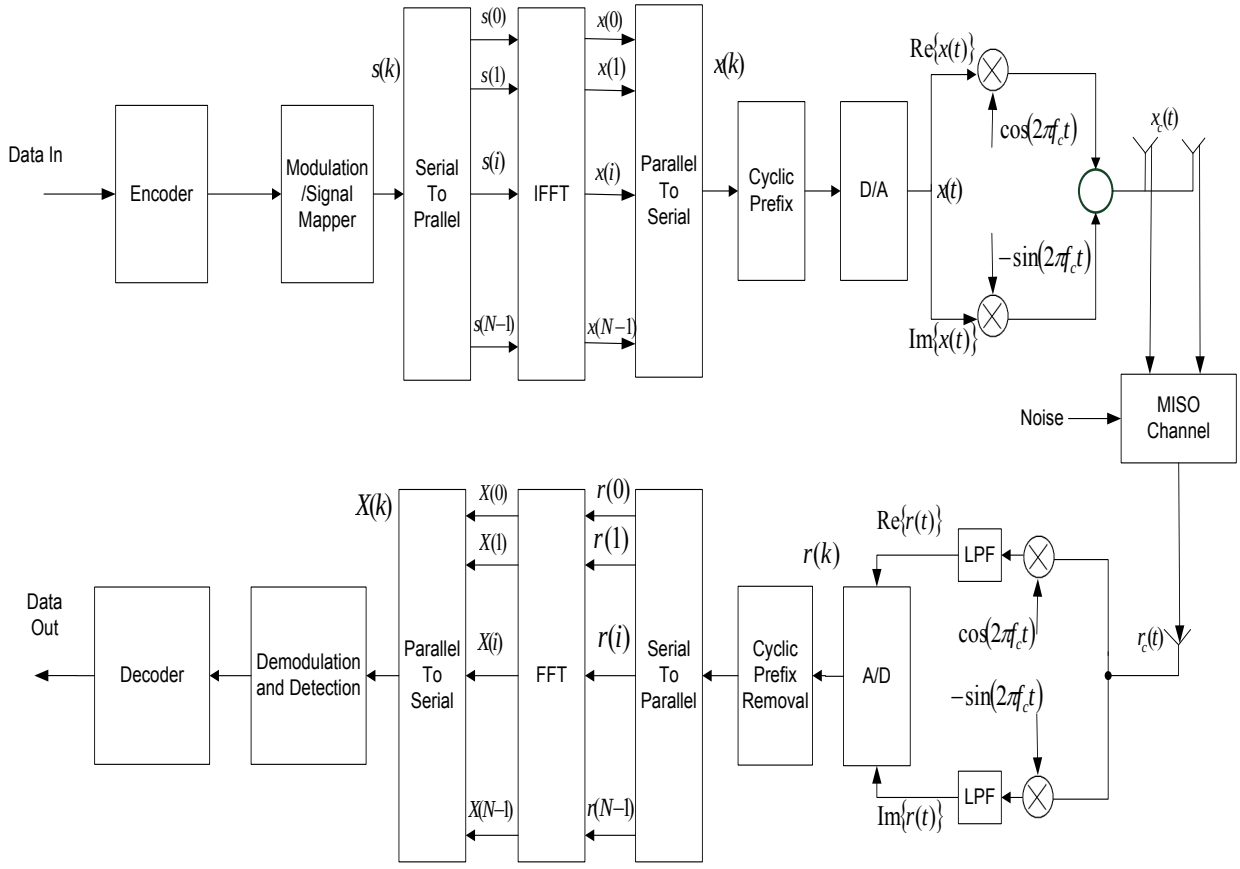

Figure 4-1: MISO OFDM Communication System

4.1 Hardware Implementation

4.1.1 Processing Units

The chosen processing units for the test bed was the TMS320C6416 DSP from Texas Instruments which comes as part of a DSP kit from Spectrum Digital. The processor operates at a frequency of 1 GHz. It contains hardware modules such as a Viterbi Decoder and a Turbo Decoder which reduces the software demand for decoding.

Choosing this DSP allowed the project to be implementable within the specified time for Masters degree. Software development takes much less development time than hardware development via FPGAs [12]. The DSP is also cheap and allows the implementation to be flexible.

The DSP at the transmitter would be responsible for implementing channel encoding, IFFT and interfacing with an external digital to analogue converter (DAC). The receiver's DSP would implement synchronization, the FFT, detection, channel estimation, decoding and interfacing with an external ADC.

4.1.2 Data Converters

In order to interface the digital processor with analogue hardware a digital to analogue converter is used at the transmitter and an analogue to digital converter is used at the receiver. In order to properly test and evaluate the real time performance of the developed channel estimation algorithms in an indoor channel, a high signal bandwidth which would be larger or very close to the channel's coherent bandwidth, had to be used so that frequency selective fading can result. In a flat fading channel, where the coherent bandwidth is much larger than the signal bandwidth, channel estimation offers little or no improvement to the system performance because the signal can be properly detected without channel estimation.

The TMSC6416 DSP kit has an on board codec capable of performing analogue to digital conversion and digital analogue conversion. The maximum sampling rate of the codec is 96 kHz. After performing a number of channel measurements in indoor environments, in [13] it was found that the coherence bandwidth in an indoor channel varied from 250 MHz to 20 MHz and a worst case RMS delay spread of 150 ns. It can be concluded that a signal

bandwidth of 96 kHz is too small for it to experience frequency selective fading in an indoor channel. Thus it would be difficult to evaluate the performance improvement of a communication system with channel estimation if the performance is just as good without the use of a channel estimation algorithm. The purpose of channel estimation is to correct the degradation of the transmitted signal caused by a dispersive channel, thus if the channel is not dispersive the use of channel estimation is redundant.

The above argument pushed the design of the testbed to make use of data converters with high sampling rate. A high signal bandwidth also allows the system to have a higher data throughput which is an added benefit. The chosen ADCs and DACs were Maxim's MAX19517 and MAX5878 respectively. The ADC and the DAC have maximum sampling rates of 130 Msps and 250 Msps respectively with resolutions of 14-bit and 10 bit respectively.

The data converters both have a parallel data interface. It allows them to operate at high speeds because the information to be converted to digital (for the ADC) or analogue (for the DAC) is presented or obtained in one clock cycle instead of several clock cycles as in the case of a data converter with a serial interface. The external memory interface module (EMIF) on the TMS320C6416 DSP was used to interface with the ADC and the DAC.

The daughter card header on the DSP kit consists of 32 bit address and data pins which allow 32 bit external devices to exchange 32 bit data between memory addresses on the DSP and the external devices. Additional hardware was designed to allow the EMIF to control 2 DACs at the transmitter and 2 ADCs at the receiver so that a full 2 by 2 MIMO communication system could be implemented but only one ADC would be used at the receiver since in this project only a MISO system was to be implemented. To illustrate how the hardware interface between the DSP kit and the ADC and the DAC was arranged, the relevant modules of the testbed design are given in Figure 4-2. The ADC and the DAC interface circuit boards are different because the MAX19517 and MAX5878 evaluation kit boards have different interface headers.

The EMIF module on the DSP also provides the sampling clock to synchronize the ADC or the DAC with the DSP and also control the sampling rate. The highest EMIF clock is 125 MHz which when used as the sampling clock will yield a signal with a significantly high bandwidth from the DAC which is in the range of the coherence bandwidth.

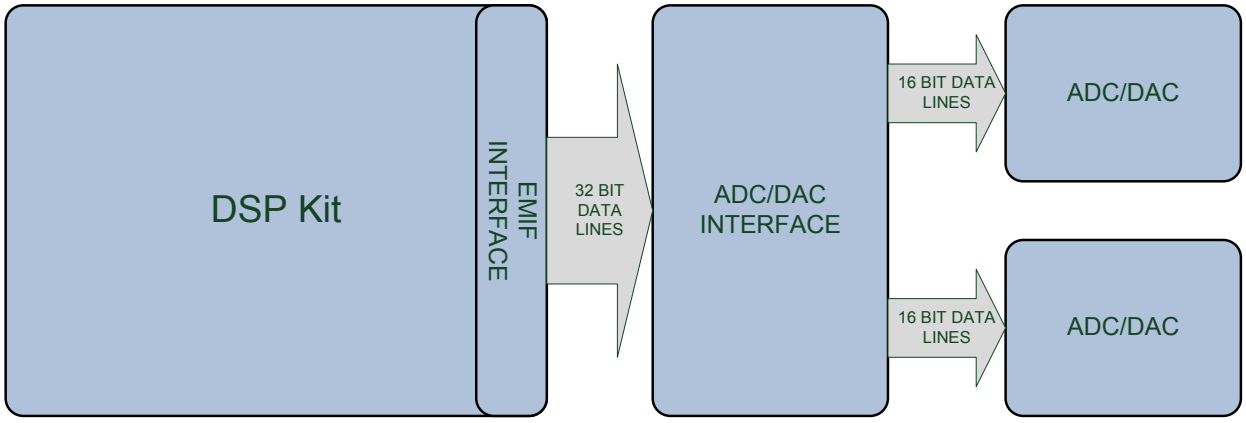

Figure 4-2: ADC and DAC interface with the DSP kit.

The ADC and the DAC both can perform in-phase and quadrature data conversion simultaneously which allows the DSP to provide complex signals to be modulated to a higher frequency at the transmitter and process complex signals at the receiver from the ADC.

4.1.3 RF Stage Hardware

The base band in-phase and quadrature signals from the DAC at the transmitter had to be modulated to an RF frequency for indoor wireless transmission. At the receiver, the received RF signal had to be demodulated back to base band and sampled by the ADC. The operating frequency used for the project was 2.4 GHz. The devices used for RF modulation and demodulation were the TRF3702 and the TR371125 evaluation modules from Texas Instruments respectively. The basic functions of the modulator and demodulator are illustrated in Figure 4-3.

The local oscillator used for the project was the MAX2750EVK which is an evaluation kit from Maxim for the MAX2750 voltage controlled oscillator (VCO). The alternative was to design and build a hardware phase lock loop (PLL) that would perform carrier recovery and synchronize the transmitter and the receiver carriers so that the RF transmitted signal can be properly demodulated.

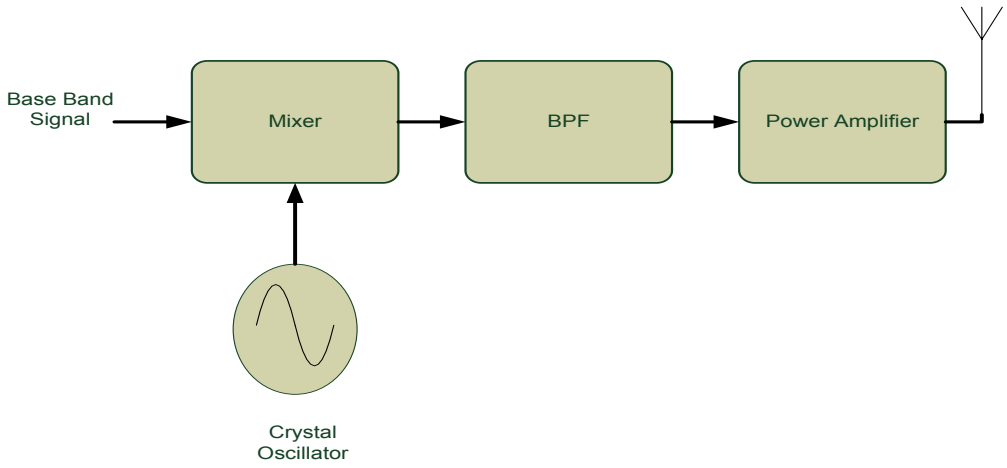

(a)

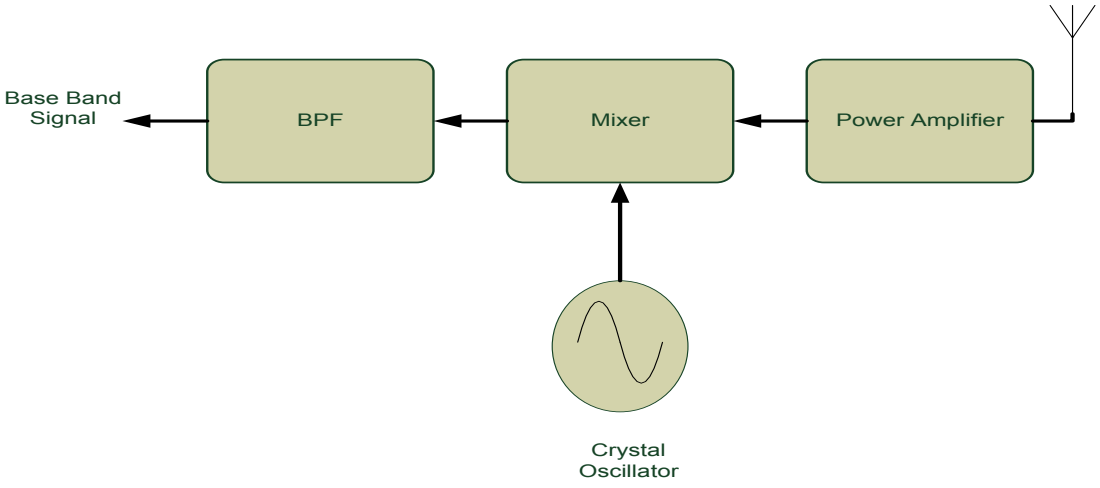

(b)

Figure 4-3: RF hardware functionality (a) modulator (b) demodulator

The TRF371125 demodulator has a bandwidth of 30 MHz. In order to accommodate this restriction the maximum subcarrier frequency was limited to this frequency. With the FFT size equal to the number of subcarriers, the sampling frequency would have to be reduced to ¼ of the maximum EMIF clock frequency which is 31.25 MHz. The transmitter's and the receiver's hardware is given in Figure 4-4.

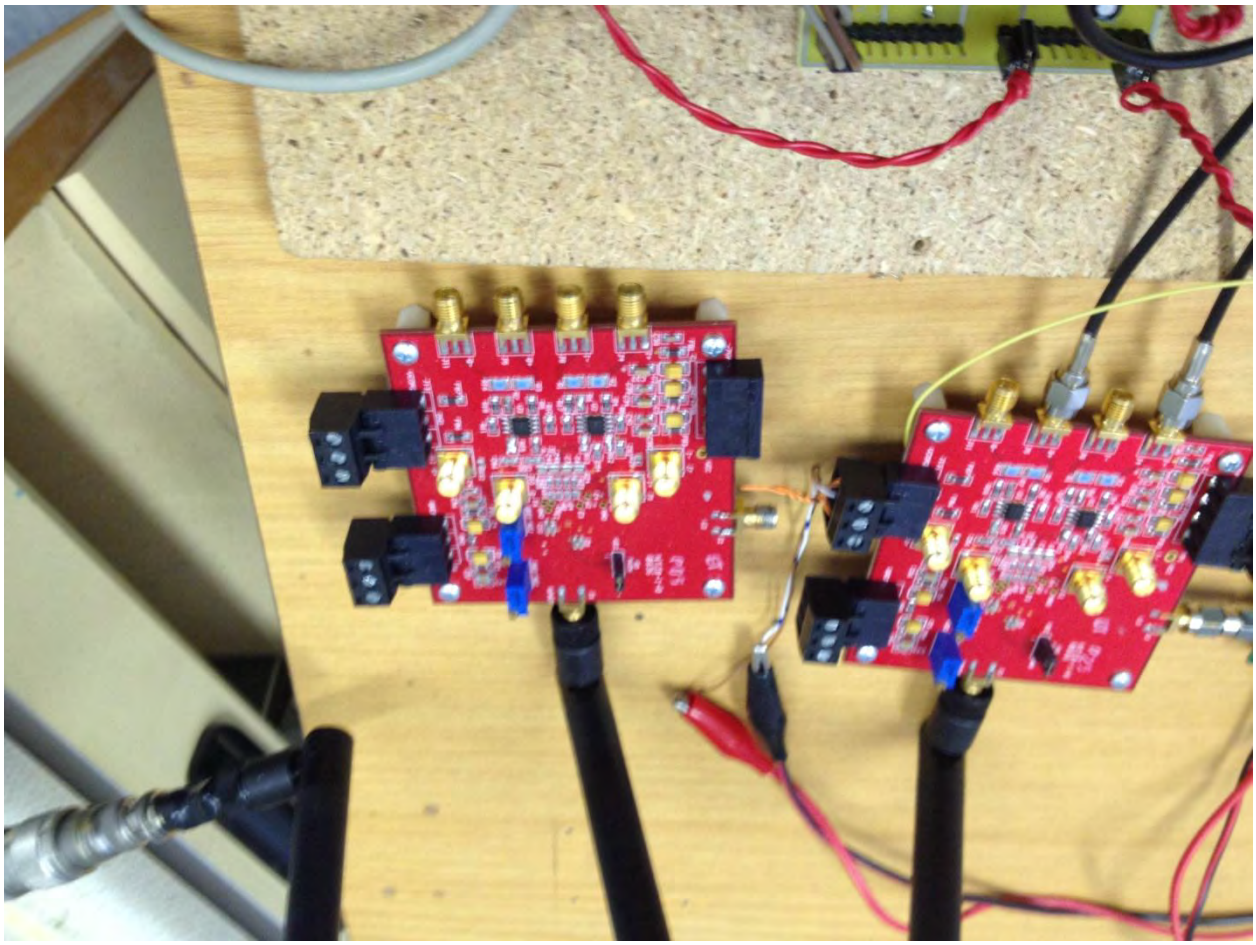

(a)

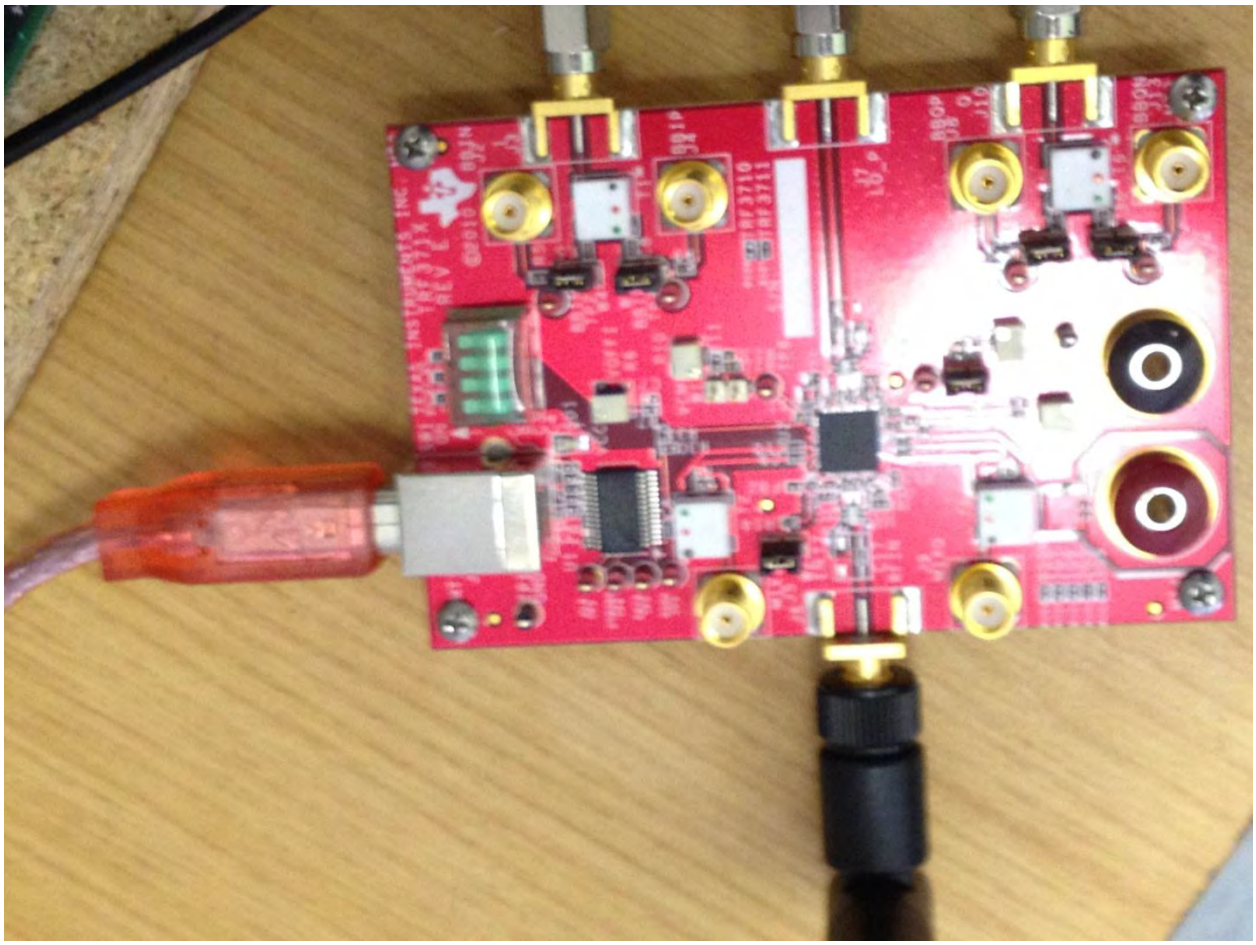

(b)

Figure 4-4: Testbed hardware (a) Transmitter modulator (b) Receiver demodulator

4.2 Synchronization

In synchronous communication systems, symbol, frame and carrier synchronization is vital in order to recover the transmitted information adequately. In OFDM, synchronization is even more important in order to keep the subcarriers orthogonal and avoid inter-carrier interference. Conventional OFDM synchronization methods use the peak of an auto-correlated received signal which consists of repeated parts. The peak of the auto-correlated signal is the sample index where symbol synchronization will be achieved.

The methods investigated for achieving synchronization in OFDM systems used symbols with repeated parts and another used cyclic prefix. The method where a symbol with repeated parts is used for synchronization was developed in [14]. The symbol consisted of 2 repeated parts where the peak of its auto-correlation function indicated the optimum symbol timing position. In [3] the repeated parts within the OFDM training symbol is increased in multiples of 2 and by making them have different signs they achieved a steeper timing metric trajectory which gives more accurate timing approximation. In [15] an OFDM timing method that exploits the cyclic nature of the cyclic prefix to obtain an adequate timing metric that estimates the optimum timing instant is presented.

4.2.1 Synchronization Using 2 Repeated Parts

A symbol with 2 identical parts in the time domain of equal length is shown in Figure 4-5. The corresponding samples of the 2 parts only differ in phase due to the frequency offset of the receiver's carrier with respect to the transmitter. The product of the samples in the first half and the complex conjugate of the corresponding samples in the second half will cancel out the channel effects and the result will have a phase given by [10],

$$\phi = \pi T \Delta f, \tag{4-1}$$

where T is the OFDM symbol period and Δf is the frequency offset. Let the received signal be given by [3]

$$r(k) = \exp(j\xi) \exp\left(\frac{j2\pi\Delta f}{N}\right) \sum_{m=0}^{K-1} h_m s(k-\tau_m) + n(k)\,, \tag{4-2}$$

where $s(k)$ is the transmitted OFDM signal, $n(k)$ is the zero mean AWGN with variance $N_0/2$, N_0 is the noise power, ξ is the carrier phase, h_m is the m^{th} channel impulse response tap with delay τ_m. The 2 repeated parts have equal length which is M=N/2. The timing metric is calculated as

$$\Lambda(d) = \frac{|P(d)|^2}{E(d)^2} \qquad 4\text{-}3$$

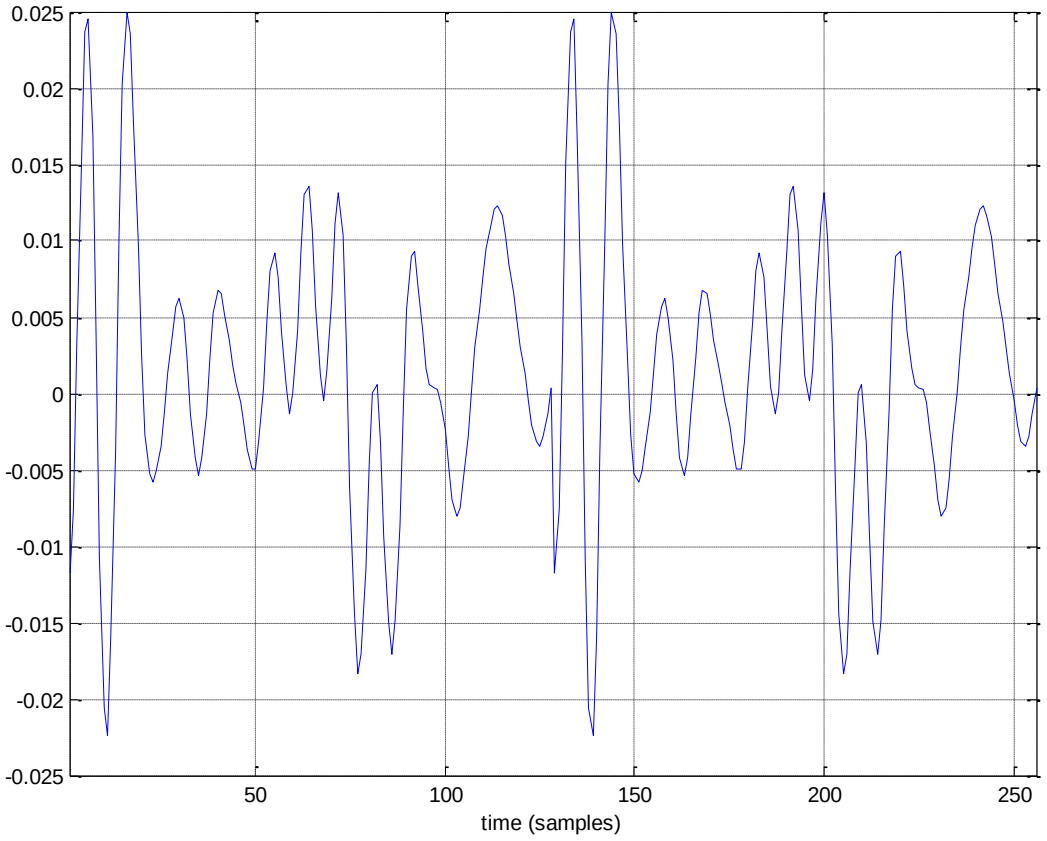

Figure 4-5: OFDM symbol with repeated parts.

where

$$P(d) = \sum_{k=0}^{M-1} r(d+k)r^*(d+M+k), \qquad 4\text{-}4$$

and

$$E(d) = \sum_{k=0}^{M-1} |r(d+M+k|^2. \qquad 4\text{-}5$$

The timing estimate is obtained with

$$\hat{\theta} = argmax(\Lambda(d)) . \qquad 4\text{-}6$$

The phase difference between the 2 repeated parts is calculated at the optimal timing instant from $P(d)$:

$$\hat{\phi} = angle(P(d)|_{d=\hat{\theta}}\,.$$

4-7

If $\hat{\phi}$ is restricted to the interval [-π, π] the frequency offset is given by

$$\Delta f = \hat{\phi}/\pi T\,.$$

4-8

The frequency offset obtained from (4-8) can only be as large as one subcarrier spacing. In order to detect larger frequency offsets a 2nd training symbol must be transmitted. The 2nd training symbol contains a pseudo-random (PN) sequence on odd subcarrier frequencies to measure the subchannels and another on even subcarrier frequencies to determine the frequency offset. The frequency offset obtained from (4-8) is used to partially correct the frequency offset of the 2 training symbols in order to reduce adjacent carrier interference by multiplying them with $exp(-j\hat{\phi}t/T)$. Let the FFT of the 2 training symbols be $X_1(k)$ and $X_2(k)$ respectively. Let the PN sequence on the even subcarrier frequencies be $v_1(k)$. The actual frequency offset is given by

$$\Delta f = \frac{\phi}{\pi T} + \frac{2z}{T}.$$

4-9

The estimate for z is obtained from the metric given by

$$B(z) = \frac{\left|\Sigma_{k\epsilon\chi} X_1^*(k+2z)v_1^*(k)X_2(k+2z)\right|^2}{2\left(\Sigma_{k\epsilon\chi}|X_2(k)|^2\right)^2}$$

4-10

where χ is the indices of even frequencies. The optimal index $\hat{z}$ should maximize $B(z)$.

4.2.2 Synchronization using Cyclic Prefix

In [15] they improve from the above method by using a cyclic prefix to obtain a timing metric. Since the last G samples of the OFDM symbol are placed at the beginning of the symbol as the cyclic prefix of length G, it follows that the OFDM symbol already contains 2 identical parts. In an observation interval of 2N +G of received samples, at least one full OFDM frame should have been captured.

The observation interval is shown in Figure 4-6 where $I \triangleq [\theta, \theta + G - 1]$ and $I' \triangleq [\theta + N, \theta + N + G - 1]$. I and I' are the intervals for the cyclic prefix and the last G samples of the OFDM symbol respectively given the timing offset θ. During the observation interval

$$E\{r(k)r^*(k+m)\}\begin{cases} \sigma_s^2 + \sigma_n^2, & m = 0 \\ \sigma_s^2 e^{j2\pi\varepsilon}, & m = N \\ 0, & otherwise \end{cases} \qquad 4\text{-}11$$

where $\sigma_s^2 \triangleq E\{|s(k)|^2\}$ and $\sigma_n^2 \triangleq E\{|n(k)|^2\}$ and the remaining samples $k \notin I \cup I'$ are mutually uncorrelated.

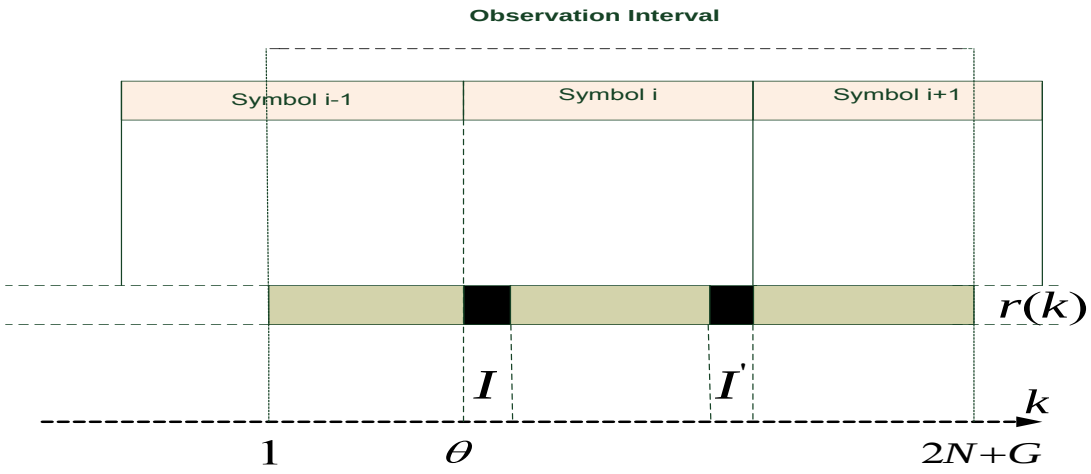

Figure 4-6 Received OFDM symbols with cyclic extension

The log-likelihood function for the timing offset θ and frequency offset ε is the probability density function of observing the 2N+G samples in $\boldsymbol{r}$ given θ and ε and is given by

$$\Lambda(\theta,\varepsilon) = \log f(\boldsymbol{r}|\theta,\varepsilon)$$

4-12

The final result is

$$\Lambda(\theta,\varepsilon) = \sum_{k=0}^{\theta+L-1}\left(2Re\left\{e^{j\pi\varepsilon}r(k)r^*(k+N)\right\} - \rho(|r(k)|^2 + |r(k+N)|^2)\right)$$

4-13

where

$$\rho \triangleq \left|\frac{E\{r(k)r^*(k+N)\}}{\sqrt{E\left\{|r(k)|^2\right\}E\left\{|r(k+N)|^2\right\}}}\right| = \frac{\sigma_s^2}{\sigma_s^2+\sigma_n^2} = \frac{SNR}{SNR+1}$$

4-14

is the correlation coefficient between $r(k)$ and $r(k+N)$. The ML estimation of θ and ε is then given by

$$\hat{\theta} = argmax(\lambda(\theta)),$$

4-15

$$\hat{\varepsilon} = -\frac{1}{2\pi}\gamma(\theta)|_{\theta=\hat{\theta}},$$

4-16

where

$$\lambda(\theta) = 2\left|\sum_{k=\theta}^{\theta+G-1} r(k)r^*(k+N)\right| - \rho\sum_{k=\theta}^{\theta+G-1}(|r(k)|^2 + |r(k+N)|^2)$$

4-17

and

$$\gamma(\theta) = \angle \sum_{k=\theta}^{\theta+G-1} r(k)r^*(k+N)\,.$$

4-18

If θ and ε are constant for several OFDM symbol periods then the observation of the OFDM signal can be extended to M frames and the log-likelihood function for θ and ε becomes

$$\Lambda(\theta,\varepsilon) \;=\; \frac{1}{M} \sum_{m=0}^{M-1} \;\Lambda_{\mathrm{m}}(\theta,\varepsilon)$$

4-19

where Λ_{m} is the log-likelihood for the m$^{\mathrm{th}}$ frame and therefore $\Lambda(\theta,\varepsilon)$ is averaged over M frames.

4.2.3 Synchronization using Multiple Repeated Parts

In [3] they improve on the method developed in [14] by using multiple repeated parts. The more repeated parts used, the steeper the timing trajectory. They developed a normalized timing metric given by

$$\Lambda_n(d) = \left(\frac{L}{L-1}\frac{|P(d)|}{E(d)}\right)^2,$$

4-20

where

$$E(d) = \sum_{l=0}^{L-1} \sum_{k=0}^{M-1} |r(d + lM + k)|^2,$$

4-21

$$P(d) = \sum_{l=0}^{L-2} b(l) \sum_{k=0}^{M-1} r(d + (l+1)M + k)\, r^*(d + lM + k) \quad ,$$

4-22

and L is the number of repeated parts and M=N/L. The vector $b(l)$ is given by

$$b(l) = p(l)p(l+1)\,,$$

4-23

where $p(l)$ is the sign pattern of the identical parts. Using different signs for the repeated parts yields a steeper timing trajectory. The steeper the timing trajectory, the more accurate the timing estimate will be in the presence of noise and channel dispersion. For an L=4 training symbol, the timing pattern that yields very steep timing trajectories was obtained to be [3]

$$p(l) = \begin{cases} - + - - \\ + + + - \\ + - + + \\ - - - + \end{cases}$$

4-24

Once the timing estimate is obtained the frequency offset is calculated by

$$\Delta\hat{f} = \frac{L}{2\pi}\sum_{m=0}^{D} w(m)\varphi(m) \qquad 4\text{-}25$$

where

$$w(m) = 3\frac{(L-m)(L-m+1)-H(L-H)}{H(4H^2-6LH+3L^2-1)} \qquad 4\text{-}26$$

$$\varphi(m) = \left[\arg\{R_y(m)\} - arg\{R_y(m-1)\}\right]_{2\pi}, 1 \le m \le H\ , \qquad 4\text{-}27$$

$$R_y = \frac{1}{N-mM}\sum_{k=mM}^{N-1} y^*(k-mM)y(k), 0 \le m \le H\ , \qquad 4\text{-}28$$

and $[x]_{2\pi}$ denotes modulo 2π, which restricts the argument to [$-\pi, \pi$]. The parameter H is a design parameter which should be less than or equal to $L-1$ whose optimal value is $L/2$. By using L repeated parts the frequency offset can be determined using one training symbol up to a value of $\pm L/2$ subcarrier spacings. L is the training pattern size and so each repeated part can have k identical subparts. This increases the frequency offset estimation range to $\pm kL/2$ subcarrier spacings.

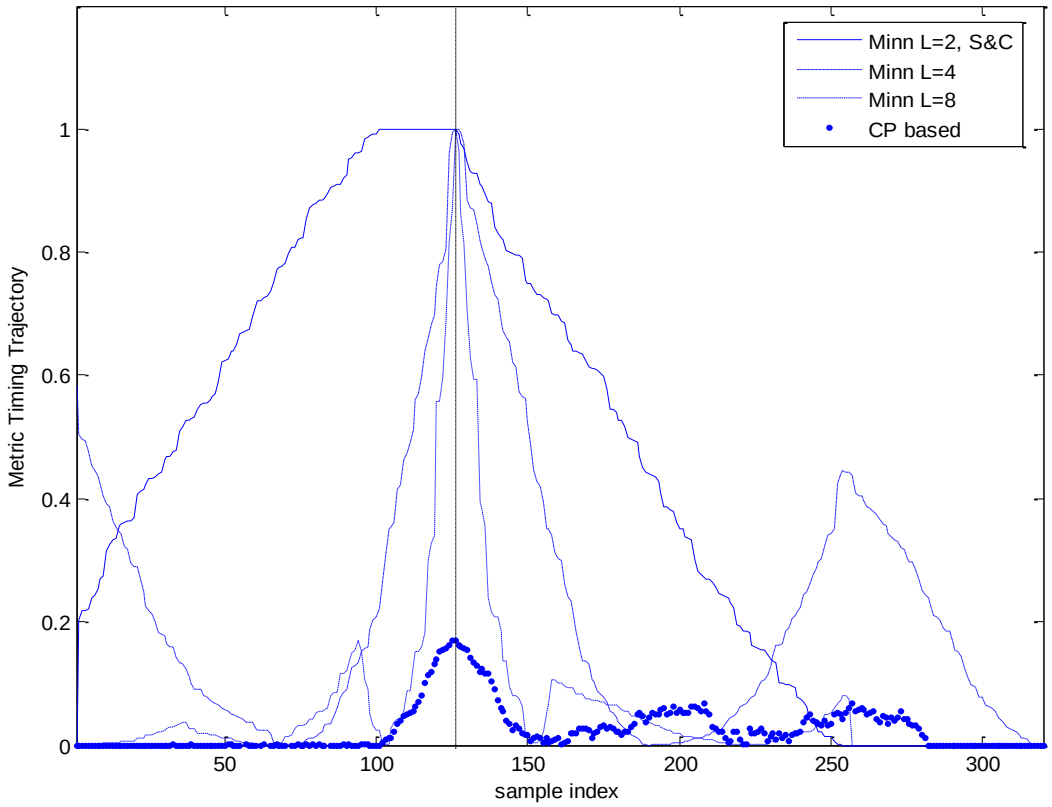

Figure 4-7: Timing metric trajectories for the different methods

The discussed symbol timing methods' trajectories are compared in Figure 4-7. A length 256 symbol sample size was used with a cyclic prefix of 25 samples and the timing delay was 100 samples. The timing position is thus at 125 samples from where sampling began since this is where the information (after cyclic prefix removal) starts. It can be seen from the Figure that the method proposed by H. Minn in [3] yields a better timing metric trajectory than S&C [14], by using multiple repeated parts with different signs instead of just 2 as proposed by S&C. Using the cyclic prefix also produces an excellent timing trajectory which performs as good as H. Minn's method when 8 repeated parts are used.

4.2.4 Fine Symbol Timing Synchronization

Since the OFDM symbols are transmitted over a wireless dispersive channel, the actual timing instant is delayed by the channel and in order to account for the channel effects , channel estimation needs to be performed to determine the channel impulse response's first tap's position [3]. After the channel impulse response's first tap's position is determined, the

approximated timing instant can be refined and hence the frequency offset. Following [3], the calculated coarse timing instant is pre-advanced by some samples such that

$$\theta_c = d_{max} - \lambda_c.$$

4-29

The received signal is given by

$$\mathbf{r}(0) = e^{j\xi}\mathbf{W}(\Delta f)\mathbf{S}\mathbf{h} + \mathbf{n}$$

4-30

where

$$\mathbf{r}(0) \triangleq [r(0), r(1), \dots, r(N-1)]^T \ ,$$

4-31

$$\mathbf{h} \triangleq [h_0, h_1, \dots, h_{K-1}]^T \ ,$$

4-32

$$\mathbf{W}(\Delta f) \triangleq diag\{1, e^{j2\pi\Delta f/N}, \dots, e^{j2\pi\Delta f(N-1)/N}\} \ ,$$

4-33

$$\mathbf{n} \triangleq [n(0), n(1), \dots, n(N-1)]^T \ ,$$

4-34

$$\mathbf{S} \triangleq \begin{bmatrix} s(0) & s(-1) & \cdots & s(-K+1) \\ s(1) & s(0) & \dots & s(-K+2) \\ \vdots & \vdots & \ddots & \vdots \\ s(N-1) & s(N-2) & \cdots & s(N-K) \end{bmatrix}.$$

4-35

The factor $e^{j\xi}$ is the phase error factor and s(k) is the known transmitted training symbol which includes the cyclic prefix. After frequency synchronization has been achieved, the frequency offset in **r** is corrected and the channel impulse response is then estimated by

$$\hat{\mathbf{h}} = [\mathbf{S}^H\mathbf{S}]^{-1}\mathbf{S}^H\mathbf{W}^H(\Delta\hat{f})\mathbf{r}(\theta_c) \tag{4-36}$$

where $(.)^H$ is the Hermitian transpose and $(.)^{-1}$ is the matrix inverse. The position of the strongest channel tap is the amount of delay caused by the channel on the transmitted signal. The strongest channel tap is given by

$$\hat{h}_{max} = max\{\hat{h}_i : i = 0,1, \ldots . K' + 1\} \tag{4-37}$$

where K' is the designed channel length estimate. The index of the strongest channel tap is given by

$$\hat{\tau}_0 = arg\ \max_l\{E_h(l) : l = 0,1, \ldots K' - K''\} \tag{4-38}$$

where

$$E_h(l) = \begin{cases} \sum_{k=0}^{K''-1}\left|\hat{h}_{l+k}\right|^2, \text{if } \hat{h}_l > \eta.\left|\hat{h}_{max}\right| \\ 0, \qquad\qquad otherwise \end{cases} \tag{4-39}$$

which is the channel energy estimate obtained from a K'' window starting from tap l. The parameter η for adjusting the threshold when calculating $E_h(l)$ since in some cases noise may be mistaken for a channel tap. The designed channel estimate has K' taps and the designed maximum channel delay spread is K'', the range of the starting tap index of the energy window is $0 \le l \le K' - K''$. The fine timing estimate is given by

$$\hat{\theta} = d_{max} - \lambda_c + \hat{\tau}_0$$

4-40

The fine timing estimate yields a better estimate of the symbol start timing instant. The drawback of using this method from [3] is that the channel delay spread has to be known *a priori* in order to design matrix S, which depends on K, appropriately. Another drawback is the computation cost which is incurred from applying (4-36), which includes matrix inversion, in order to obtain the estimate of the channel impulse response.

Looking at (4-36), the multiplications of $\mathbf{S}^H$ with $\mathbf{W}^H(\Delta\hat{f})\mathbf{r}(\theta_c)$ is simply a length K cross correlation of the known pilot repeated symbol s(k) with the frequency offset compensated received signal. Using cross correlation to achieve fine symbol timing was also used in various literatures such as in [16].

4.2.5 Fine Frequency Estimation

In [3] fine frequency estimation is achieved by calculating the maximum likelihood (ML) of the metric given by

$$\Lambda(\hat{\theta}; \Delta\tilde{f}) = \mathbf{r}^H(\hat{\theta})\mathbf{W}(\Delta\tilde{f})\mathbf{B}\mathbf{W}^H(\Delta\tilde{f})\mathbf{r}(\hat{\theta}),$$

4-41

where

$$\mathbf{B} = \mathbf{S}[\mathbf{S}^H\mathbf{S}]^{-1}\mathbf{S}^H .$$

4-42

and the parameter $\Delta\tilde{f}$ is varied from $\Delta\hat{f} - \mathrm{F}$ to $\Delta\hat{f} + \mathrm{F}$, in steps of $\Delta = \mathrm{F/J}$ subcarrier spacings, in order to find $\Delta\check{f}$ which will maximize the metric. Hence

$$\Delta\check{f} = \arg\max_{\Delta\tilde{f}} \{\Lambda(\hat{\theta}; \Delta\tilde{f}) : \Delta\hat{f} - \mathrm{F} \leq \Delta\tilde{f} \leq \Delta\hat{f} + \mathrm{F}\} .$$

4-43

The parameter J is chosen to set the step size resolution of Δ; a larger value of J results in a smaller Δ and more resolution and more trial points to evaluate the metric $\Lambda(\hat{\theta};\Delta\tilde{f})$. Variations of fine frequency synchronization exist but most are based on correlating a known training sequence $s(\mathrm{k})$ with the received sequence $r(\mathrm{k})$ and then calculating the frequency that maximizes the correlation as in (4-41).

4.2.6 Chosen synchronization scheme

OFDM synchronization using a training symbol with repeated parts can be implemented in the time domain or frequency domain. When using frequency domain training symbol, the subcarrier modulation pattern is repeated every N/L subcarriers. When using a time domain training symbol, the time domain samples are repeated every N/L samples with the relevant sign pattern. In [3] it was discovered that time domain synchronization yields better performance which results in no need for fine frequency synchronization.

In the testbed, the OFDM synchronization scheme from [3] was used with L=8 repeated parts. This was to improve the timing trajectory steepness as discussed in the above paragraph. Each repeated part also contained 2 repeated parts with the same sign. This was to improve the frequency offset estimation range, as discussed in Section 4.2.3, to $\pm kL/2 = \pm(2\times 8)/2 = \pm 8$ subcarrier spacings. The synchronization signal's pattern used was $(+\ +\ -\ -\ +\ -\ -\ -)$ which is shown in Figure 4-8. This pattern yields a steep timing metric trajectory and was presented by [3].

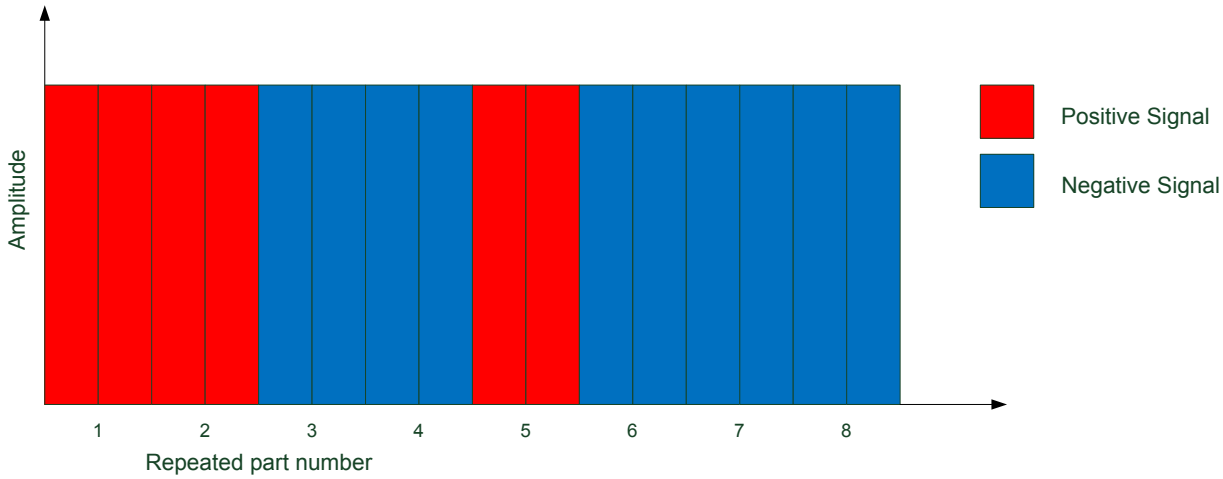

Figure 4-8: Synchronization symbol pattern.

Time domain synchronization was used which means that the repeated parts are implemented in the time domain and equations (4-21) and (4-22) are implemented using a time domain $r(k)$. The synchronization equations presented previously had to be modified in order to reduce their complexity when they are implemented on a DSP.

In the first symbol period the N complex samples of the received signal $r(k)$ are loaded into a buffer which is going to be denoted $r_B(k)$ here. Hence

$$r_B(k) = r(k).$$

4-44

In the second symbol period, the N complex samples of $r(k)$ are loaded in a buffer $r_B(k)$ after the first N complex symbols of $r(k)$ that were loaded during the first symbol period. Hence during the 2nd symbol period

$$r_B(k+N) = r(k).$$

4-45

From the 3rd symbol period onwards the 2nd N complex samples in $r_B(k)$ replace the 1st N complex samples. The 2nd complex samples in $r_B(k)$ are replaced with the new complex samples of $r(k)$ from the current symbol period. Hence from the 3rd symbol period onwards,

$$r_B(k) = r_B(k+N),$$

4-46

$$r_B(k+N) = r(k).$$

4-47

The signal buffering process for synchronization is illustrated in Figure 4-9.

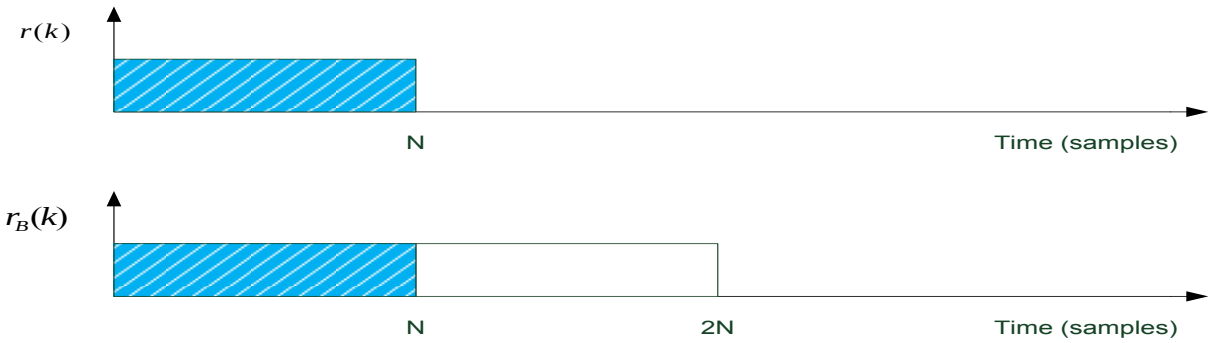
r(k)
N
Time (samples)
$r_B(k)$
N
2N
Time (samples)

(a)

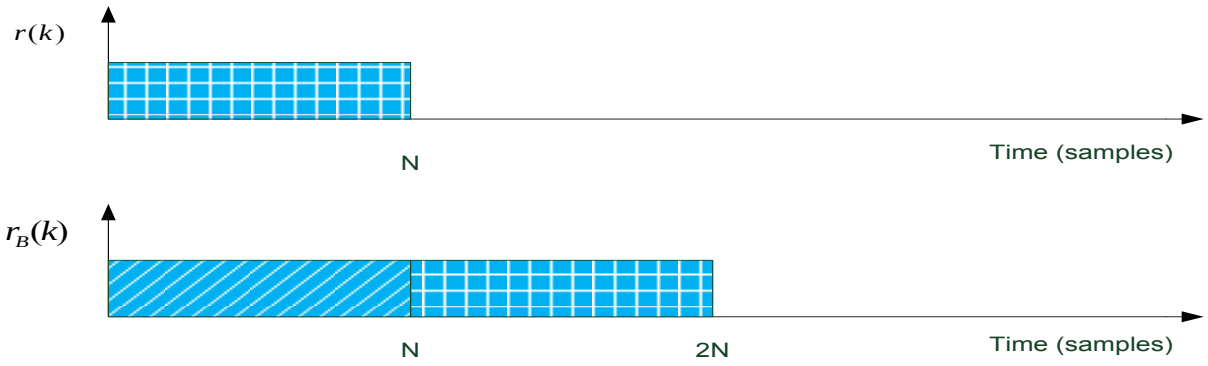
r(k)
N
Time (samples)
$r_B(k)$
N
2N
Time (samples)

(b)

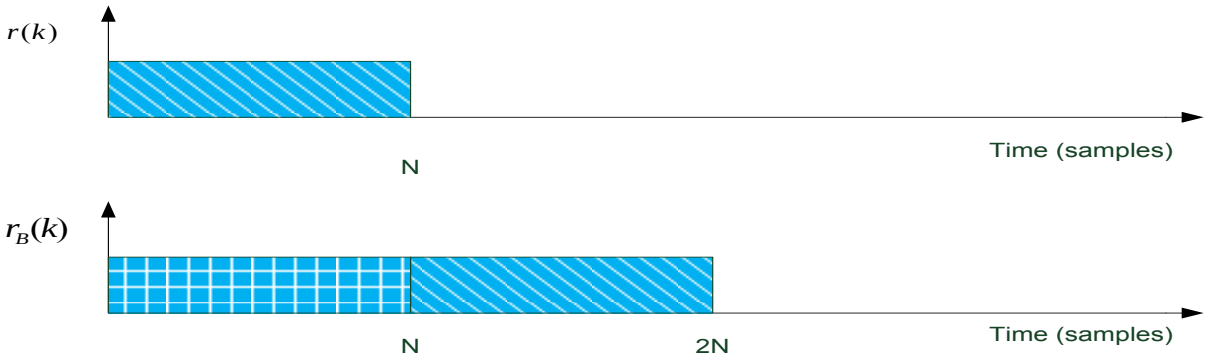
r(k)
N
Time (samples)
$r_B(k)$
N
2N
Time (samples)

(c)

Figure 4-9: Signal buffering for synchronization (a) 1st symbol period (b) 2nd symbol period (c) subsequent symbol periods.

In equations (4-21) and (4-22), for each value of d, N multiplications have to be performed to calculate $P(d)$ and $E(d)$. With the value of d varying from 0 to N-1, this implies that there will be N^2 multiplication in total. In order to reduce the complexity of $P(d)$, a variable $sumP(k)$ was introduced which is defined as

$$sumP(k) = sumP(k-1) + r\big((l+1)k_{sub}M + k\big)r^*(lk_{sub}M + k),$$

$$0 \le k \le 2N, 0 \le l \le \mathrm{L} - 2;$$

4-48

where k_{sub} is the number of sub repeated parts within a the main repeated parts which increase the frequency offset detection range and $M = N/(k_{sub}L)$. Using a length 2N window to calculate $P(d)$ and $E(d)$ and also $r_B(k)$ to store the most recent 2N complex samples, $sumP(k)$ is further defined as

$$sumP(k) = sumP(k-1) + r_B(k)r_B^*(k + k_{sub}M),$$

4-49

for the first two symbol periods and

$$sumP(k) = sumP(N - k_{sub}M + k),$$

4-50

$$sumP(N - k_{sub}M + k) = sumP(N - k_{sub}M + k - 1) + r_B(k)r_B^*(k + k_{sub}M),$$

4-51

for subsequent symbol periods. To develop a recursive implementation of $P(d)$, we use (4-22) and write

$$P(0) = \sum_{l=0}^{L-2} b(l) \sum_{k=0}^{M-1} r((l+1)M + k)\, r^*(lM + k)$$

$$= b(0)\sum_{k=0}^{M-1} r(M+k)\,r^*(k) \;\; + b(1)\sum_{k=0}^{M-1} r(2M+k)\,r^*(M+k)$$

$$+ b(2)\sum_{k=0}^{M-1} r(3M+k)\,r^*(2M+k) \; + \sum_{l=3}^{L-2} b(l)\sum_{k=0}^{M-1} r((l+1)M+k)\,r^*(lM+k)$$

$$= b(0)sumP(M-1) + b(1)[sumP(2M-1) - sumP(M-1)]$$

$$+ b(2)[sumP(3M-1) - sumP(2M-1)] + \sum_{l=3}^{L-2} b(l) \; \sum_{k=0}^{M-1} r((l+1)M + k)\,r^*(lM+k)$$

$$= \sum_{l=0}^{L-2} b(l)\,[sumP((l+1)M-1) - sumP(lM-1)]$$

4-52

where

$$sumP\big((l+1)M-1\big) = sumP(lM-1) + \sum_{k=0}^{M-1} r((l+1)M+k)\,r^*(lM+k)$$

4-53

$$P(1) = \sum_{l=0}^{L-2} b(l)\sum_{k=0}^{M-1} r\big((l+1)M+k+1\big)\,r^*(lM+k+1)$$

$$= \sum_{l=0}^{L-2} b(l)\,[sumP((l+1)M) - sumP(lM)]$$

4-54

In general the new expression for $P(d)$ is given by

$$P(d) = \sum_{l=0}^{L-2} b(l)\left[sumP\big((l+1)k_{sub}M + d\big) - sumP(lk_{sub}M + d)\right]$$

4-55

Now only N multiplications are needed to calculate $P(d)$ but a delay of N complex samples will be endured. In a similar way $sumE(k)$ and $sumR(m,k)$ are introduced to reduce the calculation complexities of $E(d)$ and $R_y(m)$ respectively.

$$sumE(k) = sumE(k-1) + |r_B(k)|^2,$$

4-56

for the 1st 2 symbol periods and

$$sumE(k) = sumE(N + k),$$

4-57

$$sumE(N + k) = sumP(N + k - 1) + |r_B(k)|^2.$$

4-58

for subsequent symbol periods. Then $E(d)$ is calculated by

$$E(d) = sumE[N + d] - sumE[d]$$

4-59

Also $sumR(m, k)$is defined as

$$sumR(m, k) = sumR(m, k - 1) + r_B(k)r_B^*(k + mM), 0 \leq m \leq H + 1$$

4-60

for the 1st 2 symbol periods and

$$sumR(m, k) = sumR(m, N - mM + k),$$

4-61

$$sumR(m, k) = sumR(m, N - mM + k - 1) + r_B(k)r_B^*(k + mM)$$

4-62

for subsequent symbol periods. To help with the derivation of the new definition for $R_y(m)$, a variable $R(m, d)$ is defined and is given by

$$R(m, d) = \sum_{l=0}^{k_{sub}L-m-1} pf(l)pf(l + m)[sumR(m, (l + 1)M + d) - sumR(m, lM + d)]$$

4-63

where $pf(l)$ is derived from $p(l)$ in Section 4.2.3 and defined as

$$pf(2l{:}\,2l+1) = p(l), 0 \le l \le L-1,$$

4-64

and its purpose is to remove the sign pattern from $r(k)$ hence $sumR(m,k)$. Now $R_y(m)$ is given by

$$R_y(m) = \frac{R(m,\hat{\theta})}{N-mM}\ , \qquad 0 \le m \le H+1$$

4-65

where , $\hat{\theta}$ is the estimated optimal timing instant obtained from symbol synchronization. The above $R_y(m)$ can now be used in (4-27) and hence to determine the frequency offset. For fine timing estimation, the factor $[\mathbf{S}^H\mathbf{S}]^{-\mathbf{1}}\mathbf{S}^H$ in equation (4-36) is calculated prior to implementation since at run time the whole equation would consume a lot of time as it involves inversion of an N by N matrix. The result of the calculation is given by

$$\hat{\mathbf{S}} = [\mathbf{S}^H\mathbf{S}]^{-\mathbf{1}}\mathbf{S}^H,$$

4-66

and (4-36) reduces to

$$\hat{\mathbf{h}} = \hat{\mathbf{S}}\mathbf{W}^H\left(\Delta\hat{f}\right)\mathbf{r}(\theta_c)\ .$$

4-67

From Figure 12 in [3], it can be seen that at low signal to noise ratio (SNR) and L=8, there is no difference between the mean square errors (MSE) of the frequency offset after only using coarse frequency offset estimation and after using fine frequency offset estimation. It was then decided to neglect fine frequency estimation to avoid the extra unnecessary computation which doesn't give profound improvement to the frequency estimation.

4.3 Detection

4.3.1 Symbol Detection

QPSK modulation was used in the testbed as in [1] in order to easily compare the performance of the 2 systems. The channel estimation algorithms developed by Dr Oyerinde in [1] make use of soft detected symbols from the detector because they yield better performance than hard decisions from the detector. After performing a FFT on the received signal, the detector demaps the received QPSK symbols by calculating the log-likelihood ratios (LLRs) of the detected bits.

For each QPSK symbol z, the LLRs of the detected bits c_0 and c_1 from the demapper are given by [17]

$$L(c_0|z) = ln\left[\frac{\Pr(c_0=1|z)}{\Pr(c_0=0|z)}\right]$$

$$= ln\left[\frac{\Pr(c_0=1,c_1=0|z) + \Pr(c_0=1,c_1=1|z)}{\Pr(c_0=0,c_1=0|z) + \Pr(c_0=0,c_1=1|z)}\right]. \quad 4\text{-}68$$

The bits c_0 and c_1 are independent of each other, hence

$$\Pr(c_0 = 1, c_1 = 1|z) = \Pr(c_0 = 1)\Pr(c_1 = 1). \quad 4\text{-}69$$

Using Bayes' rule

$$\Pr(A|B)\Pr(B) = \Pr(B|A)\Pr(A) \quad 4\text{-}70$$

which reduces () to

$$L(c_0|z) = L_a(c_0) + ln\left[\frac{\Pr(z|c_0=1,c_1=0)+\Pr(z|c_0=1,c_1=1)\exp(L_a(c_1))}{\Pr(z|c_0=0,c_1=0)+\Pr(z|c_0=0,c_1=1)\exp(L_a(c_1))}\right] \quad 4\text{-}71$$

For the testbed implementation, when using iterative demapping the *a priori* LLRs in (ln) are given by

$$L_a(c_0) = ln\left[\frac{\Pr(c_0=1)}{\Pr(c_0=0)}\right] \quad \text{4-72}$$

for c_0 and

$$L_a(c_1) = ln\left[\frac{\Pr(c_1=1)}{\Pr(c_1=0)}\right], \quad \text{4-73}$$

for c_1. Let $y[k]$ be the transmitted QPSK symbol modulated on to the k[th] OFDM subcarrier, $z[k]$ the received signal, $H[k]$ the channel transfer function and $n[k]$ the channel noise. The error probability density function (pdf) $\Pr(z[\mathrm{k}]|y[\mathrm{k}])$ is given by

$$\Pr(z[k]|y[k]) = \frac{1}{2\pi\sigma^2} exp\left[\frac{1}{2\sigma^2}\|z[k] - H[k]y[k]\|^2\right], \quad \text{4-74}$$

where σ^2 is the variance of the additive white Gaussian noise $n[k]$. Substituting (4-74) in (4-71), the following LLR approximation is obtained [17]

$$L(c_0[k]|z[k]) = L_a(c_0[k]) + \frac{1}{2\sigma^2}(max[D_{10}, D_{11} + 2\sigma^2 L_a(c_1)] - max[D_{00}, D_{01} + 2\sigma^2 L_a(c_1)]) \quad \text{4-75}$$

where

$$D_{c_0c_1} = 2\mathrm{Re}\{z[k]\}(\mathrm{Re}\{H[k]\}\mathrm{Re}\{y[k]\} - \mathrm{Im}\{H[k]\}\mathrm{Im}\{y[k]\}) + 2\mathrm{Im}\{z[k]\}(\mathrm{Re}\{H[k]\}\mathrm{Im}\{y[k]\} + \mathrm{Im}\{H[k]\}\mathrm{Re}\{y[k]\}) \quad \text{4-76}$$

In a similar way $L(c_1[k]|z[k])$ is obtained to be

$$L(c_1[k]|z[k]) = L_a(c_1[k]) + \frac{1}{2\sigma^2}(max[D_{01}, D_{11} + 2\sigma^2 L_a(c_0)] - max[D_{00}, D_{10} + 2\sigma^2 L_a(c_0)]) \quad \text{4-77}$$

For non-iterative demapping, $L_a(c_1[k]) = L_a(c_0[k]) = 0$. This concludes the detection of the QPSK modulated OFDM symbols.

4.4 Channel Estimation

There are 3 types of channel estimation schemes: blind, pilot aided and decision directed [1]. In blind channel estimation, properties of the signal structure and its second and higher order statistics are exploited in order to estimate the channel. In pilot aided channel estimation, known symbols (pilots) are transmitted with the information symbols and the receiver uses the known pilot symbols to estimate the channel. In decision directed channel estimation, decoded information symbols are used to estimate the channel impulse response.

Systems with a transceiver structure, where the transmitter and the receiver both transmit and receive information, can exchange channel state information by re-transmitting signals back and forth. The transmitter can transmit information to the receiver and the receiver can decode the information and transmit it back to the transmitter either in the next symbol period as in time division duplex (TDD) or at a different frequency as in frequency division duplex (FDD).

In blind channel estimation, the convergence of the estimated channel impulse response is slow because large data record is needed to achieve the channel estimation. Blind channel estimation also requires the channel to vary slowly in order for the statistics of the data record to yield a channel estimate that converges to the actual channel impulse response [18]. Pilot aided channel estimation is bandwidth inefficient because it uses up some subcarriers to transmit known symbols which could have been used for information. Decision directed channel estimation uses the communication bandwidth efficiently by relying on the decoded symbols to achieve channel estimation but it can suffer degradation if there errors in the decoded information and the estimated channel can diverge from the true channel over successive estimations. The transceiver method to obtain channel state information (CSI) at the receiver is both bandwidth inefficient and complex because the transmitter has to receive the resent information from the receiver and synchronization has to be maintained.

As can be seen from (4-76), channel estimation is very important for detection. Decision directed channel estimation in [1] starts off with a known pilot symbol being transmitted at first and then in subsequent OFDM symbol periods detected or decoded symbols are re-

mapped and are used as pilots for estimating the channel for the next symbol period. Since pilots are only transmitted once, block type pilot arrangement is used so that the channel state information from all subcarriers is estimated and there would be no bandwidth wastage since in the next symbol periods the pilots are generated by the receiver's detected or decoded data.

Oyerinde presented the following channel estimation algorithm in [1] which is illustrated in Figure 4-10. First the soft bits obtained from the detector are re-mapped to QPSK symbols $\bar{y}[n,k]$ using a soft mapper, where n is the OFDM symbol index and k is the OFDM subcarrier index. The re-mapped OFDM symbols are used together with the raw OFDM received signal $z[n,k]$ from the FFT to calculate the temporary channel transfer function (CTF) $\hat{H}[n]$.

From the temporary channel transfer function, a parametric channel impulse response is determined. From the parametric CIR estimator an adaptive CIR predictor is used to predict the channel conditions for the next OFDM symbol period.

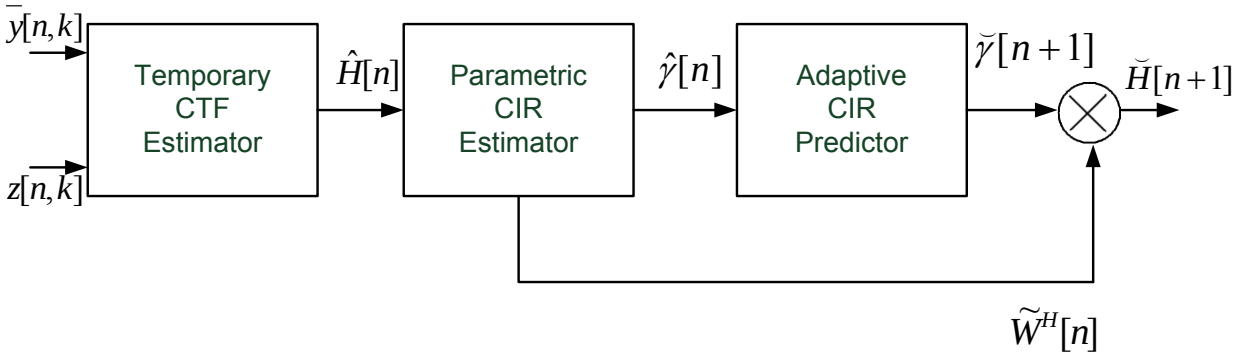

Figure 4-10: Decision Directed channel estimator for SISO OFDM

4.4.1 Channel Transfer Function Estimation

In the frequency domain, the received OFDM signal is given by

$$z[n,k] = H[n,k]x[n,k] + w[n,k] \qquad 4\text{-}78$$

where $x[n,k]$ is the transmitted signal, $H[n,k]$ is the frequency domain channel transfer function and $w[n,k]$ is the AWGN channel noise with variance σ_w^2. The parameters n and k are the temporal and frequency domain sample indices respectively. The frequency domain channel transfer function (FD-CTF) $H[n,k]$ is assumed to be complex Guassian distributed with zero mean and variance of σ_H^2. From [19] the minimum mean square error (MMSE) estimated channel transfer function is given by

$$\widetilde{H}[n,k] = \frac{\bar{y}[n,k]z[n,k]}{|\bar{y}[n,k]|^2+\frac{\sigma_w^2}{\sigma_H^2}} \quad \text{4-79}$$

where $\bar{y}[n,k]$ is the soft decision from the decoder. After the temporary channel transfer function is obtained, the channel's impulse response (CIR) is then calculated. Instead of calculating the full CIR which is known as the sample spaced channel impulse response (SS-CIR), a fractionally spaced channel impulse response (FS-CIR) is calculated instead. The SS-CIR is given by [1]

$$h[n,m] = \sum_{l=1}^{L} \gamma_l[n]c(mT_s - \tau_l) \quad \text{4-80}$$

The parameter $\gamma_l[n]$ is the FS-CIR, T_s is the sampling interval, τ_l is the temporal lag of the l^{th} path, m is the tap index. In [19] it is stated that the convolution of the transmitted signal and the SS-CIR, $h[n,m]$, will result in a signal that is dispersed over several neighbouring samples also known as leakage. The FS-CIR however produces less taps which are L in total and $L \ll K \ll N$ where L is the number of FS-CIR taps, K is the number of subcarriers and N is the FFT size. This is why the FS-CIR was chosen by [1] and will also be used in the project.

4.4.2 Channel Impulse Response Estimation

The parametric CIR estimators for determining the FS-CIR, $\gamma_l[n]$, used by [1] and [19] both actually estimated the channel's transfer function subspace using the Fast Data Projection Method (FDPM) and the deflation Projection Approximation Subspace Tracking (PASTd) algorithms respectively. Both algorithms determine the dominant eigen values of the channel

transfer function subspace and store them in $\gamma_l[n]$ which is then used as the channel impulse response. The estimated CIR and the estimated channel transfer function $\widehat{H}[n]$ are related by the equation

$$\widehat{H}[n] = \widetilde{W}[n]\hat{\gamma}_l[n] \,. \tag{4-81}$$

The matrix $\widetilde{W}[n]$ is an N by L transformation matrix with orthonormal eigen vectors of the channel transfer function covariance matrix $R_H = E\{H[n]H^H[n]\}$, where $(.)^H$ stands for Hermatian transpose.

The FDPM was used for the testbed as it formed part of Oyerinde's channel estimation algorithm. From [20] the FDPM algorithm is given by

$$\hat{\gamma}[n] = \widetilde{W}^H[n-1]\widehat{H}[n] \,, \tag{4-82}$$

$$\bar{\mu} = \mu / \left\|\widehat{H}[n]\right\|^2 \,, \tag{4-83}$$

$$T[n] = \widetilde{W}[n] \pm \bar{\mu}\widehat{H}[n]\hat{\gamma}^H[n] \,, \tag{4-84}$$

$$a[n] = \hat{\gamma}[n] - \|\hat{\gamma}[n]\|e_1 \,, \tag{4-85}$$

$$Z[n] = T[n] - \frac{2}{\|a[n]\|^2} T[n]a[n]a^H[n] \quad , \tag{4-86}$$

$$\widetilde{W}[n] = normalize\ Z[n] \,, \tag{4-87}$$

where $e_1 = [1\ 0\ 0\ \ldots\ldots\ldots 0]^T$, $normalize$ is the normalization of every column of $Z[n]$ and μ is the step size. The transformation matrix $\widetilde{W}[n]$ is initialized as follows: the first L rows of the transformation matrix are given by the L by L identity matrix and the rest of the rows are zero.

$$\widetilde{W}[0] = \begin{bmatrix} 1 & 0 & 0 & \cdots & 0 \\ 0 & 1 & 0 & \cdots & 0 \\ \vdots & \vdots & \vdots & \ddots & \vdots \\ 0 & 0 & 0 & \cdots & 1 \\ 0 & 0 & 0 & 0 & 0 \\ \vdots & \vdots & \vdots & \ddots & \vdots \\ 0 & 0 & 0 & \cdots & 0 \end{bmatrix}$$

4-88

4.4.3 Channel Impulse Response Predictor

The channel impulse response predictor predicts the channel taps for the next OFDM symbol interval which will be used for equalization. The predictor developed by Oyerinde in [1] was variable step size normalized least mean square (VSSNLMS) algorithm. It is derived from the well known least mean square (LMS) algorithm in Digital Signal Processing. The LMS algorithm provides a good balance between computation complexity and performance and this is why it was chosen for this real time application.

Given the soft symbol $\bar{x}[n]$, the estimated channel impulse response for the previous symbol interval $\hat{h}[n]$ and an error $e[n]$ given by

$$e[n] = z[n] - \hat{\gamma}^T[n]\bar{x}[n] ,$$

4-89

where $z[n]$ is the received signal. According to the LMS algorithm the channel impulse response is updated as

$$\hat{\gamma}[n+1] = \hat{\gamma}[n] + \mu e[n]\bar{x}[n],$$

4-90

where μ is the step size. When $\bar{x}[n]$ is very large the LMS algorithm experiences a gradient noise amplification problem which is dealt with by normalizing $\bar{x}[n]$. This gives rise to the normalized LMS algorithm which is given by

$$\hat{\gamma}[n+1] = \hat{\gamma}[n] + \mu e[n] \frac{\bar{x}[n]}{\|\bar{x}[n]\|^2}.$$

4-91

The choice of the step size μ is very critical because if it is very small it will reduce the sensitivity of wrong error adjustments at steady state but the convergence of the algorithm will, however, be very slow. If the step size is too large, the algorithm will be too sensitive to error misadjustements but will provide fast convergence and tracking. Thus it is best that the step size be variable so that it can give good performance both in the transient stage of tracking and also in steady state. The update of the step size was then developed to be given by

$$\mu[n] = \mu[n-1] + \frac{\rho e[n] e[n-1] \bar{x}^T[n] \bar{x}[n-1]}{\|\bar{x}[n-1]\|^2},$$

4-92

where ρ is a positive constant that controls the adaptive behavior of the step size. The optimal value of the step size is reported by [1] to be between 0 and 2 and thus it was limited to this range. The procedure continues from estimating the channel using the FDPM algorithm and now the task is to predict $\check{\gamma}_m[n+1]$ of the next symbol interval. Replacing $\bar{x}[n]$ in the above equations with $\hat{\gamma}[n]$ obtained from the FDPM algorithm, the step size update is now given by

$$\mu[n] = \mu[n-1] + \frac{\rho Re\{e[n] e^*[n-1] \hat{\gamma}^T{}_m[n] \hat{\gamma}_m[n-1]\}}{\|\hat{\gamma}_m[n-1]\|^2}$$

4-93

The FS-CIR is predicted using the channel predictor coefficient filter $p_m[n]$ which is updated using the VSSNLMS algorithm given by

$$p_m[n+1] = p_m[n] + \mu[n] e_m^*[n] \frac{\hat{\gamma}_m[n-1]}{\|\hat{\gamma}_m[n-1]\|^2},$$

4-94

where $e_m[n]$ is now given by

$$e_m[n] = \hat{\gamma}_m[n] - \check{\gamma}_m[n] = \hat{\gamma}_m[n] - p_m^H[n-1]\hat{\gamma}_m[n-1].$$

4-95

The predicted channel taps for the next symbol interval are then calculated by

$$\check{\gamma}_m[n+1] = p_m^H[n]\hat{\gamma}_m[n].$$

4-96

The channel predictor coefficient filter are initialized to

$$p_m[0] = [1\ 0\ 0\ \ldots\ \ldots\ 0]^T.$$

4-97

4.5 Channel Coding

In order to achieve better performance in terms of reliability in a communication system channel coding needs to be employed. In channel coding, redundant bits (parity bits) are added to the information codeword which help detect and correct errors in the codeword at the receiver. The performance of the communication system is increased at the expense of a lower information rate because less information bits are transmitted per unit frame of bits.

There are many channel coding schemes in literature and they vary with performance and complexity. In order to easily compare the results from the testbed with the simulation results from [1], the Turbo Coding channel coding scheme was chosen which was also used in [1]. The Turbo Coding scheme improves system performance by combining 2 encoders (block or convolutional) which give independent parity symbols with the aid of an interleaver at the second encoder input. The independent parity symbols will be used at the receiver to recover the transmitted information with the aid of 2 independent component decoders.

4.5.1 Turbo Encoder

A simple Turbo encoder is shown in Figure 4-11. Usually recursive systematic convolutional encoders are used which give better performance at low SNR than non-systematic convolutional codes. This ensures that a low weight input, which is an input bit stream with lots of zeros, will not always give a low weight output using a recursive encoder [21].

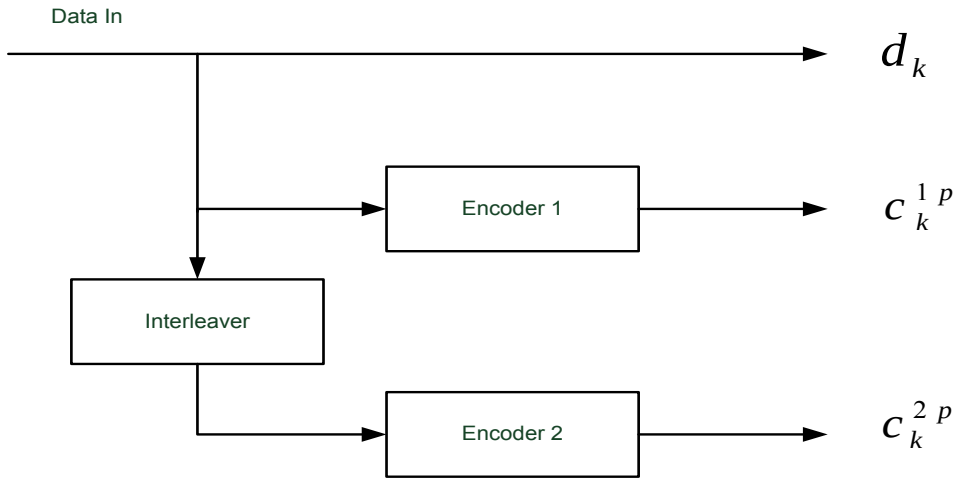

Figure 4-11: Turbo Code encoder

A (7,5) non-systematic encoder is shown in Figure 4-12, which consists of 2 parity bits for every input data bit. For such a ½ rate convolutional code the output is given by

$$\boldsymbol{c}_1(D) = \boldsymbol{d}(D)\boldsymbol{g}_1(D) \tag{4-98}$$

$$\boldsymbol{c}_2(D) = \boldsymbol{d}(D)\boldsymbol{g}_2(D). \tag{4-99}$$

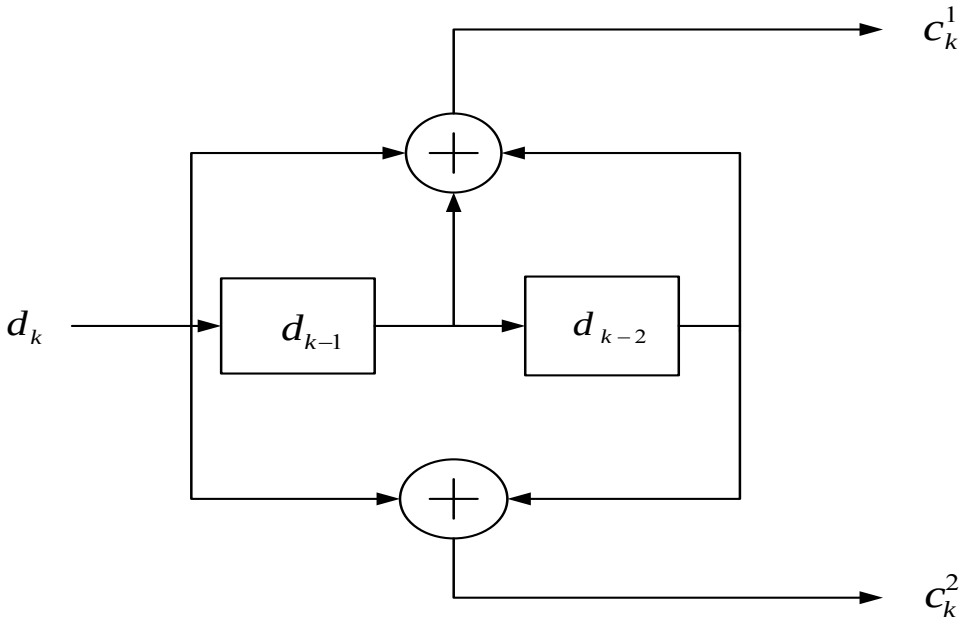

Figure 4-12: Convolutional Encoder (Non-Systematic)

To convert the non-systematic to a systematic recursive encoder, the first output bit must be the input bit and there must be feedback from the previous inputs. This is achieved by dividing the 2 equations above by $\boldsymbol{g}_1(D)$,

$\boldsymbol{c}_1(D) = \boldsymbol{d}(D)$, and

4-100

$$\boldsymbol{c}_2(D) = \boldsymbol{d}(D)\ \frac{\boldsymbol{g_2}(D)}{\boldsymbol{g_1}(D)}.$$

4-101

Previously the outputs were given by

$c_k^1 = \sum_{i=0}^{k-1} g_{1i} d_{k-i}$, and

4-102

$$c_k^2 = \sum_{i=0}^{k-1} g_{2i} d_{k-i}.$$

4-103

Now we define a new encoder input a_k given by

$$a_k = d_k + \sum_{i=1}^{k-1} g_{1i}\, d_{k-1},$$

4-104

such that

$$c_k^1 = d_k$$

4-105

$$c_k^2 = \sum_{i=0}^{k-1} g_{2i} a_{k-i}.$$

4-106

The (7, 5) Recursive Systematic Convolutional encoder is shown in Figure 4-13. For the Turbo encoder, the systematic bit (information bit) and the parity bits from the 2 encoders are transmitted. The output sequence from the transmitter is $[d_k, c_k^{1p}, c_k^{2p}]$.

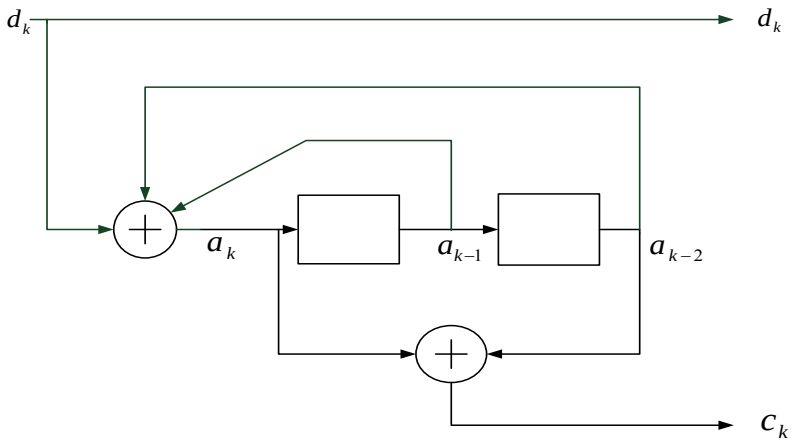

Figure 4-13: (7.5) Recursive Systematic Convolutional Enconder

4.5.2 Turbo Decoder

The Turbo decoder is shown in Figure 4-14. The received symbols are demultiplexed and fed to their corresponding component decoders. The component decoders use log likelihood ratios (LLR) to get soft estimates of the input symbols. The LLRs are a reliability measure of the input symbols.

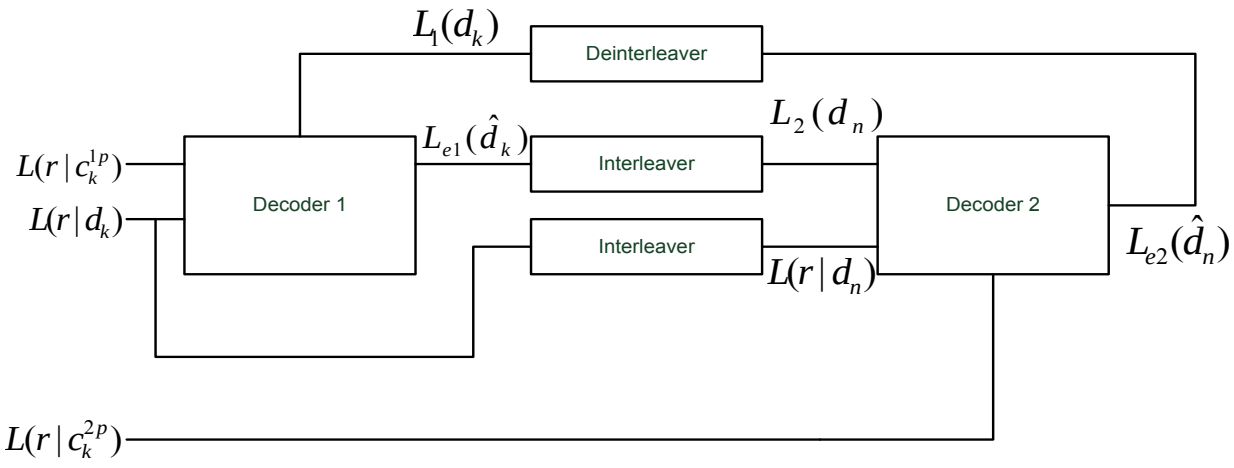

Figure 4-14: Turbo Code Decoder

The value $L(r|d)$ comes from the demodulator output as a test statistic of r under the possibilities of $d = +1$ and $d = -1$. To emphasize this $L(r|d)$ is usually written as $L_c(r)$. The value $L(d)$ is the *a priori* information of d at the decoder input and is zero for equally likely values of d.

The decoders each use the soft inputs to decode the received information. The decoders are used in an iterative process which requires them to exchange their own statistics on the received symbols, which are obtained during the decoding process, with each other in order to improve their own estimates. The interleavers at the Turbo encoder and Turbo decoder make the information obtained by the decoders uncorrelated and thus independent.

The process continues iteratively till a sufficient statistic on the received information is obtained. The convergence of the decoders to the same value is not guaranteed and thus a fixed number of iterations which will achieve a good enough estimate are usually used [21].

The decoding method of decoders is usually suggested to be the MAP [21] and the Forward Backward Algorithm [11] since the Viterbi Algorithm doesn't provide soft outputs to be used in the iterative decoding process. The Viterbi Algorithm has been modified to a Soft Output Viterbi Algorithm which provides soft outputs for the use in iterative decoding. A Turbo Coding scheme using a SOVA decoder and a (7,5) systematic encoder, BPSK modulation and a length 1000 interleaver was simulated for an additive white Gaussian noise (AWGN) channel and the performance is given in Figure 4-15.

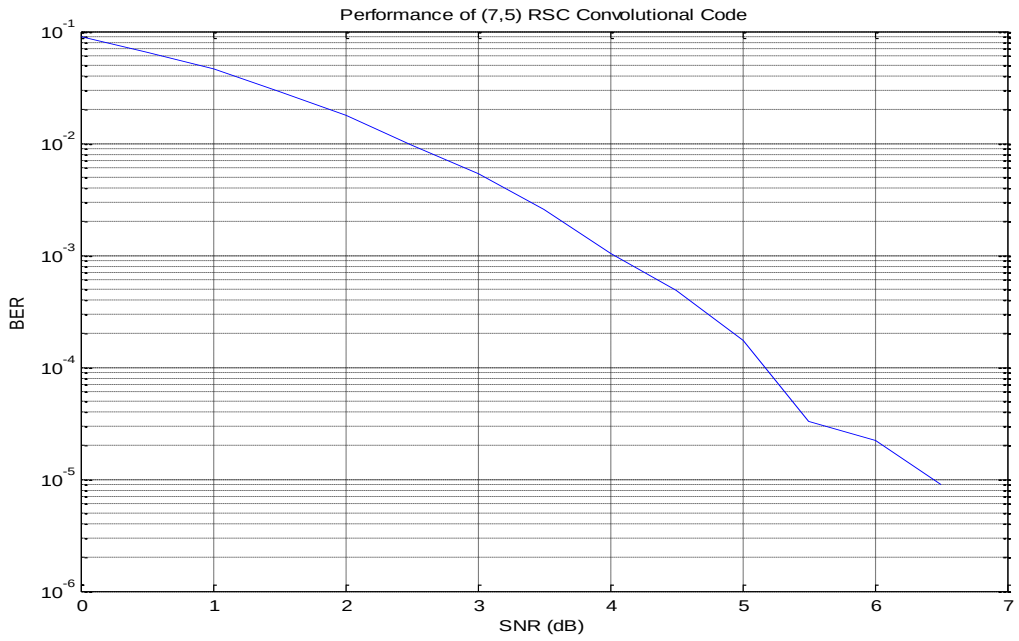

Figure 4-15: Performance of the (7,5) Convolutional Code using a recursive systematic encoder.

The TMS320C6416 DSP has an on chip hardware Turbo decoder which allows the DSP to perform Turbo decoding and other tasks simultaneously. The Turbo Decoder Coprocessor (TCP) module on the DSP can be used in Stand Alone or Shared Processing mode. In Stand Alone mode, the decoder takes the systematic and parity LLRs from the detector and the interleaver indices table and calculates hard decisions which yield the transmitted information bits. In Shared Processing the decoder takes the systematic and parity LLRs from the detector and the interleaver indices table and calculates soft decisions which are the extrinsic LLRs from one of the component decoders. The extrinsic LLRs are now supplied to the other component decoder by the user (software) as *a priori* LLRs along with the corresponding systematic and parity LLRs and the interleaver table. The other decoder now

calculates its own extrinsic LLRs. The user must calculate the hard the hard decisions from the given extrinsic LLRs and the channel LLRs after the chosen amount of iterations have elapsed.

Since extrinsic LLRs from the decoder are needed for iterative decoding, the TCP module was configured for Shared Processing mode. The enhanced data memory addressing (EDMA) module on the DSP was used to send configuration, systematic and parity, interleaver table and *a priori* information to the TCP module. The EDMA module is a hardware module that allows the DSP to move large amounts of information from the source to destination addresses in a very short of time while other tasks are being performed. Since the data movement is carried out in hardware, it is much more efficient than using software routines such as *for* loops.

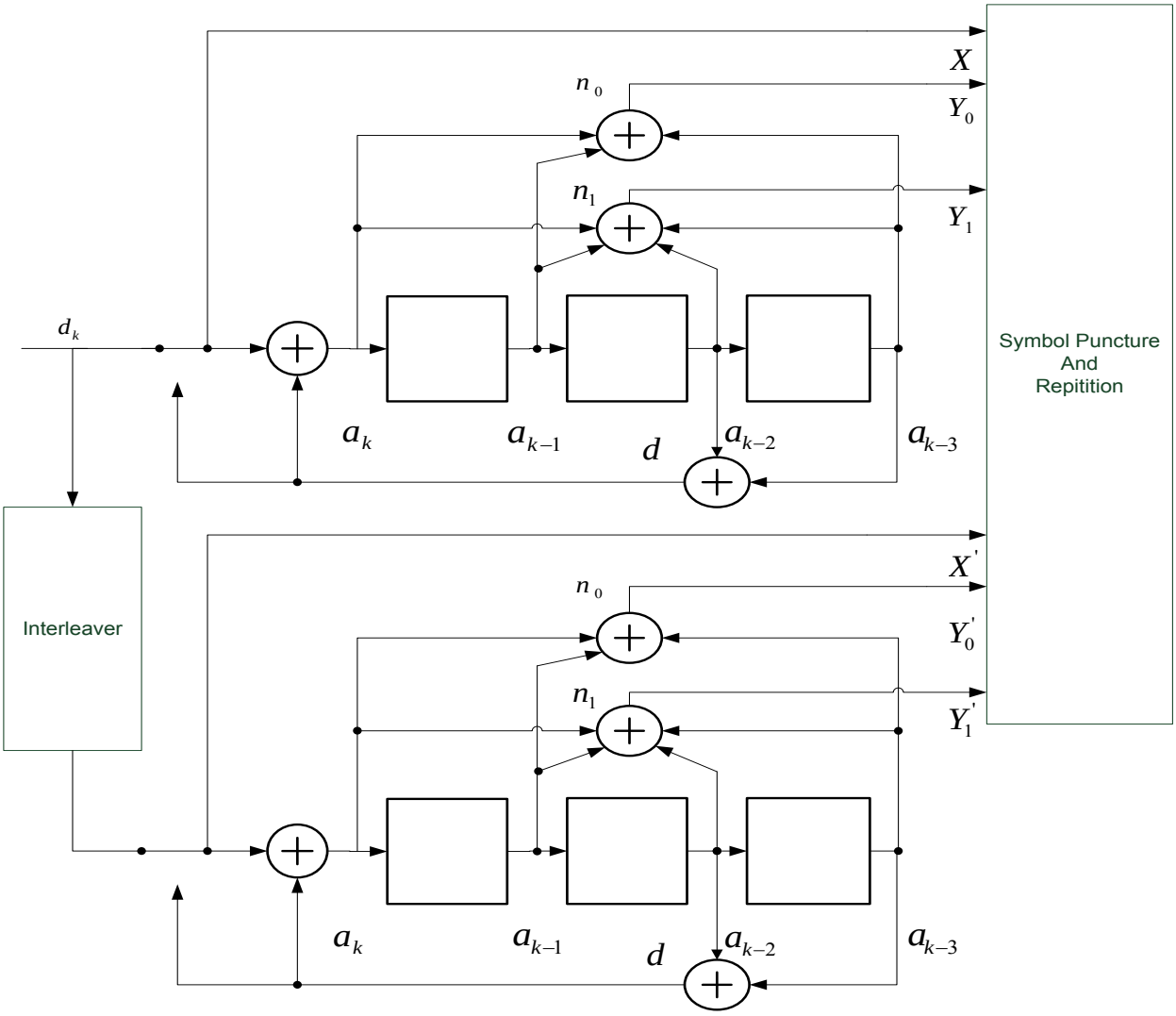

Figure 4-16: 3GPP Standard Turbo Encoder

The TMS320C6416 DSP's TCP module supports 3GPP and ISO 2000 standards. The 3GPP2 standard was used for the TCP module whose Turbo encoder is shown in Figure 4-16 with polynomials given by

$$d(D) = 1 + D^2 + D^3 ,$$

4-107

$$n_0(D) = 1 + D + D^3 ,$$

4-108

$$n_1(D) = 1 + D + D^2 + D^3.$$

4-109

X, Y_0 and Y_1 are the systematic and parity bits respectively. A 1/3 rate Turbo encoder was used which required only $n_0(D)$ and $d(D)$ polynomials from the component encoders.

4.6 Decision Directed Channel Estimation SISO OFDM systems

4.6.1 Non –Iterative

The non-iterative SISO decision directed channel estimation OFDM communication system block diagram developed in [1] is given in Figure 4-17.

In the non-iterative decision directed channel estimation, after the received signal has passed through the FFT block to become $z[n,k]$, the soft demapper recovers the soft transmitted bits by implementing (4-75) and (4-77) for QPSK modulation which was the modulation used in the project. In these equations, the channel transfer function is needed for the detection of the soft symbols.

The demapped soft bits are re-mapped into QPSK symbols and are used to estimate the current CTF, the current CIR and the CIR for the next symbol period. Initially known pilot symbols are used to estimate the CTF and then in subsequent symbol intervals the demapped soft decisions are remapped to determine the CTF. The QPSK soft mapping is given by [22]

$$\bar{y}[n,k] = D_n^{00} + D_n^{01} + D_n^{10} + D_n^{11}$$

4-110

where

$$D_n^{i,j} = \Pr[\hat{c}_i = p]\,\Pr\left[\hat{c}_j = q\right] f_{map,2}(\hat{c}_i, \hat{c}_j)$$

4-111

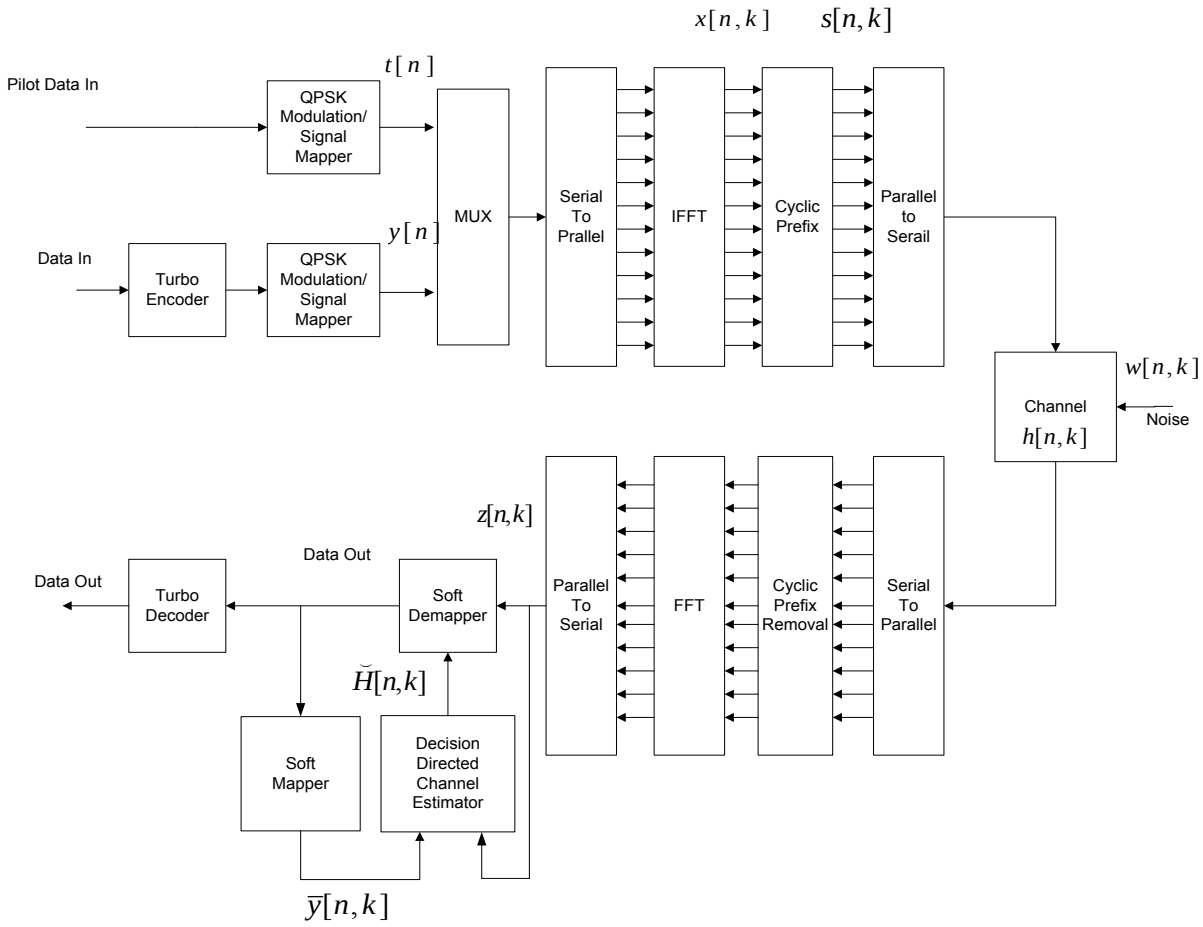

Figure 4-17: Non- Iterative Decision Directed Channel Estimation for SISO OFDM

The function $f_{map,M}()$ maps the soft decision arguments to a 2^MPSK constellation. The probability density functions in (4-111) are given by

$$\Pr[\hat{c}_k = 0] = \frac{1}{2}\left(1 - \tanh\left(\frac{L(\hat{c}_k|z[n,k])}{2}\right)\right)$$

4-112

$$\Pr[\hat{c}_k = 1] = \frac{1}{2}\left(1 + \tanh\left(\frac{L(\hat{c}_k|z[n,k])}{2}\right)\right)$$

4-113

After a full frame of symbols, which consists of many OFDM symbols, has been received, all the soft decisions are sent to the Turbo decoder to determine the hard decisions which will be estimates for the transmitted bits. A modification was made to the system given in Figure 4-17 with regard to the channel estimation procedure.

Since the testbed was to be implemented for an indoor channel, where the channel variation with time is very small due to slow movements of the transmitter and the receiver terminals indoors, the channel estimation can be performed once for every frame of decoded OFDM symbols. The Turbo decoder can provide the soft mapper with extrinsic likelihoods for all the decoded bits from the decoded frame. The decision directed channel estimator can use them to estimate the current channel and predict the channel for the next frame of OFDM symbols. The modified system is given in Figure 4-18.

At the end of the frame, the CTF is calculated for each received OFDM symbol and the CTFs are averaged and only one CIR is calculated which is used to predict the CIR for the next frame of OFDM symbols. The benefit of the modified system given in Figure 4-18 was that the detection process was faster because the CTF estimation, CIR calculation and CIR prediction are performed only once per frame instead of being performed for every received OFDM symbol as in Figure 4-17.

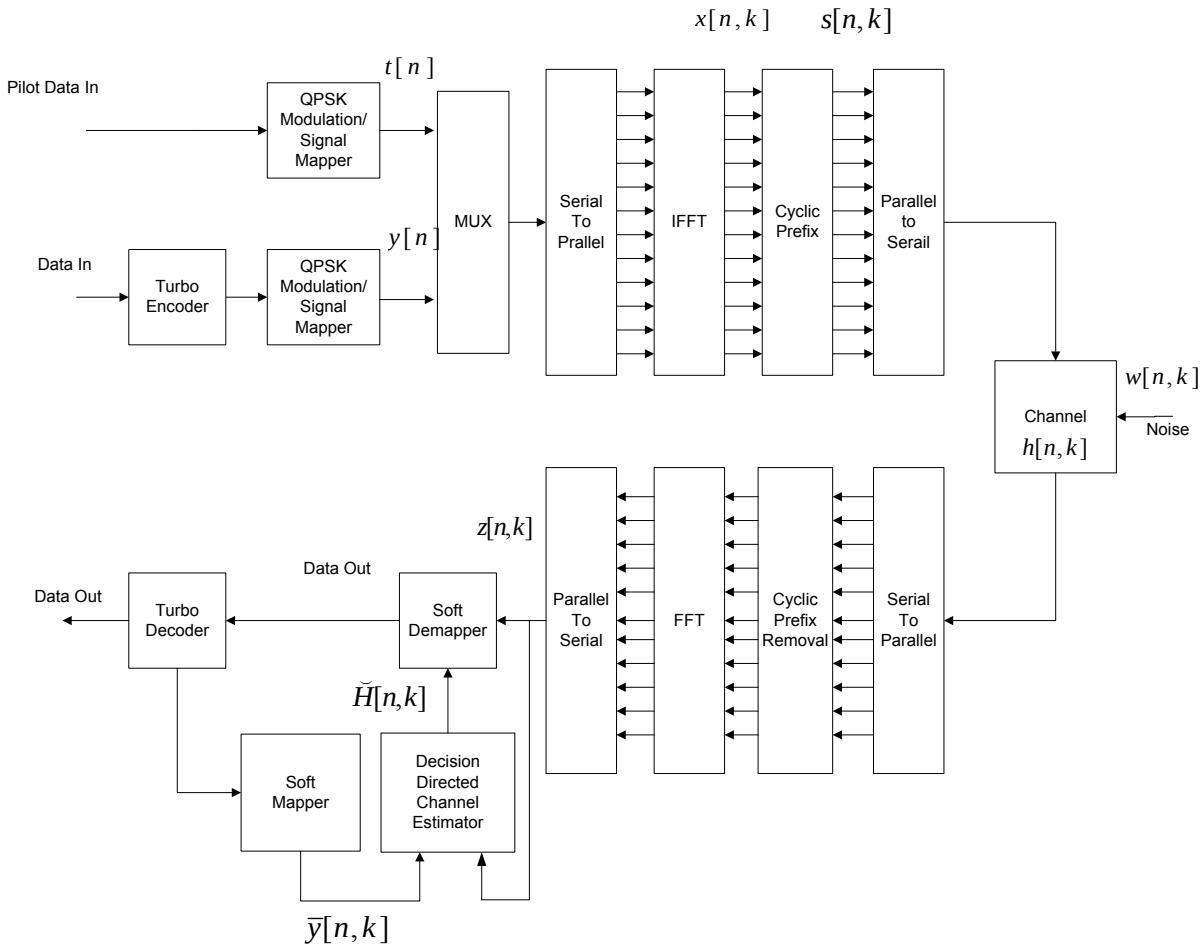

Figure 4-18: Modified Non- Iterative Decision Directed Channel Estimation

Another benefit of using the system in Figure 4-18 was improved performance in terms of bit error rate. The soft decisions from the decoder are more accurate than the soft decisions from the detector so using the soft decisions from the decoder to perform CTF estimation yields more accurate channel estimates and hence better decoded results. In the system in Figure 4-17, a few errors in the detected and remapped symbols causes errors in the CTF and CIR calculations. The errors in the CTF and CIR yields more errors in the detected soft decisions of the next OFDM symbol period and this continues until the CTFs and CIRs diverge from the true CTF and CIR. In a small enough frame, the divergence of the estimated CTF from the true CTF can be small enough to still achieve properly decoded symbols because the Turbo decoder will be able to correct the errors.

In [1], frame length is equal to the amount of bits in one OFDM symbol. In that case the channel estimation which is performed once per frame is also performed for every OFDM symbol. In the implementation given in Figure 4-18 the Turbo code frame length consists of a larger number of OFDM symbols and that is why averaging was used in order to predict a single CTF for the next frame of OFDM symbols.

4.6.2 Iterative

In Chapter 5 of [1], Oyerinde modified the system given in Figure 4-17 and made the detection iterative at the end of the frame after all the symbols in a frame have been received. For every received OFDM symbol, the CTF estimator uses remapped soft decisions from the detector together with the current received OFDM symbol and estimates the CTF. Then the CTF is used to estimate the CIR, which is then used to predict the CIR of the next OFDM symbol period. This process continues as in the system given in Figure 4-17. At the end of the frame the Turbo decoder becomes involved in the symbol detection and channel estimation procedure as given in Figure 4-19.

In the system in Figure 4-19, the extrinsic LLRs from the decoded frame of OFDM symbols are used to perform soft mapping of all the OFDM symbols within the frame. For this system in Chapter 5 of [1] the frame is equal to one OFDM symbol hence the channel estimation process for each received OFDM symbol uses soft decisions from the Turbo decoder and not the detector. This yields better results than using soft decisions from the detector. After a predetermined number of iterations the decoder calculates the hard decisions of the received OFDM symbol.

The benefit of the system in Figure 4-19 is that the decoder is involved in the detection process and the channel estimates are calculated from the soft decisions from the decoder and not the detector and this yields better results. With the frame being equal to one OFDM symbol, the detection and decoding has to be done for every received OFDM symbol. Pipelining, which is performing the n^{th} detection and decoding iteration for the 1^{st} OFDM symbol and the n^{th} -1 iteration for the 2^{nd} OFDM symbol and so on, cannot be achieved since the detection of the k^{th} OFDM symbol depends on the final CTF and CIR obtained from the iterative detection of the $(k-1)^{th}$ OFDM symbol. Hence the system with iterative decision directed channel estimation is slower than the system with non-iterative decision directed

channel estimation since every OFDM symbol has to undergo iterative detection and channel estimation is performed n times per OFDM symbol, where n is the number of iterations.

In order to reduce the complexity of the system in Figure 4-19, the symbols were detected using the channel impulse response obtained from the first symbol in a frame as in Figure 4-18. During the detection and decoding iterations, the CTFs corresponding to the OFDM symbols in a frame are calculated and the average CTF is used to determine the CIR and then predict the CIR for the next iteration and if the iteration was the last one then it is used for the next frame. The averaging of the CTFs corresponding to the OFDM symbols in the frame works because the indoor channel was assumed to be slow fading due to slow movements within buildings of the transmitter and the receiver. Hence all the OFDM symbols within the frame would have been transmitted through channels with similar impulse responses.

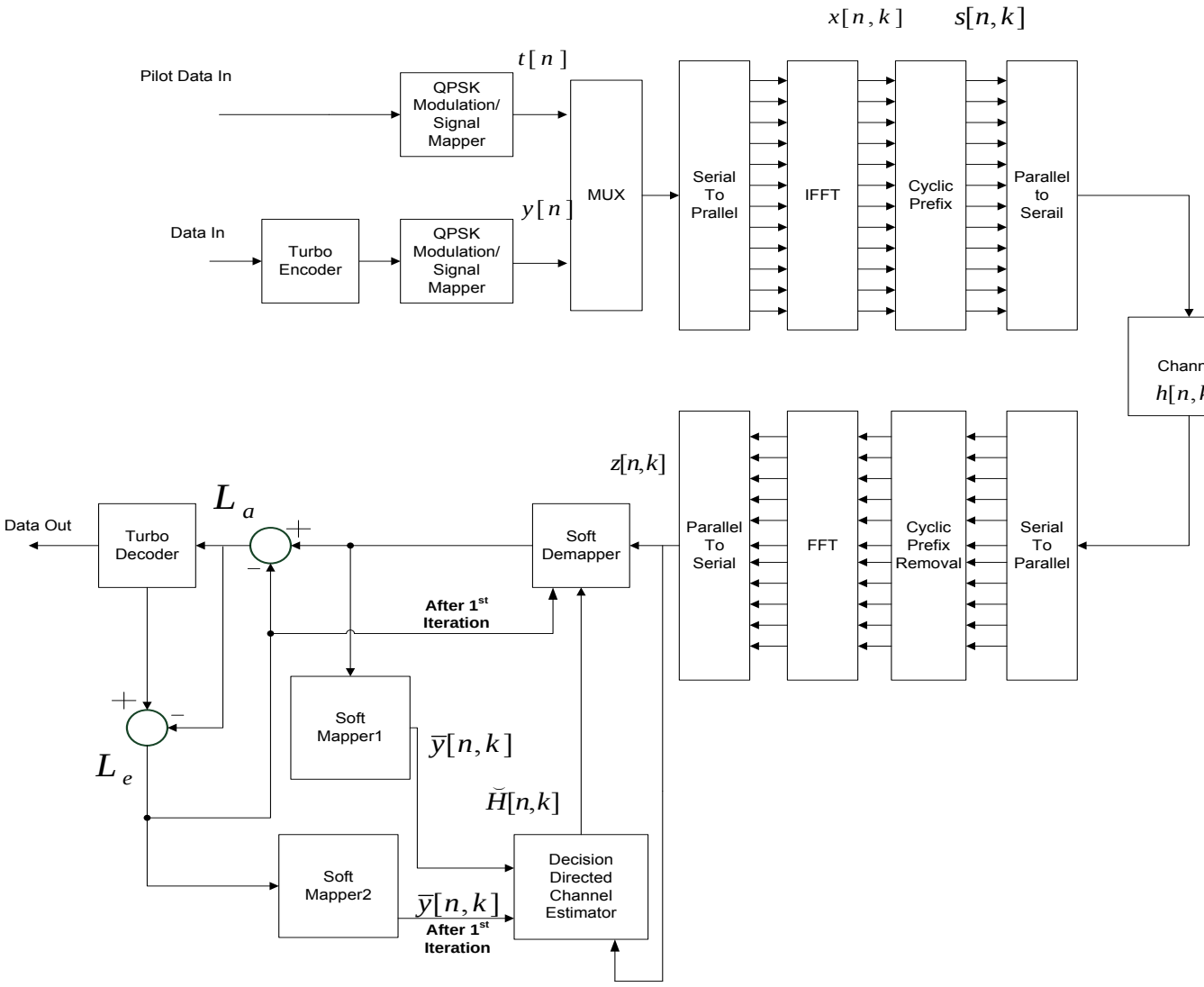

Figure 4-19: Iterative Decision Directed Channel Estimation

4.7 Decision Directed Channel Estimation for MISO OFDM systems

In this section, the work presented in Sections 4.2 through 4.6 is extended for MISO OFDM communication systems. Only 2 transmitter antennas were used in the project and the Alamouti scheme was the selected space time (ST) coding method to achieve transmitter diversity which also keeps the information rate equal to that of a SISO OFDM system.

4.7.1 Synchronization

The synchronization for the MISO OFDM communication system is similar to that of the SISO case. Here the synchronization training symbol is sent from the 2 antennas simultaneously. This simplifies the synchronization procedure instead of transmitting it from 1 antenna in the 1st symbol period and from the other in the 2nd symbol period. The 2nd method is more complex when it comes to combining the training symbol in order to achieve transmitter diversity. Hence the first method was used at the cost of not exploiting transmitter diversity.

After modifying (4-2), the received training symbol for the MISO OFDM communication system is given by

$$r(k) = \exp(j\xi)\exp\left(\frac{j2\pi\Delta f}{N}\right)\left(\sum_{m1=0}^{K_1-1} h_{m1}s(k-\tau_{m1}) + \sum_{m2=0}^{K_2-1} h_{m2}s(k-\tau_{m2})\right) + n(k)\,. \quad \text{4-114}$$

The modulators share a local oscillator so they have the same phase error ξ and frequency offset Δf with respect to the receiver oscillator. The receiver receives many versions of $s(k)$ because of the 2 dispersive channels created by antenna separation. Without any space time coding, the receiver cannot distinguish between the signals that were received via the 1st channel and the signals that were received via the 2nd channel. To the receiver, it is as if the training signal was received via one channel which is a combination of the 2 channels. The effective received signal in this case is given by

$$r(k) = \exp(j\xi)\exp\left(\frac{j2\pi\Delta f}{N}\right)\sum_{m=0}^{K_T-1} h_m s(k-\tau_m) + n(k)\,.$$

where $K_T = K_1 + K_2$. The received signal for this type of synchronization for a MISO OFDM system is the same as received signal for a SISO OFDM system and the method of synchronization is the same. The draw back as mentioned before is that there is no diversity gained from using the 2 antennas. Diversity can be exploited in subsequent symbol intervals when information is transmitted.

4.7.2 Channel Estimation

The channel estimation procedure discussed in Section 4.4 is also used for the MISO OFDM communication system. The 2 MISO channels' CTFs are estimated using MMSE channel estimator. The CTF are used to estimate the parametric CIR. The parametric CIR is then used to predict the CIR for the next MISO OFDM symbol periods. The MISO OFDM communication system using iterative DDCE is given in Figure 4-20.

4.7.2.1 MISO Channel Transfer Functions Estimation

In Section 3.3, the space time code structure of the Alamouti scheme was discussed where the received symbols for the 1st and 2nd intervals are given by

$$r_0 = h_0 s_0 + h_1 s_1 + n_0 \tag{4-115}$$

$$r_1 = -h_0 s_1^* + h_1 s_0^* + n_1 \tag{4-116}$$

respectively. The MIMO extension of the MMSE channel estimator is given by [1]

$$\tilde{H}_{ij} = \frac{\sum_{i=1}^{M_R} r_i s_i^*}{\sum_{i=1}^{M_R} |s_i|^2 + \frac{\sigma_{n_i}^2}{\sigma_{H_{ij}}^2}} \tag{4-117}$$

One could implement (4-117) by transmitting the 1st pilot symbol from the 1st antenna in the 1st symbol interval and the 2nd pilot symbol from the 2nd antenna in the 2nd symbol interval. Then the 2 channels' CTFs can be estimated from the corresponding training symbols. However in this project the channel estimation was derived directly from the Alamouti scheme.

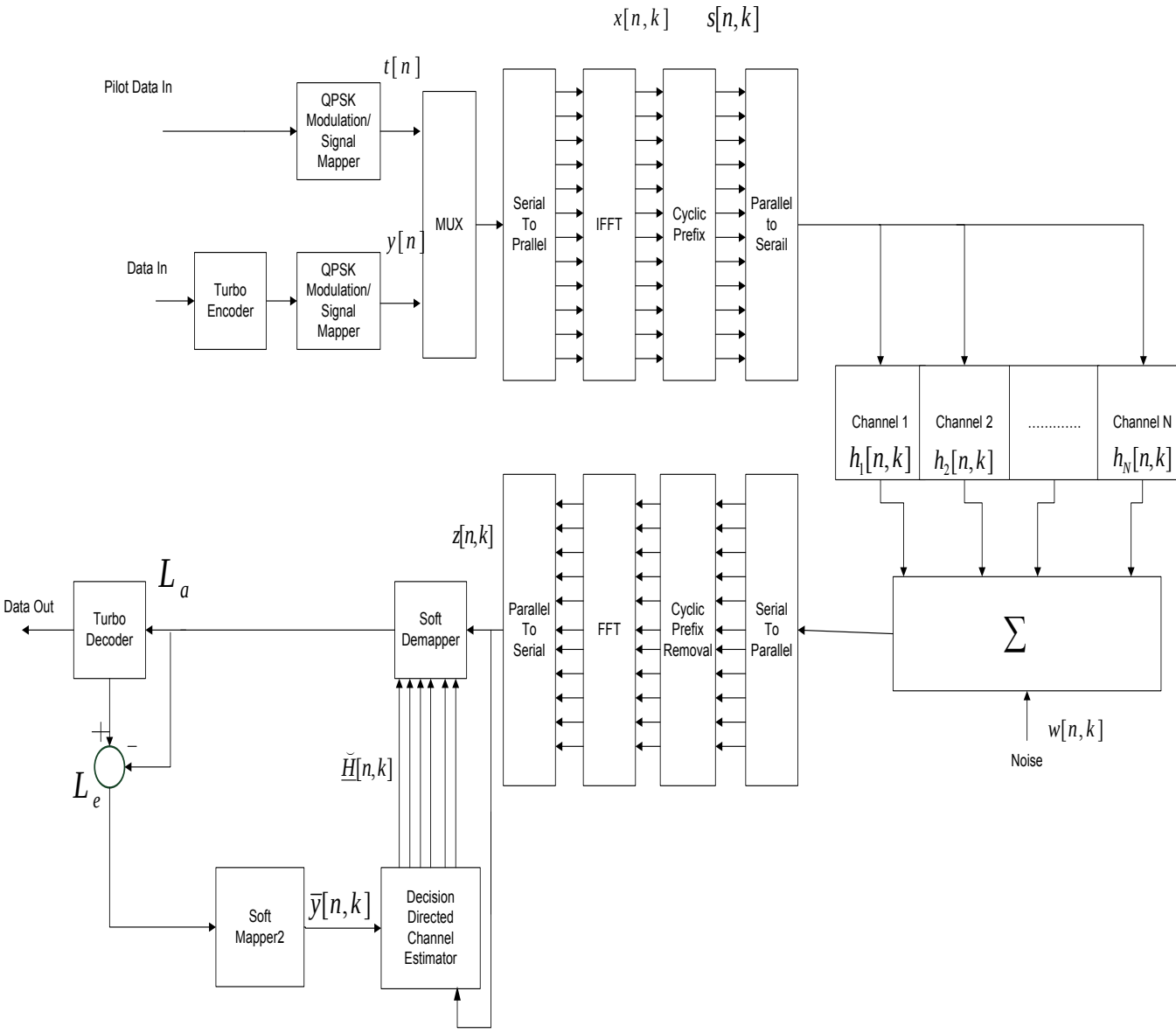

Figure 4-20: Decision directed channel estimation block diagram for MISO OFDM.

Through the 1st channel h_0 : the transmitted signal is s_0 and the received signal is r_0 in the 1st symbol interval. During the 2nd interval the transmitted signal is $-s_1^*$ and the received signal is r_1. Thus using (4-117) for the estimate for channel h_0 we get

$$\widetilde{H}_0 = \frac{r_0 s_0^* - r_1 s_1}{|s_0|^2 + |s_1|^2 + \frac{\sigma_0^2}{\sigma_{h_0}^2} + \frac{\sigma_1^2}{\sigma_{h_1}^2}} ,$$

4-118

where $\sigma_0^2 = \sigma_1^2$ are the variances of the AWGNs n_0 and n_1 respectively, and $\sigma_{h_0}^2 = \sigma_{h_1}^2$ are the channel variances. In the same the way the estimate for h_1 is given by

$$\widetilde{H}_1 = \frac{r_1 s_0 + r_0 s_1^*}{|s_0|^2 + |s_1|^2 + \frac{\sigma_0^2}{\sigma_{h_0}^2} + \frac{\sigma_1^2}{\sigma_{h_1}^2}} ,$$

4-119

4.7.2.2 Channel Impulse Response Estimation

After the CTFs for the 2 channels are obtained, the CIR is estimated as in Section 4.4.2. For the 2 channels, the FDPM procedure is now as follows after modifying equations (4-82) through (4-87)

$$\hat{\gamma}_i[n] = \widetilde{W}_i^H[n-1]\widehat{H}_i[n] ,$$

4-120

$$\bar{\mu}_i = \mu_i / \left\| \widehat{H}_i[n] \right\|^2 ,$$

4-121

$$T_i[n] = \widetilde{W}_i[n] \pm \bar{\mu}_i \widehat{H}_i[n] \hat{\gamma}_i^H[n] ,$$

4-122

$$a_i[n] = \hat{\gamma}_i[n] - \|\hat{\gamma}_i[n]\| e_1 ,$$

4-123

$$Z_i[n] = T_i[n] - \frac{2}{\|a_i[n]\|^2} T_i[n] a_i[n] a_i^H[n] ,$$

4-124

$$\widetilde{W}_i[n] = normalize\ Z_i[n] ,$$

4-125

4.7.2.3 Channel Impulse Response Prediction

The process of predicting the CIR for the next symbol period using the VSSNLMS algorithm is now extended for the MISO case as follows: The step size update is given by

$$\mu_i[n] \quad = \quad \mu_i[n-1] \quad + \qquad \frac{\rho Re\{e_i[n]e_i^*[n-1]\hat{\gamma}_{i,m}^T[n]\hat{\gamma}_{i,m}^T[n-1]\}}{\left\|\hat{\gamma}_{i,m}[n-1]\right\|^2}$$

4-126

The FS-CIRs are now predicted using the channel predictor coefficient filters $p_{i,m}[n]$ which are updated using the VSSNLMS algorithm given by

$$p_{i,m}[n+1] = p_{i,m}[n] + \mu_i[n]e_{i,m}^*[n]\frac{\hat{\gamma}_{i,m}[n-1]}{\left\|\hat{\gamma}_{i,m}[n-1]\right\|^2},$$

4-127

where $e_{i,m}[n]$ is now given by

$$e_{i,m}[n] = \hat{\gamma}_{i,m}[n] - \check{\gamma}_{i,m}[n] = \hat{\gamma}_{i,m}[n] - p_{i,m}^H[n-1]\hat{\gamma}_{i,m}[n-1].$$

4-128

The predicted channel taps for the next MISO OFDM symbol interval are the calculated by

$$\check{\gamma}_{i,m}[n+1] = p_{i,m}^H[n]\hat{\gamma}_{i,m}[n].$$

4-129

The channel predictor coefficient filters are initialized to

$$p_{i,m}[0] = [1\ 0\ 0\ \ldots\ \ldots\ 0]^T.$$

4-130

4.8 Conclusion

In this chapter the design and implementation of the MISO OFDM test bed was presented. The hardware required to realize the communication system was discussed as well as the commercially available products selected for the project. The software end of the test bed was presented which included synchronization, channel estimation, detection and decoding.

Chapter 5

5 Results

In this chapter the results of the implementation of the test bed are presented. At first the simulation results of the SISO OFDM and the MISO OFDM communication systems are presented. Then the hardware results are discussed.

5.1 Simulation Results

The system's sampling rate was 31.25 MHz which is a ¼ of the DSP's EMIF module clock frequency for transferring parallel data (see Section 4.1.2). The number of subcarriers used was 64 and a cyclic prefix of 16 samples which made the number of samples per OFDM symbol equal to

$80\ samples\ per\ symbol \times 2 = 160.$

Every OFDM symbol has a real and imaginary part hence there are 160 samples per OFDM symbol. The symbol period is

$$\frac{160\ samples\ per\ OFDM\ symbol}{31\ 250\ 000\ samples\ per\ second} = 5.12\mu s.$$

The date rate is

$$\frac{126\ bits\ per\ symbol\ period}{5.12\mu s} = 24.6\ Mbits/s$$

Only 63 subcarriers are modulated out of the 64 and the DC subcarrier was unutilized. As mentioned in Section 4.5, the TCP module of the TMS320C6416 DSP has 2 modes. In Stand Alone mode the TCP calculates hard decisions from the systematic and parity LLRs. In Shared Processing mode the TCP calculates extrinsic LLRs from the systematic, parity and a priori LLRs from the previous iteration. In order to implement iterative DDCE, the TCP had to be used in Shared Processing mode. In Shared Processing mode the minimum frame length is

5114. The frame length used was a multiple of the number of systematic bits per OFDM symbol, which with QPSK modulation is

$63\ subcarriers \times code\ rate\ \times bits\ per\ subcarrier = 63 \times \frac{1}{3} \times 2 = 42$.

The minimum frame length selected was 5166. The communication systems presented in Figure 4-17 to Figure 4-20 were simulated and the results are given in Figure 5-3 and Figure 5-4. For the SISO and MISO OFDM systems, the simulation parameters were as given in Table 5-1. The system performance depends on the number of iterations used in the decoding and channel estimation stages at the receiver. The graphs that show how the system performance improves with the number of iterations are given in Figure 5-1 and Figure 5-2. In Figure 5-1and Figure 5-2 it can be seen that the Turbo decoder improves in decoding the transmitted information as more iterations are used. The channel estimation used in these simulations was non-iterative.

Table 5-1: Table of simulation parameters

Parameter	**SISO OFDM**	**MISO OFDM**
Frame length	5166	5166
FFT size	64	
Number of sub carriers	63	
Cyclic prefix length	16	
Modulation	QPSK	
RF frequency	2.4 GHz	
Sampling frequency	125 Msps	
Coding		
Channel coding	Turbo code 3GPP2 standard	
Iterations	8	
Code rate	1/3	
Space time coding	N/A	Alamouti
Cannel Estimation		
ρ	0.002	

Predictor filter length	10	
M	3	
Step size	0.98	
Channel (hyperLAN/2 standard channel model [**4**])	Power (dB)= 0, -0.9, -1.7, -2.6, -3.5, -4.3, -5.2, -6.1, -6.9, -7.8, -4.7, -7.3, -9.9, -12.5, -13.7, -18.0, -22.4, -26.7, Delay(ns)= 0, 10, 20, 30, 40, 50, 60, 70, 80, 90, 110, 140, 170, 200, 240 290, 340, 390	Power 0(dB)= 0, -0.9, -1.7, -2.6, -3.5, -4.3, -5.2, -6.1, -6.9, -7.8, -4.7, -7.3, -9.9, -12.5, -13.7, -18.0, -22.4, -26.7 Power 1(dB)=0 ,-0.9, 0, 0, -2.5, -2.7, -4.2, -6.1, 0, -6.8, -4.7, 0 ,0, -12.5, -13.7, 0, -22.4, -26.7 Delay0(ns)= 0, 13, 22, 32, 41, 53, 63, 72, 83, 92, 111, 141, 173, 202, 243, 293, 343, 391 Delay1(ns)= 6, 16, 29, 35, 46, 59, 61, 78, 80, 96, 117, 132, 184, 209, 253, 297, 366, 399

In the simulations it was found that a system that uses remapped symbols from the detector yields bad channel estimates because errors in the estimated channel increase with OFDM symbols and so at the end of the frame the estimated channel would've diverged significantly from the true channel. This system's results were not presented here. The reason that this deviates from the behavior predicted in [1] is that here the frame consists of many OFDM symbols (5166 information bits/ 21 information bits per OFDM symbol= 246 OFDM symbols). Hence LLRs from the Turbo decoder are only used after 246 OFDM symbols after decoding has been performed and by this time the CTFs obtained from using the demapper's LLRs would have deviated from the true CTF. The demapper's LLRs are less accurate than the LLRs from the decoder so this is what would cause the divergence.

In Figure 5-3 and Figure 5-4, the simulated systems all used remapped decoded symbols for channel estimation. From the figures it can be seen that there was no benefit for iterative

detection in an indoor channel with a frame consisting of many OFDM symbols. This is because the soft remapped decoded symbols from the first iteration of the Turbo decoder may have many errors because the decoder has not converged to suitable decisions.

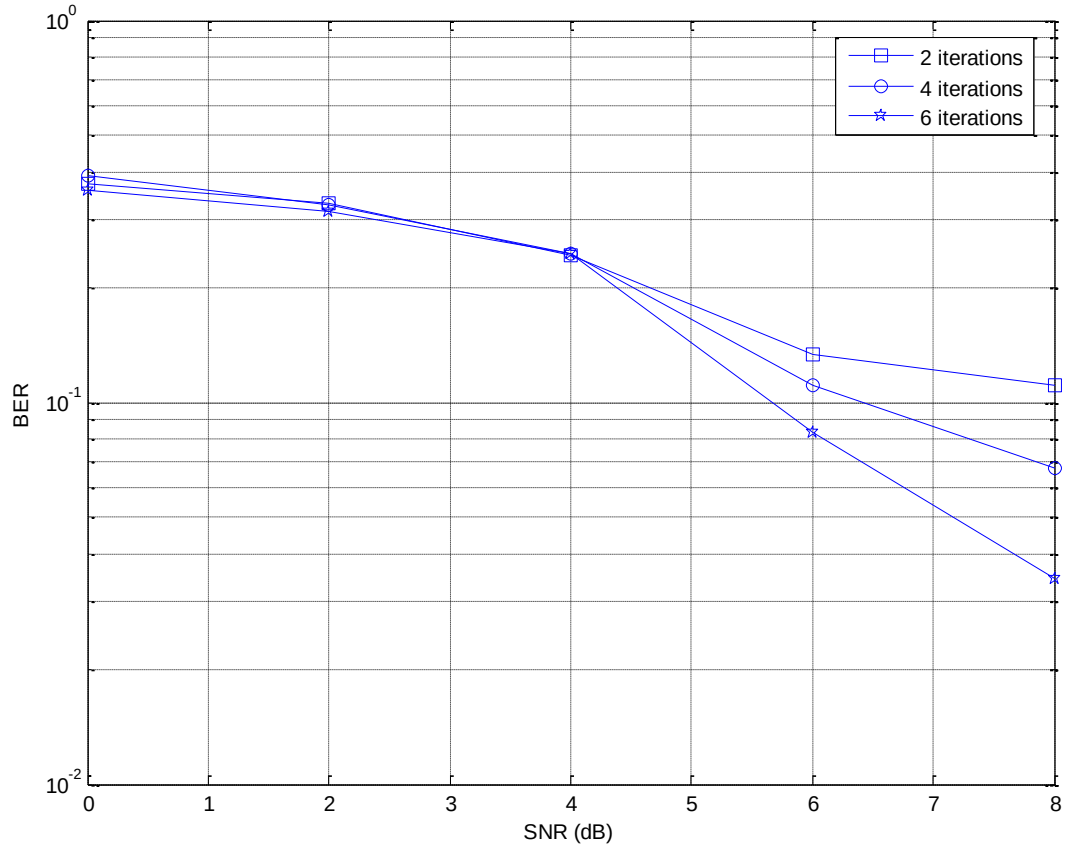

Figure 5-1: SISO OFDM system performance for different number of iterations

Hence the errors in the symbols obtained in the first iterations will cause the channel estimates obtained from them to have errors and hence produce more errors in the decoding for the next iterations. This causes the estimated channels to diverge from the true channels. This deviates from the behavior predicted in [1] because there the frame consisted of only one OFDM symbol and there was no need for averaging. The subsequent frames are detected using a final CTF estimate from the iterative DDCE process. The CTF averaging during the iterative DDCE process for the simulated systems causes the estimated CTF to deviate from the true CTF with every DDCE iteration.

The results obtained for SISO and MISO OFDM are similar to those obtained in Chapter 6 of [1] where the system using space diversity gives better performance than a SISO system. Thus there is a performance gain with using multiple antennas at the transmitter. Since the Alamouti Space Time coding scheme was used, the data rate of the MISO OFDM system is the same as the SISO OFDM case.

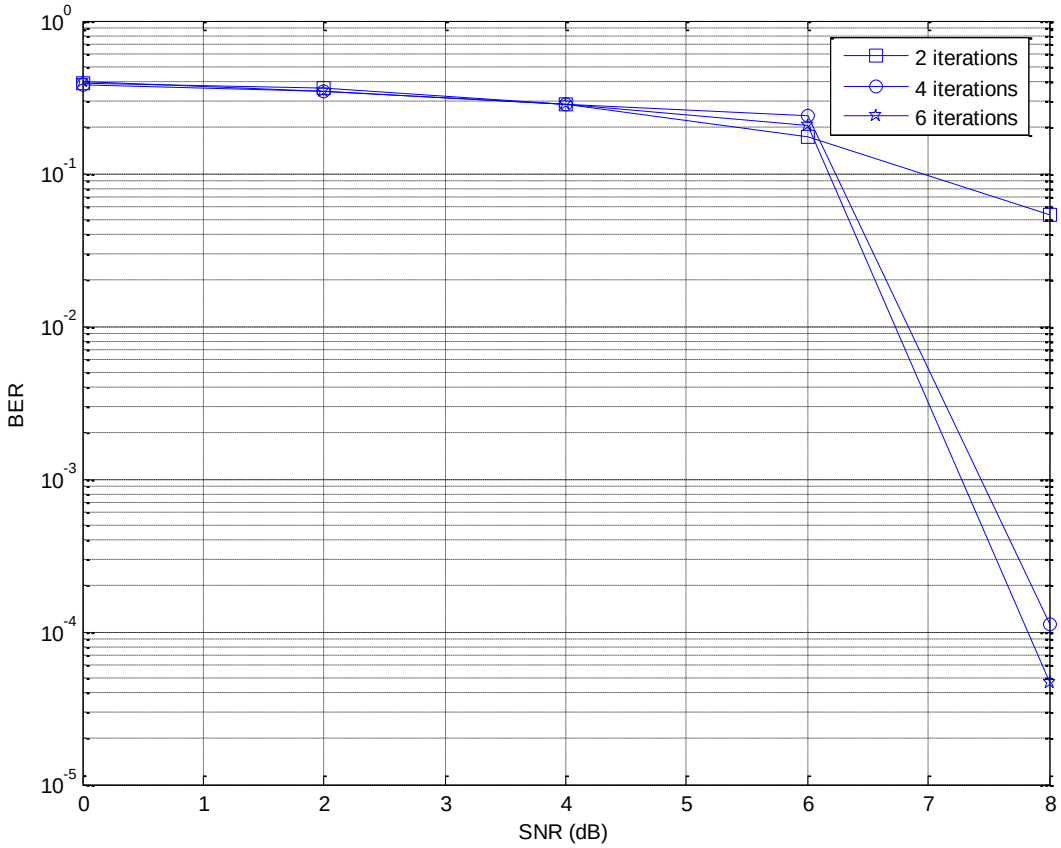

Figure 5-2: MISO OFDM system performance for different number of iterations

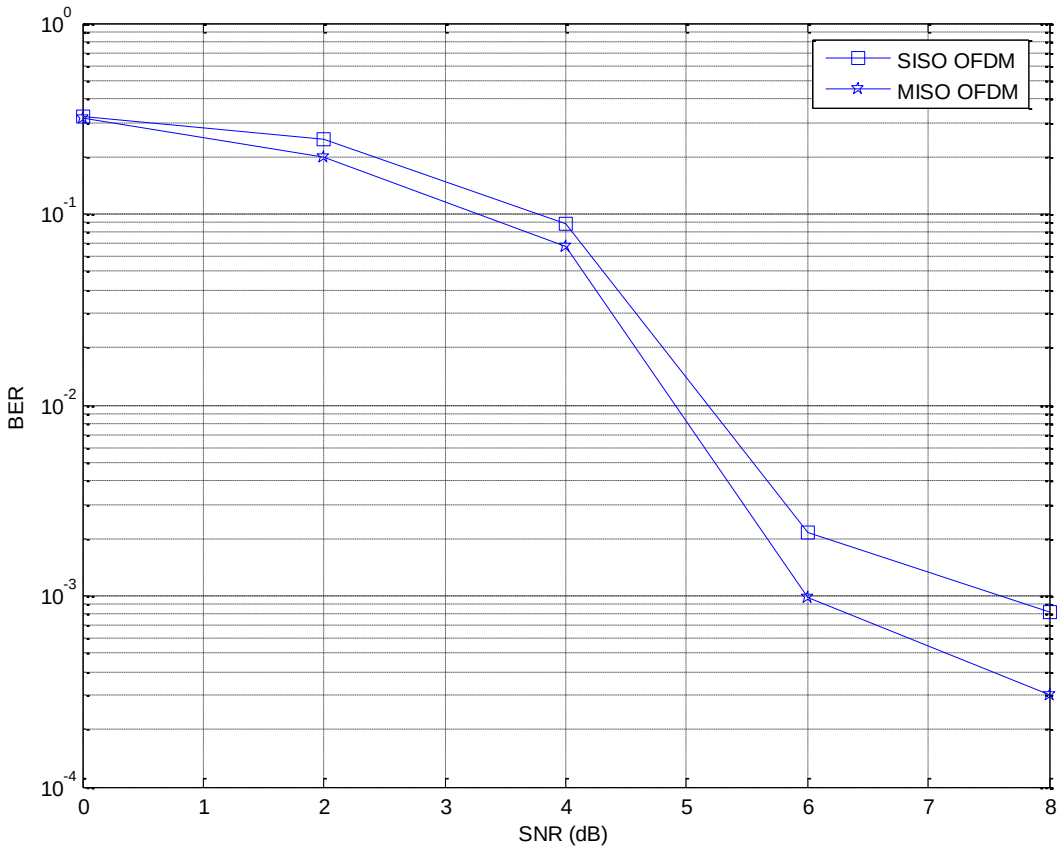

Figure 5-3: Performance of SISO and MISO OFDM systems for Non-Iterative DDCE.

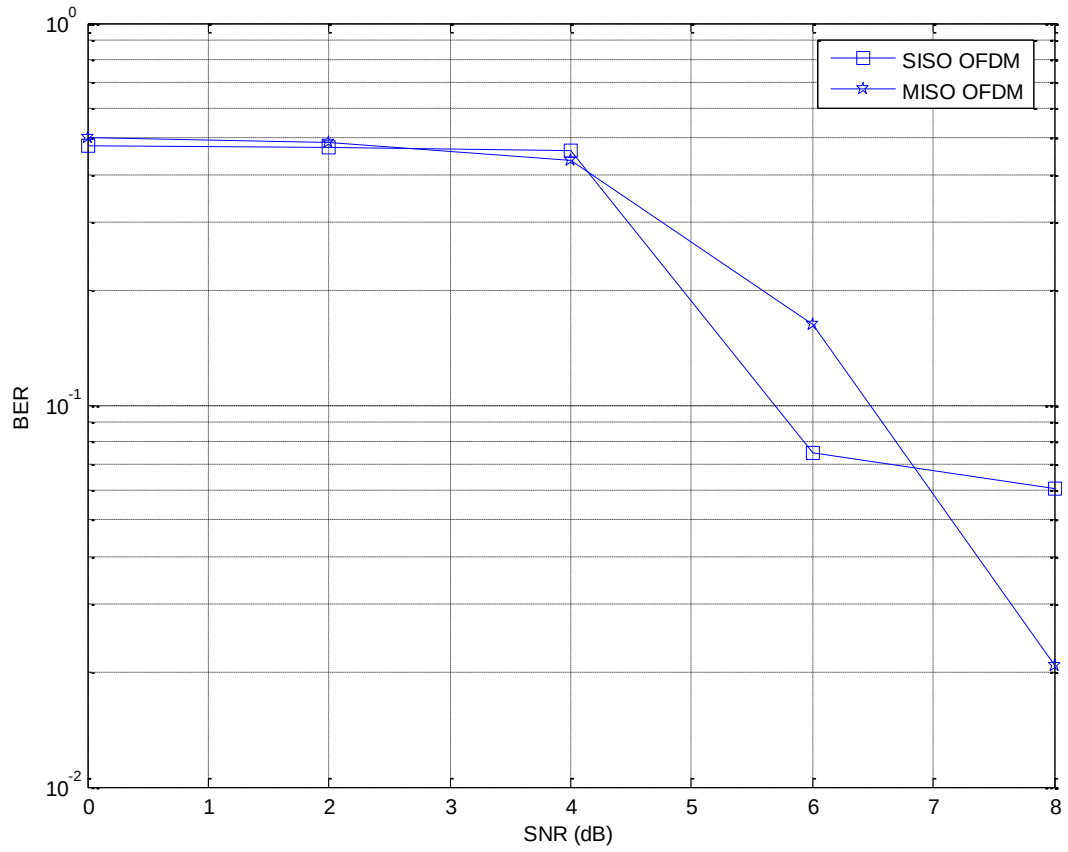

Figure 5-4: Performance of SISO and MISO OFDM systems for Iterative DDCE.

In the systems without iterative channel estimation, the channels are estimated from symbols obtained after the last iteration of the Turbo decoder. At this stage the decoder has converged to better decisions than those at the initial stages of decoding. Using decoded symbols with less errors yields better channel estimates and hence the non-iterative decision directed channel estimation outperforms the iterative version for an indoor channel using a frame consisting of many OFDM symbols.

5.1 Implementation Results

The different tasks for the receiver DSP are given in Table 5-2. The tasks include synchronization, channel estimation, detection and decoding for SISO OFDM.

Table 5-2: Profiling Statistics for the Receiver DSP

Task	CPU Cycles
Synchronization	
Coarse Time Synchronization	470 656
Coarse Frequency Synchronization	179 067
Fine Time Synchronization	507 821
Fine Frequency Synchronization(J=100)	613 623 507
Fine Frequency Synchronization(J=10)	64 074 239
Moving 64*2 *10 data	63 982
Moving 64*2 *64 data	412 892
10X64 Matrix Multiplication	249 539
Channel Estimation (Estimation, FDPM and predictor) (64 carriers)	
Estimation	102 610
FDPM and predictor	522 672 (372 280 excl VSSNLMS)
Demodulation	
Demodulation (N-1 carriers) 126 bits	260 117
Decoding	
Decoding only	42 731 952
Decoding only (iterative)	292 593 672
Receiver	
Full Receiver (excl sync, FL=5166)	57 104 392
Full Receiver (excl sync, FL=5166) (iterative)	349 179 464
Receiving and detection only	30 480 360

From the table, it can be seen that it took about 1 million clock cycles to achieve synchronization (coarse time, coarse frequency and fine time synchronization with fine frequency synchronization not used). The system clock of the DSP is 1 GHz so that makes the time to achieve synchronization equal to 1ms. This means that for that for the symbol period of 1.28**µ**s the number of received OFDM symbols during the synchronization process is $1\ ms/5.12\mu s = 195$ symbols. This makes buffer size required to store incoming samples while the system performs synchronization equal to $195\ symbols\ \times 160\ samples\ per\ symbol = 31200$ samples. With each sample taking 2 bytes the total memory needed to buffer the received samples is 62.4 kB.

The time taken to detect and decode a whole frame, where the shared processing is used for the TCP and non-iterative decoding, is $57000000\ cycles/1\ GHz = 57ms$. As mentioned before, pipelining of frames is not possible since the next frame has to be detected using the final CTF predicted in the current frame. While the receiver detects and decodes the current frame for the 57 ms interval, the next frame's symbols need to be stored in memory. The number of symbols for the next frame that need to be stored while DSP decodes the current frame is

$$\frac{57\ ms\ per\ processing\ time}{5.12\mu s\ per\ symbiol} \approx 10\ 000\ symbols\ per\ processing\ time.$$

The memory required is

$$10\ 000\ symbols\ \times 160\ samples\ per\ symbol\ \times 2\ bytes\ per\ symbol = 3.2\ MB.$$

For the iterative DDCE receiver the processing time is about 6 times that of the non-iterative DDCE receiver so the memory required in that case is 19.2 MB. The TMS320C6416 didn't have enough memory to store the received samples while performing synchronization, channel estimation, detection and decoding. The memory was used up by variables and code for the project. The DSP could only offer 16 KB of data memory (RAM) and 1 MB of internal RAM.

The tasks also need more processing power the DSP could offer. Even with more memory there would still be problems. The unprocessed samples would accumulate in the buffer because the rate at which the samples are retrieved from the buffer and processed is much less than the rate at which the buffer is populated with received samples. According to [12], for a real time implementation of a testbed the better choice would've been an FPGA based

platform. The reason is that the DSP implement software which is sequential. Even when using the DSP BIOS threads to run tasks simultaneously, the overall time processing bottleneck and memory doesn't increase. For an FPGA the processing is concurrent since the device implements the tasks in hardware. This means that the tasks run simultaneously, without any time slicing.

In [12] they implemented a DSP based test bed that has a bandwidth of 4 kHz which is a bandwidth similar to the implementation discussed in Section 5.2. But for such a low bandwidth, there would be no need for channel estimation in an indoor channel as discussed in Section 4.1.2. In FPGA based testbeds in [23], [24] and [25] the channel estimation algorithm was simple. The MMSE channel estimator implemented in the project was similar in terms of complexity to those channel estimators and was 102 000 clock cycles for the DSP according to Table 5-2. Together with channel prediction, the total number clock cycles for performing the channel estimation scheme would be 600 000. This is only about 6 times the single MMSE channel estimation. The matrix calculations involved in the FDPM and VSSNLMS algorithms are the main cause for the large number of clock cycles needed for implementing all the channel estimation modules used by Oyerinde.

Using the hardware comparisons stated above, one could conclude that in a system such as that in Figure 4-18 Oyerinde's channel estimation algorithms could be viable. The reason is that although the complexity of the full channel estimation algorithm in [1] is 6 times that of the mentioned FPGA based systems in terms of DSP clock cycles, it is only performed once per frame. For the other receiver configurations, Figure 4-17 and Figure 4-19, the channel estimations is performed for every OFDM symbol and involves the Turbo Decoder for the iterative case. These types of systems are less likely to be viable especially because no pipelining is possible since the next OFDM symbol's CIR is only known after the processing of the previous OFDM symbol.

The hardware aspect of the testbed was successfully implemented. A MISO OFDM could be transmitted from the transmitter to the receiver. A 16 subcarrier OFDM symbol was generated by the transmitter DSP and it is converted to analogue form by 2 DACs. The 2 DACs are each connected to an RF modulator. The RF modulators translate the baseband signals from the DACs to a frequency band of 2.4 GHz. The OFDM signals are demodulated by the receiver's demodulator. The EMIFA clock frequency was 31.25 MHz and since the real and

imaginary signals are interleaved, the effective sampling frequency of the OFDM signal was 15.625 MHz which then was the bandwidth of the OFDM signal.

In Figure 5-5 the demodulated MISO OFDM signal is given including the individual antenna contributions to the total received signal. It can be seen from the figure that the received MISO OFDM signal is the sum of the 2 received signals which arrive via different paths. The RF frequency MISO OFDM signal is also given in Figure 5-6. The peak OFDM subcarrier power measured at the demodulator was -50 dBm. The peak noise power was measured to be -80 dBm. This was thermal noise measured with source signals disconnected at frequency range ending at 20 MHz as can be seen in the spectrum analyzer screen in Figure 5-5 (a).

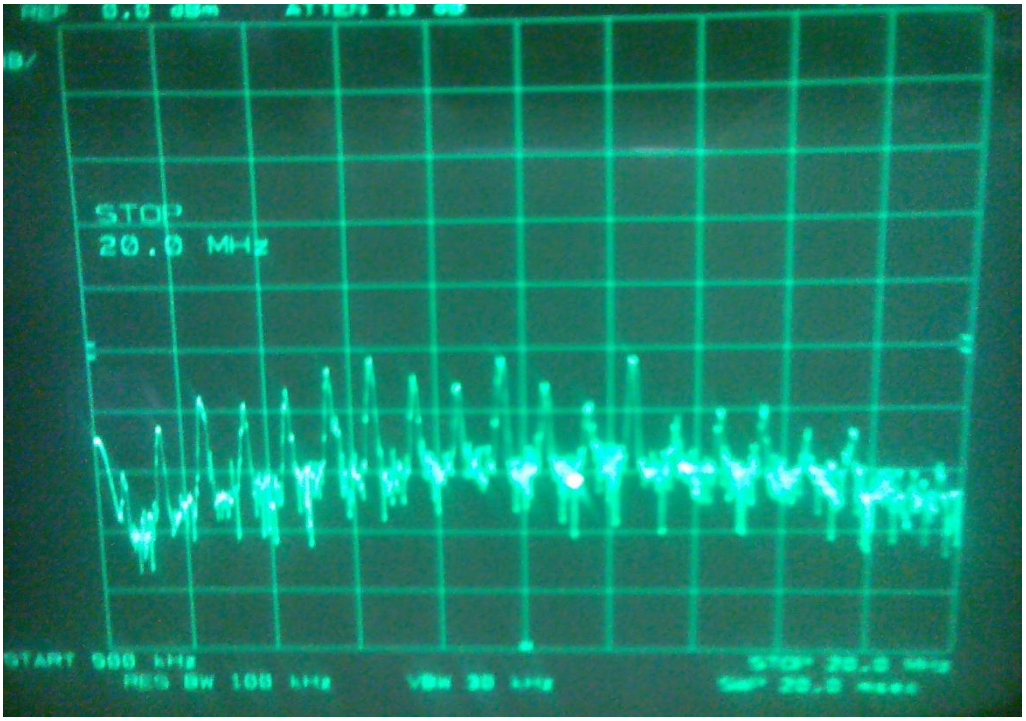

(a)

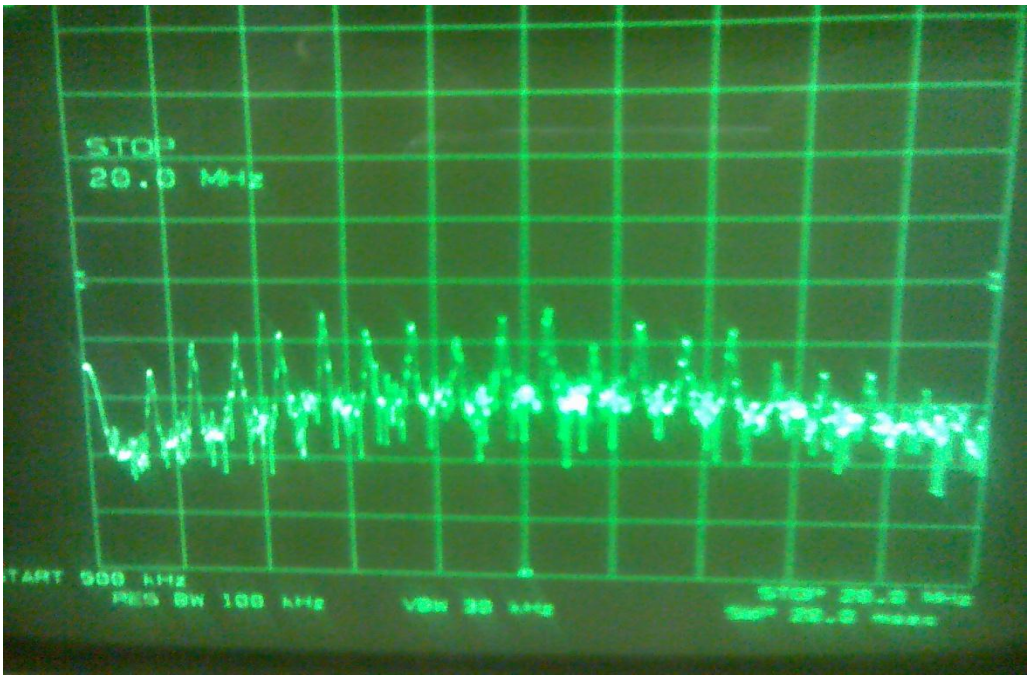

(b)

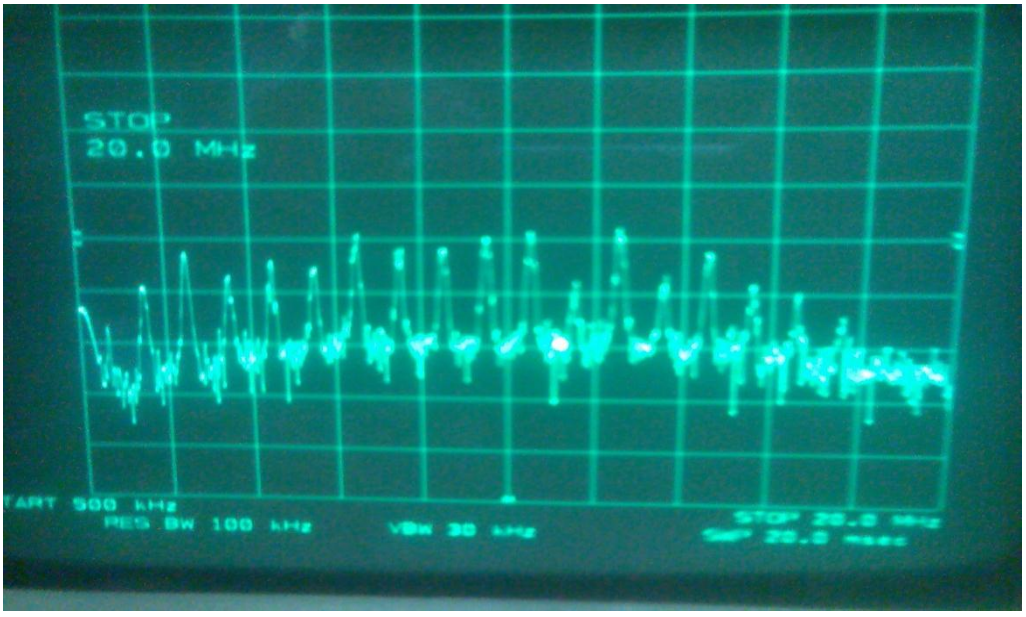

(c)

Figure 5-5: MISO OFDM spectrum for 16 subcarriers (a) 1st antenna contribution (b) 2nd antenna contribution (c) Total received MISO OFDM signal.

Figure 5-6: RF frequency MISO OFDM signal.

As mentioned in Chapter 4, the reason such a high operating bandwidth was used was because an indoor channel has a very small delay spread. In order for the channel estimation algorithms to be useful they must help cancel out the distortion caused by the multipath fading. For an indoor channel of RMS delay spread of 50 ns, the coherent bandwidth is 20 MHz which is close to the bandwidth used. If the testbed was to be deployed in an outdoor environment, the delay spread would have been in the order of microseconds which would've allowed the system bandwidth to be reducible such that the DSP can cope with the real time demand.

5.2 DSP Implementation of a Baseband SISO OFDM Communication System

In this section a simple OFDM communication system is presented. The communication was between 2 TMS320C6416 DSP kits where one acts as the transmitter and the other the receiver. The main focus of the implementation was to achieve synchronization and correct detection of the transmitted data. Channel coding and estimation wasn't included in the

implementation because the channel was not time varying. A more robust communication system could be developed from the current implementation in order to complete the testbed.

The system implemented is given in Figure 3-1. The communication consists of a binary source. The binary data is mapped using a signal mapper which maps the data to points on the M-ary constellation map. The serial symbols are converted to parallel and an inverse Fast Fourier Transform (IFFT) is used to convert the frequency domain symbols to time domain. The time domain samples which are in parallel are converted to serial samples. A cyclic prefix is added to prevent inter-symbol interference (ISI) due to the multipath channel and a digital to analogue converter (DAC) is used to convert the digital signal into analogue.

The complex signal cannot be transmitted as it is, since it has an imaginary component so it is separated into real and imaginary. The real part is modulated by a cosine signal and the imaginary signal is modulated with a sine signal and the 2 signals are added together and transmitted over the channel as one real signal as given in (3-2).

At the receiver the signal is separated in to 2 branches. One branch multiplies the received signal with a cosine signal and the other multiplies it with a sine signal. The outputs of the multipliers are low pass filtered and the real and imaginary components of the transmitted signal are recovered as given in (3-3). The real and imaginary signals are sampled with analogue to digital converters (ADC) and the cyclic prefix is removed from the samples. The samples are converted to parallel and a Fast Fourier Transform (FFT) is used to convert the samples into the frequency domain. The parallel symbols are converted to serial and are mapped back into binary.

5.2.1 Transmitter

The sampling frequency used on the DSP boards was 48 kHz. The carrier frequency f_c used was 6 kHz and this allowed $48/6 = 8$ samples per carrier period. The highest frequency component of the baseband OFDM signal must be much smaller than 6 kHz so that the information signal can be modulated by the carrier. The OFDM symbols had 16 data symbols which achieved the requirement that the highest subcarrier's frequency be smaller than the carrier frequency. The bandwidth of the baseband signal would be 48 kHz since the BPSK symbols would occupy all the frequency components in the frequency domain and the frequency variable k varies from 0 to N-1. The carrier frequency spacing would be

$\frac{F_s}{N} = \frac{48000}{16} = 3\ kHz.$

In order to make the bandwidth of the symbols much smaller than the sampling frequency and the carrier frequency of 6 kHz, an up sampled N_u point IFFT had to be used instead of the N= 16 point IFFT for only the 16 used subcarriers. Since the FFT algorithm requires that N_u be a power of 2, and $N_u = 1024$ point IFFT was used and this gave a bandwidth of

$\frac{16F_s}{N_u} = \frac{16(48000)}{1024} = 750\ Hz$

and the subcarrier frequency spacing would be 750/16= 46.875 Hz. The carrier frequency is 8 times the bandwidth. The DSP kit used was the C6416 DSK from Texas Instruments and it came with a software library for implementing FFT and IFFT functions that were written in assembly and interfaced with C and are optimized for the TMS320C6416 DSP. In the library, the complex variables are 1 by 2n arrays where n is the number of complex elements and the real and imaginary components corresponding to the same complex number are stored next to each other with the real part being first. The transmitted signal $x_c(t)$ would have 2048 elements (1024 real and 1024 imaginary parts).

The synchronization scheme used was that of Schmidl & Cox [14] which corresponds to that of Minn [3] for L=2. In OFDM synchronization, a symbol with repeated parts must first be transmitted before those carrying information in order to achieve timing and frequency synchronization. From [3] the timing metric for 2 repeated parts is given by (4-3), (4-4) and (4-5). The frequency offset estimation was calculated using (4-8).

In the implementation the OFDM symbol consisted of the following data

$$d(k) = [1\ 1\ 0\ 1\ 1\ 0\ 0\ 1\ 1\ 1\ 0\ 1\ 1\ 0\ 1\ 0] \qquad 5\text{-}1$$

The data is mapped to M-ary symbols and the symbols consist of real components only since BPSK modulation was used. The mapped data is given by

$$s(k) = [1\ \ 1\ -1\ \ 1\ \ 1\ -1\ -1\ \ 1\ \ 1\ \ 1\ -1\ \ 1\ \ 1\ -1\ \ 1\ -1] \qquad 5\text{-}2$$

An IFFT is performed on the symbols and the result, showing only the real part, is given in Figure 5-7. Since a 1024 point IFFT was performed instead of a 16 point IFFT, the frequency

domain representation of $x(t)$ will be as shown in Figure 5-8 and it can be seen that only the first 16 components contain information symbols.

The baseband signal signal's components are modulated according to (3-2) to obtain $x_c(t)$. The high frequency signal is shown in Figure 5-9.

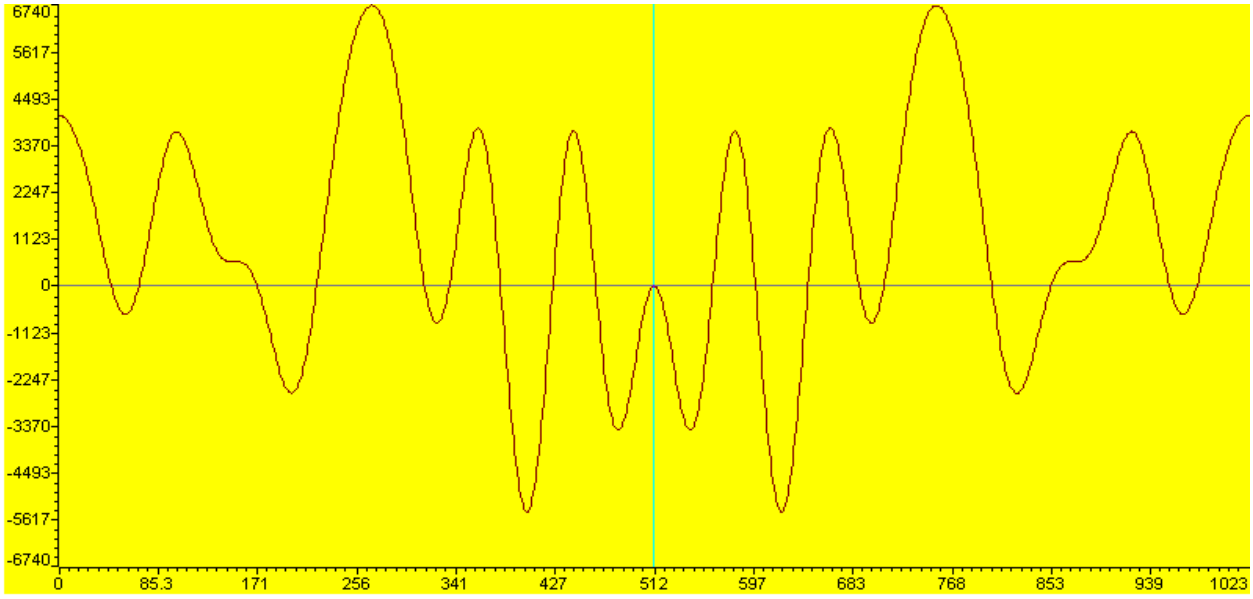

Figure 5-7: Real part baseband signal$x(t)$.

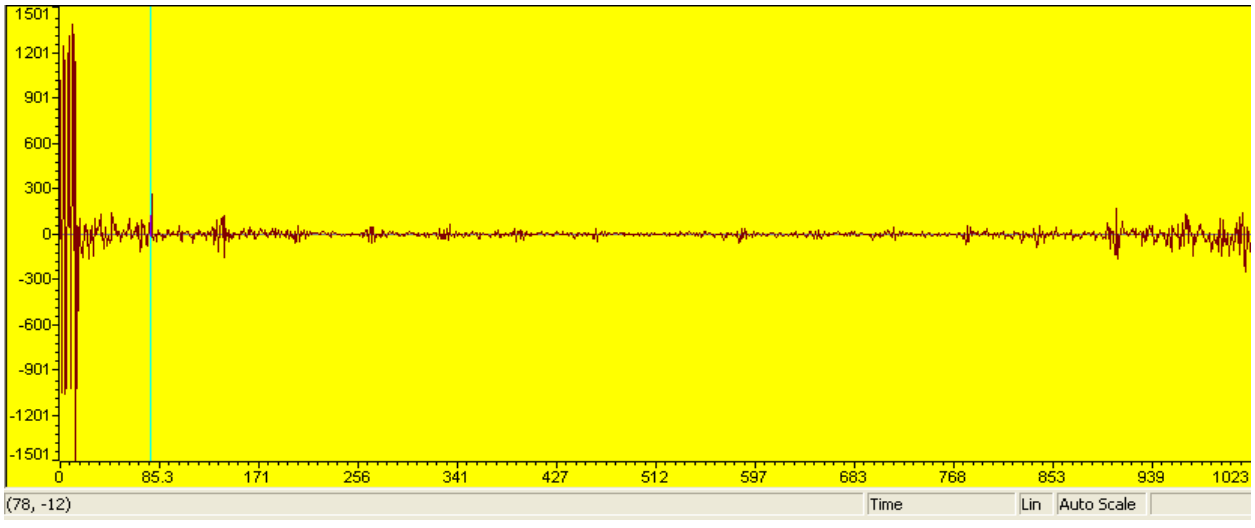

Figure 5-8: Real part of $X(k)$

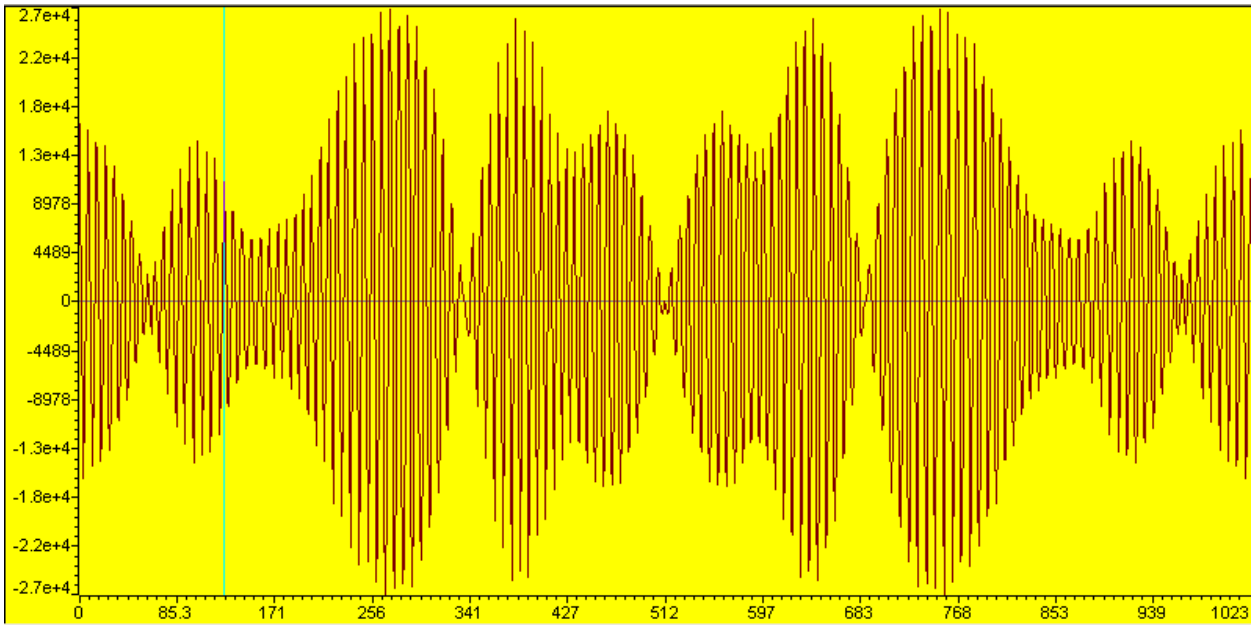

Figure 5-9: Transmitted high frequency signal $x_c(t)$

The 1st OFDM symbol that is transmitted consists of 2 repeated parts which are samples 256 to 767 of $x_c(t)$ and are 512 samples in total. The same symbol is then transmitted over the rest of the OFDM intervals. This completes the transmitter side of the implemented SISO OFDM communication system.

5.2.2 Receiver

At the receiver, the received signal is split into 2 branches. One branch's signal is multiplied with a cosine signal and the other branch is multiplied with a sine signal in order to recover the baseband signal's real and imaginary components respectively as given in (3-3) which after low pass filtering the real and the imaginary parts of the baseband transmitted signal is obtained.

The low pass filter used was a simple first order low pass filter with transfer function given by

$$H(j2\pi f) = \frac{1}{1+j\frac{f}{800}}, \qquad 5\text{-}3$$

which rejects the double frequency terms by 25 dB. In a more advance implementation a better low pass filter with a large attenuation in the stop band would be used. Since this was a simple implementation the filter given in (5-3) was adequate. After filtering and synchronization the correctly received baseband signal (real part) after 4 OFDM symbols is shown in Figure 5-10.

Initially the receiver collects samples for an interval of 2N, where N is the OFDM symbol period, and then it calculates the metric from those samples. A metric threshold of 0.9 was used to tell if any symbol with a repeated part had been received, if not the receiver collects the next N samples and uses them and the last N samples in the 2N interval to calculate the next timing metric. An interval of 2N was used because within only one OFDM interval the cross-correlation of the 1st and 2nd parts may not have a maximum in that period and the maximum delay that can be found would be N/2. With an observation interval of 2N the correct maximum delay of N can be found from the cross-correlation of the 2 parts.

Since in the implementation the same symbol is continuously transmitted and contains a repeated part only at the beginning, the repeated part used was from samples N/4 to 3N/4-1 which were 256 to 767. This prevents correlation of the symbol with the repeated part with the next symbol with no repeated part since they are the same. The 1st received symbol which has a repeated part is shown in Figure 5-11.

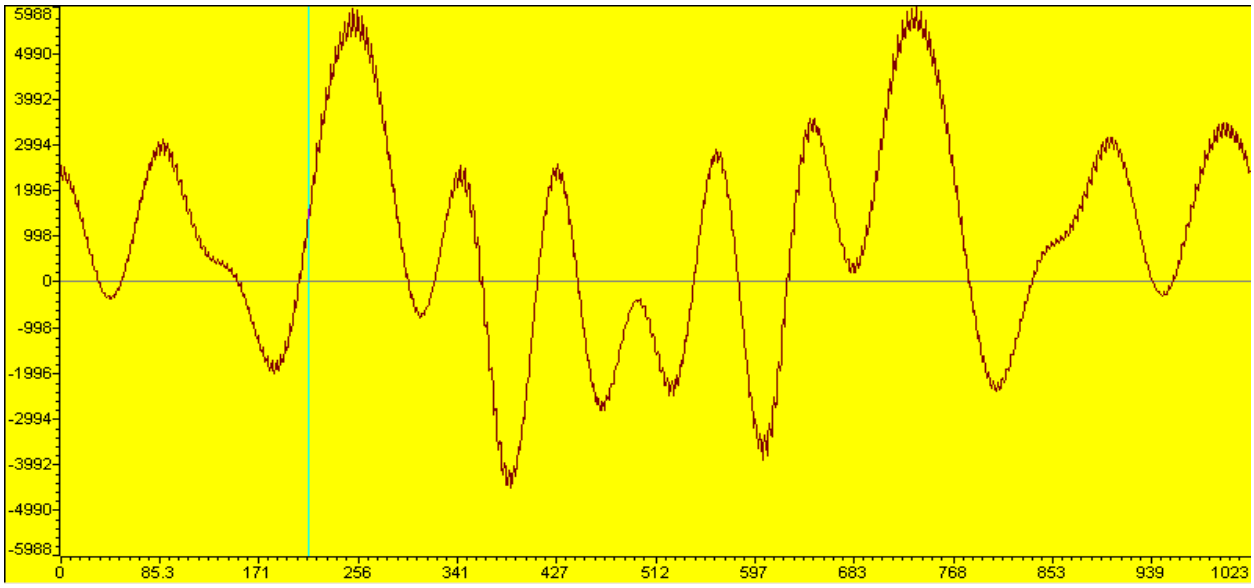

Figure 5-10: Recovered real part of baseband signal after 4 OFDM symbol periods.

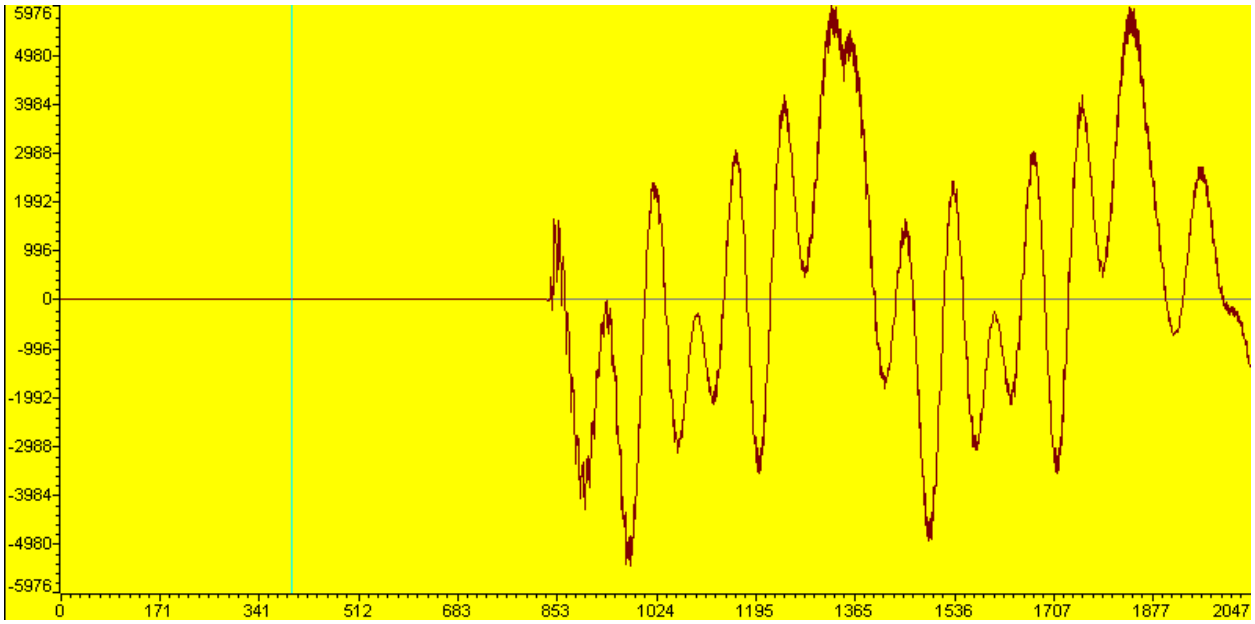

Figure 5-11: Received repeated OFDM signal's real part at low frequency after filtering.

From the OFDM symbol with a repeated part, the timing metric is calculated using Equations (4-3), (4-4) and (4-5). Figure 5-12 to Figure 5-14 depict $P(d)$, $E(d)$ and $\Lambda(d)$ respectively from the 1st 2 OFDM symbols that give a timing metric greater than 0.9. Also in Figure 5-14 a table of the information obtained from $\Lambda(d)$ is shown where symbol, delay2, d_max , d and fe are the number of symbols received after detecting a metric greater than 0.9, the delay caused by calculations of the metric, the index corresponding to the maximum of the metric, the difference between d_max and delay2, and the frequency error.

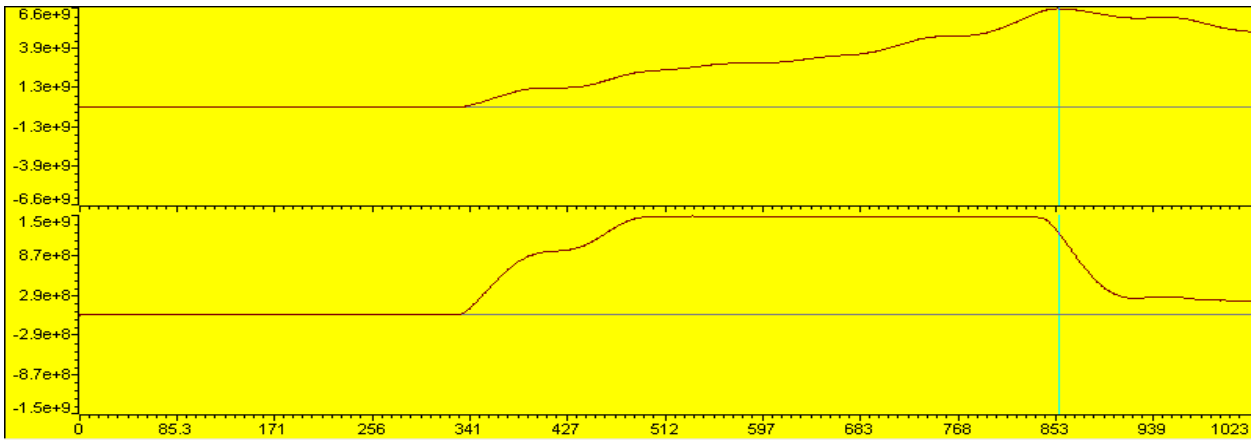

Figure 5-12: $P(d)$

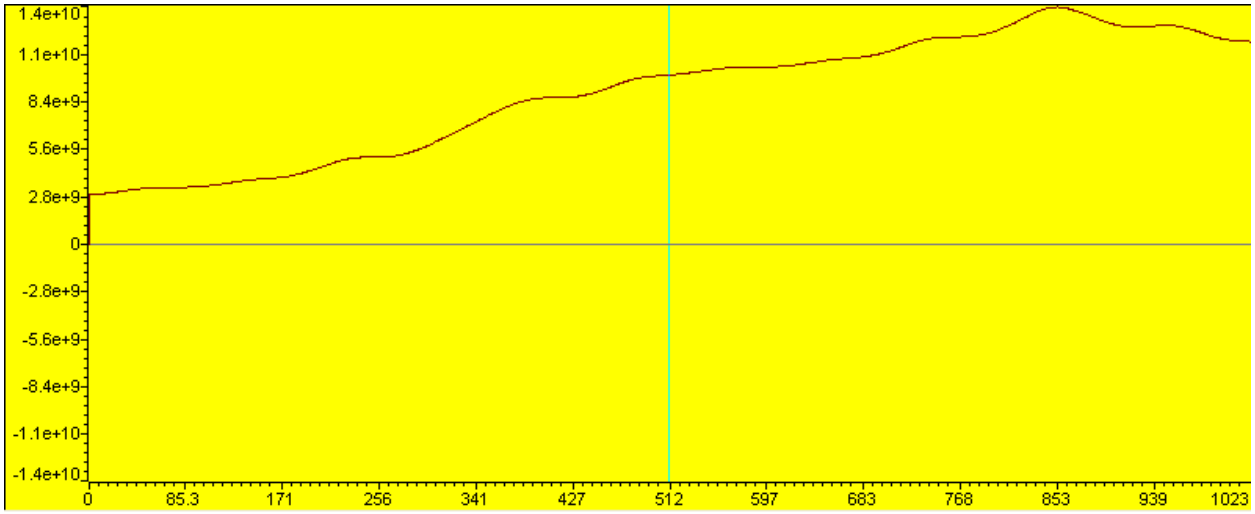

Figure 5-13: $E(d)$

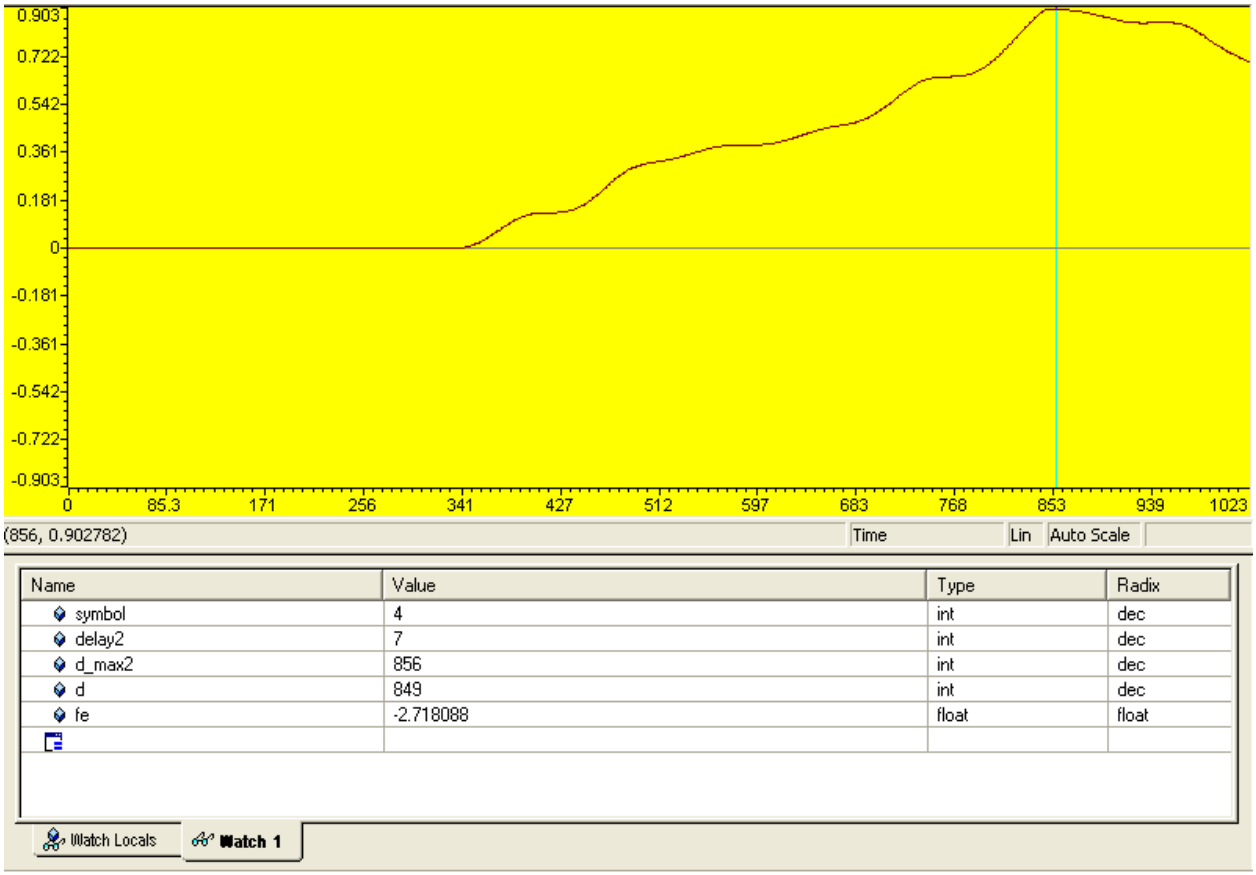

Figure 5-14: $\Lambda(d)$ and timing data

After correcting the timing and frequency offsets, an FFT is performed on the received symbol and the result is shown in Figure 5-15 and Figure 5-16. From the frequency bins, the transmitted BPSK symbols can be recovered and the mapped back into binary data. As can be seen from the enlarged FFT in Figure 5-16 the BPSK symbols are 1 1 -1 1 1 -1 -1 1 1 1 -1 1 1 -1 1 -1 which are the same as the transmitted BPSK symbols.

The FFT algorithms from the DSP's library which were written in assembly gave a delay of only 477 microseconds which is negligible compared to the symbol period of 21.33 milliseconds. The performance of the algorithms is good considering that the FFT size is 1024 which is very large.

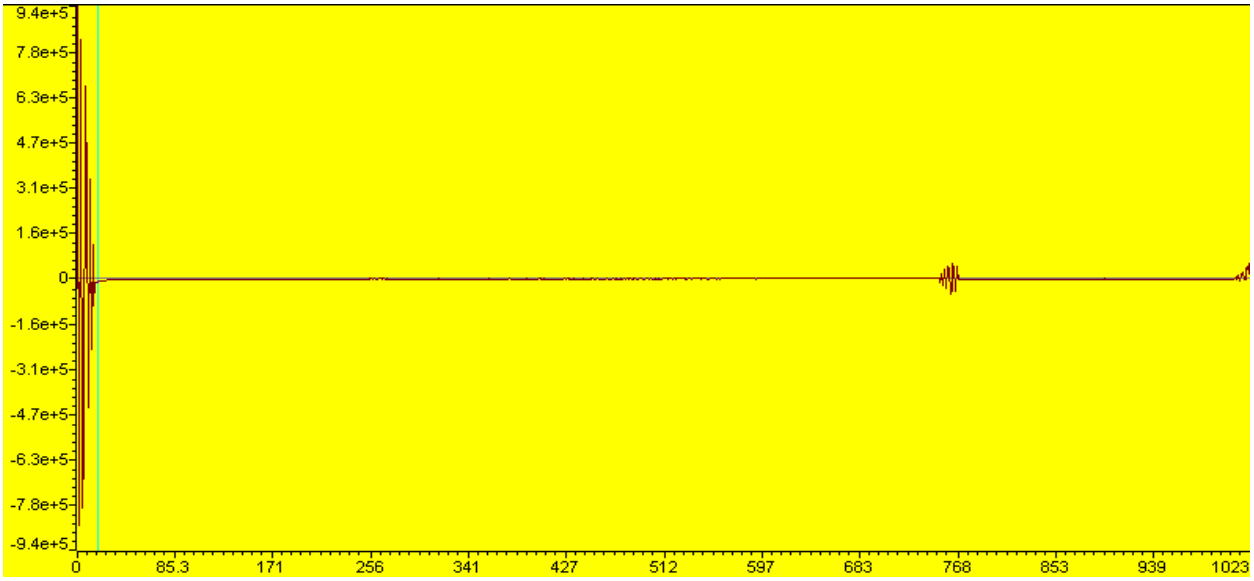

Figure 5-15: Real part of FFT of synchronized OFDM symbol after 4 periods.

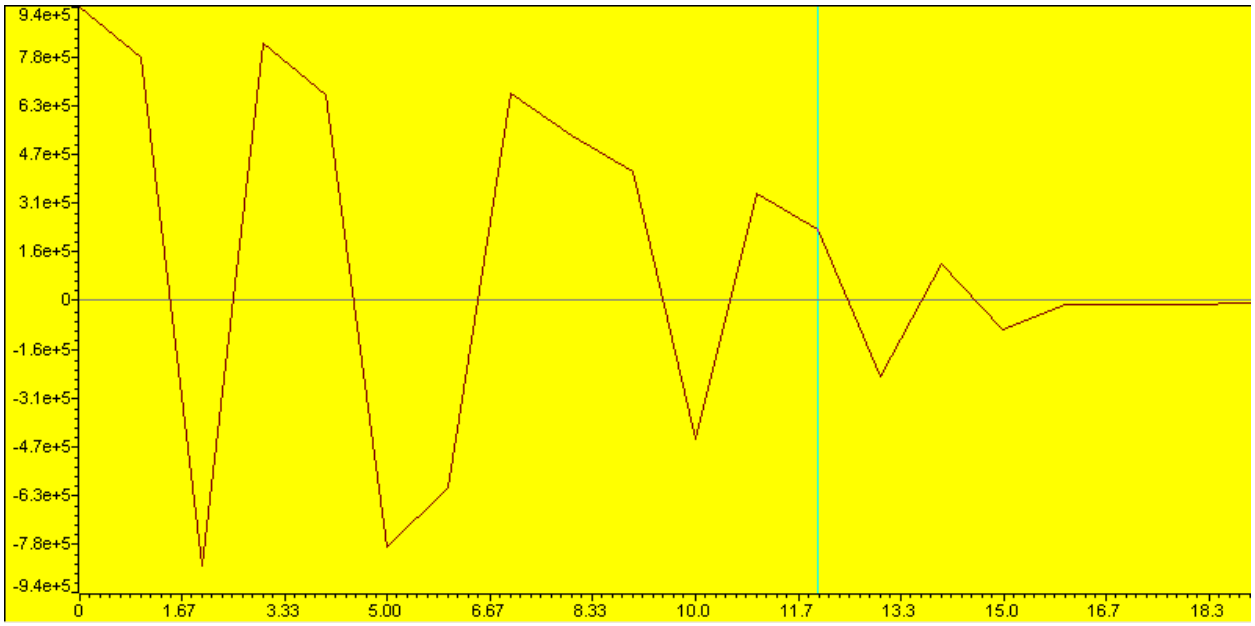

Figure 5-16: Real part of Enlarged FFT of synchronized OFDM symbol after 4 periods.

5.3 Conclusion

In this chapter, the simulation and the implementation results for the testbed were presented. The processing requirements of the testbed were not achievable due to the indoor channel having a high coherent bandwidth which the communication system has to reach in order for the channel estimation algorithms to be correctly evaluated. A DSP cannot cope with the processing requirements of such a high system bandwidth and so the implementation of the testbed could not be fully realized for an indoor channel. A qualitative evaluation was however performed based on the DSP's clock cycles and it was concluded that a non-iterative DDCE can be implemented with an FPGA with reasonable cost. The iterative DDCE takes up a lot of clock cycles to be implemented and is very likely not to be realizable. The analogue front end results of the MISO OFDM communication system were also presented. Also a base band implementation of a SISO OFDM communication system was presented which illustrated the achievement of synchronization and detection of an OFDM signal. In Chapter 6, it is suggested that this testbed should be improved with the use of an FPGA and that this DSP based system was better suited for an outdoor environment because the system bandwidth demands, for the sake of demonstration, would be much lower.

Chapter 6

6 Conclusion and Recommendations

6.1 Conclusion

The theory of MISO OFDM communication systems was developed in this thesis and the implementation of the system was presented. The project was implemented for evaluating the real time performance of the channel estimation algorithms developed in [1]. The development included finding the optimal synchronization scheme, channel coding scheme, RF hardware, analogue front end hardware and the processor for the project.

The processor chosen for the project was a digital signal processor (DSP) which allowed the development of the baseband processing to be achieved within a short space of time. The drawback of the DSP was that it could not process high bandwidth signals which were required in order to properly validate the channel estimation algorithms developed by [1]. A qualitative evaluation was made and it was concluded that iterative channel estimation algorithms were very demanding for real time systems and the non-iterative counterparts were a better solution.

It was also found from the simulation results that the non-iterative channel estimation algorithms yielded better system performance than the iterative channel estimation algorithms. This means that the non-iterative channel estimation algorithms have 2 benefits: less complexity and better performance over the iterative channel estimation algorithms. The reasons why this aspect differed from what was obtained in [1] was because a different frame structure and channel was used in this project.

The hardware aspects of the project were properly implemented. A MISO OFDM signal could be sent from the transmitter to the receiver. With a fast enough processor the signal at the receiver could be processed in order to recover the transmitted information. It was also concluded that the DSP based testbed was better suited for an outdoor channel where the delay spread is larger and allows the system bandwidth to be reduced in order to still get

frequency selective fading. For indoor channels an FPGA must be used at the expense of high cost and longer development time.

6.2 Recommendations and future work

The processing aspect of the testbed can be improved by the use of an FPGA in order to support the high bandwidth required by the indoor testbed so that practical feasibility of channel estimation algorithms can be evaluated.

The distance of the receiver from the transmitter was limited to 3 meters because the transmitted signal could not be detected beyond that range. An additional RF power amplifier at the receiver or transmitter would further increase the maximum distance of the receiver from the transmitter that allows the transmitted signal to be detectable.

8 References

[1] O.O. Oyerinde and S.H. Mneney, *Channel Estimation for SISO and MIMO OFDM Communication Systems(PhD Thesis)*. Durban, South Africa: University of KwaZulu Natal, 2010.

[2] R.L.G. Cavalcante & I. Yamada, "A Felxible Peak-To-Average Power Ratio Reduction Scheme for OFDM Systems by Adaptive Projected Subgradient Method," *IEEE Transactions on Signal Processing*, vol. 57, no. 4, pp. 1458-1468, April 2009.

[3] K. B. Letaief and H. Minn V. K. Bharg, "A Robust Timing and Frequency Synchronization for OFDM Systems.," *IEEE Transactions on Wireless Communications*, vol. 2, pp. 822-839, July 2003.

[4] S. Worrall, E. Sofe, M Goldshtein and A. Navarro C.H. Liew, "Fixed and Mobile Channels Identifications," *Suit*, vol. 64, no. IST-4-028042, July 2006.

[5] D. Gesbert, C. B. Papadias & A. Van der Veen H. Bölcskei, *Space Time Wireless Systems: From Array Processing to MIMO Communications*.: Cambridge University Press, 2006.

[6] D. Tse and P. Viswanath, *Fundamentals of Wirelss Communications*. New York: Cambridge University Press, 2008.

[7] J.B. Anderson & R. Vaughan, *Channels, Propagation and Antennas for Mobile Communications: IEE Electromagnetic Wave Series no. 50.*, 2003.

[8] R.L. Peterson & R.E. Ziemer, *Introduction to Digital Communication*, 2nd ed.: Prentice-Hall, 2001.

[9] M.C. Chiu and J. S. Lin R. C. T. Lee, *Communications Engineering: Essentials for Computer Scientists and Electrical Engineers*. West Sussex, England: John Wiley & Sons, 2007.

[10] S. Glisic, *Advanced Wireless Communications: 4G Technologies*. Chichester, West Sussex, England: John Wiley & Sons, 2004.

[11] N. Benvenuto and G. Cherubini, *Algorithms for Communications Systems and their Applications*. West Sussex, England: John Wiley & Sons Ltd, 2005.

[12] W. Zhu, C. Oberli, D. Browne, J. Bhatia, J. F. Frigon, J. Wang, P. Gupta, H. Lee, D. N. Liu, S. G. Wong, M. Fitz and B. Daneshrad R. M. Rao, "Adaptive Antennas and MIMO Systems for Wireless Systems: Multi-Antenna Testbeds for Research and Education in Wireless Communications," *IEEE Communications Magazine*, vol. 42, no. 12, pp. 72 - 81, December

2004.

[13] S. Salous and D. Eden V. Hinostroza, "High Resolution Indoor and Indoor to Indoor Measurements," *European Cooperation in the Field of Scientific Techinical Research*, May 2002.

[14] D.C. Cox & T.M. Schimdl, "Robust Frequency and Timing Synchronization for OFDM," *IEEE Transactions on Communications*, vol. 45, no. 12, pp. 1613 - 1621, December 1997.

[15] P. O. Borjesson, M. Sandell J. J. Van der Beek, "ML Estimation of Time and Frequency Offset in OFDM Systems," *IEEE Transactions on Signal Processing*, vol. 45, no. 7, pp. 1800- 1805, July 1997.

[16] A.N. Mody & G.L. Stuber, "Synchronization Of MIMO OFDM Systems," *Proceedings of GLOBECOM*, vol. 1, pp. 509 - 513, 2001.

[17] J. Spiedel and R.H. Yan S. te Brink, "Iterative Demapping for QPSK Modulation," *Electronics Letters*, vol. 34, no. 15, pp. 1459-1460, July 1998.

[18] E. Biglieri and M. Lops D. Angelosante, "Sequential Estimation of Multipath MIMO OFDM Channels," *IEEE Transactions on Signal Processing*, vol. 57, no. 8, August 2009.

[19] J. Akhtman and L. Hanzo, "Decision Directed Channel Estimation Aided Employing Sample Spaced and Fractionally Spaced CIR Estimators," *IEEE Transactions on Wireless Communications*, vol. 6, no. 4, pp. 1171 - 1175, April 2007.

[20] X.G. Doukopoulos and G.V. Moustakides, "Fast and Stable Subspace Tracking ," *IEEE Transactions on Signal Processing*, vol. 56, no. 4, pp. 1452 - 1465, April 2008.

[21] A. Goldsmith, *Wireless Communications*, 2nd ed. New York: Cambridge University Press, 2005.

[22] S. Jelting and J. Speidel F. Sanzi, "A Comparative Study of Iterative Channel Estimators for Mobile OFDM Systems," *IEEE Transactions on Wireless Communications*, vol. 2, no. 5, pp. 849-859, September 2003.

[23] G. Caire, J. Corrat, A.R. Dias, A.G. Fábregas, K. Gosse, M. Guillaud, Z. Li, X. Miet, A. Peden, S. Rouquette, D.T.M. Slock and Y.Toutain P. Bernadin, "MIMO OFDM Testbed for Wireless Local Area Networks," *EURASIP Journal on Applied Signal Processing*, pp. 1-20, 2006.

[24] W. Zhu, B. Daneshrad, J. Bhatia, H. Kim, K. Mohammed, S. Sasi, A. Shah J. Chen, "A Real Time 4X4 MIMO OFDM SDR for Wireless Networking Research," in *15th European Signal Processing Conference (EUSIPCO 2007),* Poznan Poland, September 2007, pp. 1151-1155.

[25] T.C.W Shenck, A. van Zelst, "Implementation of a MIMO OFDM Based Wireless LAN System," *IEEE Transactions on Signal Processing*, vol. 52, no. 2, pp. 483-494, February 2004.

[26] M. Ergen, A. Puri and A. Bahai S. Coleri, "Channel EstimationTechniques Based on Pilot Arrangement in OFDM Systems," *IEEE Transactions on Broadcasting*, vol. vol. 48, no. No. 3, pp. 223- 229, September 2002.